



A University of Sussex DPhil thesis

Available online via Sussex Research Online:

<http://sro.sussex.ac.uk/>

This thesis is protected by copyright which belongs to the author.

This thesis cannot be reproduced or quoted extensively from without first obtaining permission in writing from the Author

The content must not be changed in any way or sold commercially in any format or medium without the formal permission of the Author

When referring to this work, full bibliographic details including the author, title, awarding institution and date of the thesis must be given

Please visit Sussex Research Online for more information and further details



Electroencephalogram Signal Acquisition in Unshielded Noisy Environment

Mohsen Fatoorechi

Submitted for the degree of Doctor of Philosophy

University of Sussex

September 2014

Declaration

I hereby declare that this thesis has not been and will not be submitted in whole or in part to another University for the award of any other degree.

Signature:

Mohsen Fatoorechi

UNIVERSITY OF SUSSEX

DOCTOR OF PHILOSOPHY

ELECTROENCEPHALOGRAM SIGNAL ACQUISITION IN UNSHIELDED

NOISY ENVIRONMENT

SUMMARY

Researchers have used electroencephalography (EEG) as a window into the activities of the brain. High temporal resolution coupled with relatively low cost compares favourably to other neuroimaging techniques such as magnetoencephalography (MEG). For many years silver metal electrodes have been used for non-invasive monitoring electrical activities of the brain. Although these electrodes provide a reliable method for recording EEG they suffer from noise, such as offset potentials and drifts, and usability issues, e.g. skin preparation and short circuiting of adjacent electrodes due to gel running. Low frequency noise performance is the key indicator in determining the signal to noise ratio of an EEG sensor. In order to tackle these issues a prototype Electric Potential Sensor (EPS) device based on an auto-zero operational amplifier has been developed and evaluated. The absence of $1/f$ noise in these devices makes them ideal for use with signal frequencies $\sim 10\text{Hz}$ or less. The EPS is a novel active electrode electric potential sensor with ultrahigh input impedance. The active electrodes are designed to be physically and electrically robust and chemically and biochemically inert. They are electrically insulated (anodized) and scalable. These sensors are designed to be immersed in alcohol for sterilization purposes. A comprehensive study was undertaken to compare the results of EEG signals recorded by the EPS with different commercial systems. These studies comprised measurements of both free running EEG and Event Related Potentials. Strictly comparable signals were observed with cross correlations of higher than 0.9 between the EPS and other systems.

Acknowledgements

There have been many individuals in my life who have affected it with their presence bit by bit, being instrumental in getting me to this point. I would like to thank my supervisors Dr. Helen Prance and Prof. Robert Prance for their tireless help and continuous support for me and my work. My regards are extended to all my colleagues in the STRC lab, in specific Martin Nock for all the help and advice he gave me. The Sackler centre for allowing access to their research facilities, and in particular David and Jim, for allowing me to use their time generously and educate me on various topics while we waited for our experiments to conclude. Atefeh, for patiently awaiting me, while I was writing this thesis and giving me courage. Ali, for providing me company and tolerating me as a flatmate. Last but not least I thank my parents for their support and trust in me.

This has been a long journey that without the help of my family, colleagues, and friends would not have been possible. . .

Contents

Acknowledgements	iii
Contents	iv
List of Figures	vii
List of Tables	ix
1 Introduction	1
2 Background	4
2.1 Introduction	4
2.2 Activities of the Brain	4
2.2.1 Electrical activity	5
2.2.1.1 Electrode Positioning	6
2.2.2 Magnetic activity	6
2.2.3 Neuroimaging	7
2.3 Interpretation of Brain Activities	8
2.3.1 Spontaneous EEG	9
2.3.2 ERPs	10
2.3.3 Source Localisation	12
2.3.4 Brain Computer Interface	13
2.4 Methods of measuring EEG	13
2.4.1 Wet (Gel) Electrode	13
2.4.2 Dry Electrode	15
2.4.3 Insulated Electrode	16
2.4.4 Quasi-Dry Electrode	19
2.5 Electric Potential Sensor	20
2.5.1 EPS Design for EEG Recording	21
2.5.2 Noise	23
2.5.2.1 Noise Coupling Through USB Cable	24
2.5.2.2 EEG Artefacts	25
2.5.2.3 Shielded Room	27
2.5.3 EPS Configuration	28
2.5.3.1 Present Design	30
2.5.3.2 Different EPS Designs	31
2.6 Discussion	32

3	Spontaneous EEG	34
3.1	Introduction	34
3.2	Alpha Rhythm	34
3.2.1	Alpha Blocking	35
3.3	Alpha Detection using EPS	36
3.3.1	Methodology	37
3.3.2	Signal Processing	42
3.3.3	Results	46
3.4	Comparison with Conventional Sensors	49
3.4.1	ANT EEG Monitoring System	50
3.4.1.1	Methodology	51
3.4.1.2	Results	53
3.4.2	g.tec EEG Monitoring System	57
3.4.2.1	Methodology	57
3.4.2.2	Results	58
3.5	Discussion	60
4	Sensory ERPs	62
4.1	Introduction	62
4.2	Sensory ERP	62
4.2.1	Visually Evoked Potential	64
4.2.2	Signal Processing	66
4.3	Pattern Reversal Experiment	67
4.3.1	Methodology	68
4.3.2	Results	70
4.4	Flashing LED Experiment	72
4.4.1	Experiment Design	73
4.4.2	Results	75
4.5	Discussion	76
5	Cognitive ERPs	78
5.1	Introduction	78
5.2	Cognitive ERP	78
5.3	Oddball Paradigm	80
5.3.1	Methodology	80
5.3.2	Signal Processing	82
5.3.3	Results	82
5.4	Face Processing Experiment	83
5.4.1	Methodology	84
5.4.2	Signal Processing	86
5.4.3	Results	86
5.5	Recording Artefacts	87
5.5.1	Key Stroke	87
5.5.2	Referencing Artefacts	88
5.5.3	Trigger Signals	91
5.5.4	Movement Artefact	91
5.6	Discussion	94

6	Wireless Connectivity	96
6.1	Introduction	96
6.2	Wireless Standards	97
6.2.1	IEEE 802.15.4 Design	97
6.3	Data measurements	103
6.3.1	ECG	103
6.3.2	EEG	104
6.3.3	Frequency Bands	106
6.4	Mobility Data	107
6.5	Discussion	108
7	Conclusion	112
A	Appendices	126
A.1	Appendix A	126
A.1.1	MATLAB	126
A.1.1.1	FFT routine	126
A.1.2	C Code	126
A.1.2.1	Sensor Node	126
A.1.2.2	CC2420 Driver	133
A.1.3	LabView	135
A.2	Appendix B	138
A.2.1	g.tec	138
A.3	Appendix C	139
A.3.1	UART Converter	139
A.3.2	gtec Interface	139
A.3.3	Wireless Communication Board Design	139

List of Figures

2.1	10-20 System	7
2.2	Free Running EEG	11
2.3	Gel Electrode	14
2.4	EPS Design	21
2.5	EPS strongly coupled	21
2.6	EPS Noise	24
2.7	Drift EPS vs. AgCl	25
2.8	USB Noise	26
2.9	Size and Grounding Variation	30
3.1	Alpha Blocking Demo	36
3.2	connector	38
3.3	Sensor Block Diagram	38
3.4	AmpBoxV1	38
3.5	Head Gear	40
3.6	Skin EPS Interface	41
3.7	Demo Signals	43
3.8	System Gain and Filter	44
3.9	Frequency Response of System and Sensor	45
3.10	Alpha Blocking Time Domain	46
3.11	Alpha Blocking Frequency Domain	47
3.12	Referencing 50 Hz removal	48
3.13	Referencing Common mode noise PSD	48
3.14	Referencing Drift Removal	49
3.15	Raw time domain EPS ANT Alpha	53
3.16	Frequency domain EPS ANT Alpha	54
3.17	Complete EPS ANT Alpha	55
3.18	Effect of Drift and Eye Blink	56
3.19	Effect of Drift on Cross-Correlation	56
3.20	g.LADYbird sensor	58
3.21	Alpha Signal g.tec comparison Frequency domain	59
3.22	Alpha Signal g.tec comparison Time domain	60
4.1	Primary sensory areas	64
4.2	Checkerboard stimulus and its reverse pattern	68
4.3	Checkerboard Sensor Position	69
4.4	VEP signal recording	70
4.5	VEP trials	71
4.6	VEP ANT comp	72

4.7	VEP Stimulator	73
4.8	gtec Setup	74
4.9	VEP gtec Compare	76
4.10	VEP components	77
5.1	Oddball XO Experiment	81
5.2	Oddball XO Results	83
5.3	Image of a face with variations	85
5.4	Face Perception	87
5.5	Key Stroke	88
5.6	Spatial attention experiment results	90
5.7	Trigger Noise	92
5.8	Movement Artefact	93
6.1	Overview of wireless design	100
6.2	Network Protocol	101
6.3	LabView Front Panel	101
6.4	Time domain wireless ECG	104
6.5	Frequency domain wireless ECG	105
6.6	Alpha Wireless	105
6.7	Alpha Wireless Frequency	106
6.8	Wireless vs. wired Alpha	107
6.9	Band Power	108
6.10	Raw Walking Data	109
6.11	Drift Strength	110
7.1	EPIC	114
A.1	LabView Block Diagram Part 1	136
A.2	LabView Block Diagram Part 2	137
A.3	Alpha Signal g.tec comparison	138
A.4	USB UART Converter	139
A.5	g.tec Interface	140
A.6	Wireless Board Part 1	141
A.7	Wireless Board Part 2	142

List of Tables

2.1	Frequency bands of free running EEG and their classification	10
2.2	Size and ground connection effects on recording alpha signal	30

Chapter 1

Introduction

The study of the human body has been enhanced by the discovery of the wide range of electrical signals it exhibits. Specifically, electroencephalography (EEG) is used to monitor the human brain. This has opened new frontiers for medics and researchers alike, acting as a window to the activities of the brain. The effectiveness of this window and the clarity of the picture it provides is partly limited by the structure of human head, its tissue, and the skull that protects it. However, the tools used for capturing these activities, biopotential electrodes, impose further degradation to this picture.

A number of sensor designs exist for the recording of EEG, and other biopotentials. A category of sensors work based on forming a resistive contact to the surface of scalp through a wet (gel) or dry medium. Another method for capturing EEG is to couple capacitively to the scalp using insulated electrodes. Current recording methods suffer from three restrictions. The first is noise, such as offset potentials and drifts, caused by the interfacing to the body and the electrodes or the intrinsic noise of the electronics used. The second is usability, for example skin preparation and short circuiting of adjacent electrodes due to gel running. The third is the invasiveness of current technology, not limited to the

human body but also to the life of the participant in an experiment. A better method of recording EEG should enable continuous measurement of EEG to be made while the participant is allowed to perform their daily routines without being restricted to a shielded room.

The Electric Potential Sensor (EPS) is an active electrode sensor. An insulation layer can be placed in front of the active electrode forming a half capacitor plate when in mechanical contact with a signal source. The EPS does not rely on a resistive contact to make measurements as a displacement current is drawn by coupling capacitively to the signal source. As a generic electric field measurement technology, the EPS has many applications including biopotential recording. It has been shown previously that it is possible to record specific EEG signals using the EPS. However, these measurements have been performed inside a screened room in order to reduce noise present from external sources.

In the following chapters some of the generic problems of the EEG recording methods such as low frequency noise , movement artefact, long term monitoring, usability, and half-cell potential are discussed and addressed. Furthermore some problems that are specific to capacitive measurement of the EEG, such as effect of static charge on the sensors, sensor size and shape are encountered. Previously low coupling capacitances have been investigated for use in EEG sensors, such as an air gap. This work focuses on probing effects of increasing the coupling capacitance and minimising its variations by introducing a small amount of moisturising agent to the skin electrode interface. Therefore, forming a quasi-dry capacitive sensor. The content of this thesis can be divided into three major parts. The first part provides a background on methods of recording brain activities with a review of different electrode technologies used for collecting EEG. A novel low noise

active electrode sensor is introduced which includes description and characterization of the sensor developed for this work.

The second part reflects on different EEG signal categories and investigates whether it is possible to collect them using the EPS and how the results compare to other commercial systems. This part includes sections on spontaneous EEG and event related potentials. A number of studies have been conducted based on previously published experiments. The aims of these studies were: First, to assess the low frequency noise performance of EPS, to ascertain if it was analogous to, or lower than, conventional electrodes within a 0.1-10 Hz bandwidth. Secondly, I wanted to compare EPS and standard electrode EEG recordings from free running EEG and Event Related Potential (ERP) paradigms, in order to investigate if the signals were broadly comparable.

The final part is devoted to the development of a low power wireless module that would incorporate EPS and enable recording of EEG while a person is mobile. This section is analysed based on both the quality of the EEG signal it records, and the limitations of current devices and wireless standards.

Chapter 2

Background

2.1 Introduction

A discussion is provided on the methods of recording brain activities. The electrical activity of the brain is looked at in more detail in this chapter. A number of different electrode technologies such as wet, dry and capacitive are currently available. A new approach has recently been followed which forms an electrode that is positioned between dry and wet electrodes named quasi-dry electrode[1]. This is followed by a description of a sensor design based on the Electric Potential Sensor (EPS) that is capable of recording various brain electrical activities.

2.2 Activities of the Brain

The recording of potentials can be divided to two general categories of perturbative and non-perturbative measurements[2]. A further distinction in categories of measurement is

whether they are based on invasive methods. In this work the focus is based upon non-invasive technologies, and furthermore the introduction of a non-perturbative method of monitoring brain activity.

2.2.1 Electrical activity

The electroencephalogram (EEG) represents oscillations of brain electric potential recorded from electrodes positioned on the head. The first electrical activity from a brain was recorded by Richard Caton. In 1875, while working on the theory of the electrical basis of epilepsy, he recorded the signs of electrical activity in an animal brain[2]. In his work he placed unipolar electrodes inside the brain and on the surface of the skull. The currents were recorded using a galvanometer. He mentioned the increase of currents in case of sleep and variations in baseline which were unrelated to cardiac activities. More crucially he noticed that these activities would disappear in the case of the animal's death[3].

However, in relation to recording these activities from the human brain, it was not until 1924 that work of Hans Berger lead to the first recording of electrical activities from a human brain. In his early work he characterised patterns such as Alpha and Beta waves, and he coined the term electroencephalogram (EEG) to describe the method of recording these phenomena[3].

The relatively low input impedances of conventional acquisition systems using silver-silver chloride (Ag/AgCl) electrodes ($10^6 - 10^7 \Omega$) have been shown to significantly distort the scalp recorded electrical potentials due to volume conductance. A general property of electrical currents is to follow the path of least resistance, which causes activity from a cortical dipole to spread out the further from the source it is and also to be smeared or diverted as it tries to pass through the highly resistant skull[4].

2.2.1.1 Electrode Positioning

The internationally standardized 10-20 system is usually employed to record the EEG. All the signals are recorded against a reference signal, that can be the signal from an electrode anywhere on the head or the average of all electrodes[5]. Depending on the type of the signal recorded and the effect of interest the reference electrode can change. A linked mastoid is used as the reference signal in some studies, where a mathematical average of the two signals is used. This is explained in more detail in chapter 5. Another typical reference point is the tip of the nose[6].

Electrode positioning on the head is demonstrated in Figure 2.1. Points M1 and M2 are the locations for the mastoids. It should be noted that A1 and A2 point to the ear lobes. Furthermore, a ground position is included on the 10-20 system. this position is used in recording with conventional gel electrode systems.

2.2.2 Magnetic activity

Associated with the electric field of the brain is a magnetic field. A recording of these activities is called magnetoencephalogram (MEG). Both the EEG and the MEG originate from the same source but exhibit different patterns[8]. Some of the limitations of EEG have been addressed by using superconducting quantum interfering device (SQUID) magnetometer systems, which unlike Ag/AgCl electrodes do not require direct mechanical contact with the scalp [9]. Unfortunately, SQUID systems are very expensive, mainly due to the requirement for cryogenic cooling of the sensors and the necessity of a magnetically shielded chamber to attenuate the Earth's own large magnetic field and external noise. However, it is clear from the data published using SQUID magnetometers that the recording of signals with no electrical connection to the body affords great benefits, including

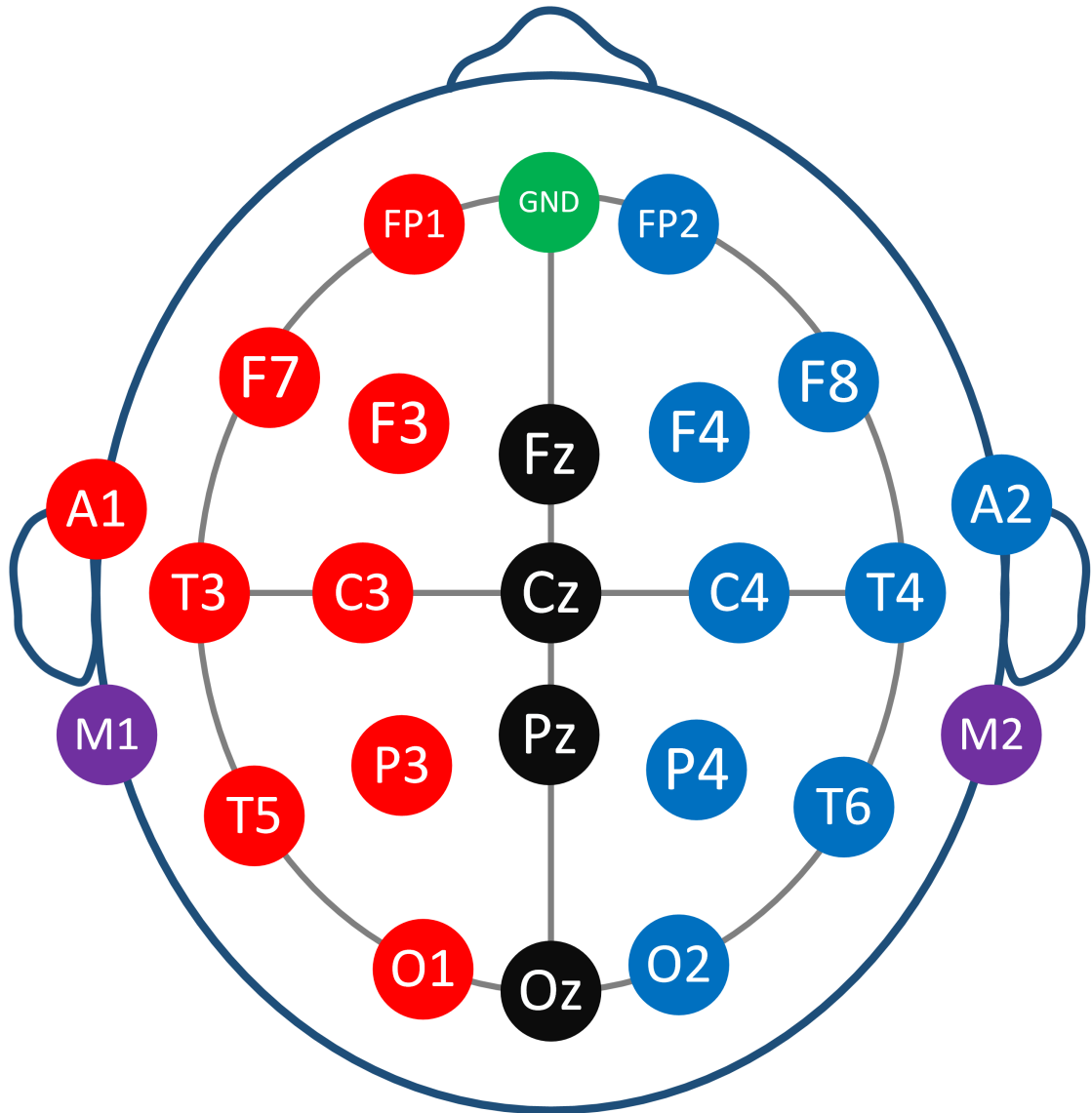


FIGURE 2.1: Electrode positioning according to 10-20 system, if looked at from top of the head. Cz is measured to be in equal distance from the Inion and the Nasion of human skull. This distance is further used to find the position of adjacent sensor based on 10% or 20% of that distance. Positions M1 and M2 indicate the left and right mastoid. The GND position is a separate electrode used as ground in conventional EEG systems[7].

enhanced case of the three dimensional (3D) reconstruction of the underlying sources of scalp recorded signals[4].

2.2.3 Neuroimaging

Both EEG and MEG record the changes in the brain in real time, given a high temporal resolution of below 100 ms[10]. However, they have poor spatial resolution compared to brain

imaging techniques such as functional magnetic resonance imaging (fMRI) or positron emission tomography (PET)[11]. Unlike EEG and MEG methods, where the variations caused by neurons were recorded by means of electromagnetic measurements, neuroimaging relies on blood oxygen levels or blood flow in brain tissue. These methods provides researchers with images of cross sections of the brain[12]. This helps with localising the sources of activity for a particular cognitive event with a much higher resolution than it is possible with the models available for the EEG and MEG. It is possible to resolve sources with a resolution of merely 3 to 5 mm using PET scanner. Apart from the high costs associated with these methods they have a poor temporal resolution, typical PET scan image takes between 45 to 60 seconds to develop[13].

2.3 Interpretation of Brain Activities

The interaction of neurons or assemblies of neurons is known to be the source of the brain's dynamic behaviour. These exchanges between neurons are performed through the medium of electrochemical currents passing between them. Parts of these activities can be measured in the form of a surface potential on the scalp. Electrical activities of the brain recorded from the scalp electrodes have provided medical professionals and researchers with a valuable tool to study and treat mental illnesses. EEG dynamics can be altered in the presence of a stimulus which can be in the form of a visual or audible cue. When brain signals are recorded in the absence of such stimuli, it is understood as spontaneous or free running, as opposed to being interpreted based on a trigger signal[6].

Presenting a stimulus gives rise to activities in neurons which alters the potentials recorded on the scalp, creating event related potentials. These potentials are observable given the

information about the stimulus trigger, and are the subject of chapters 4 and 5. Based on the nature of the brain activity the recorded signal can be divided into two categories[6]:

- Spontaneous (Free-Running) EEG
- Event Related Potentials (ERPs)

Sensory

Cognitive

ERPs are the responses of brain to specific stimuli such as visual or audible events. They are recorded by time averaging single stimulus waveforms to remove the background spontaneous EEG activities. The number of stimuli required to produce an averaged ERP may be anything between ten to several thousands, depending on the application[14].

2.3.1 Spontaneous EEG

In the absence of specific stimuli, the recorded brain activity presents certain characteristics. These activities are categorized based on frequency bands and the state of the mind they can represent and are called spontaneous or free-running EEG[6]. This will be covered in more detail in chapter 3. In the case of the spontaneous EEG, changes in the shape or amplitude level of specific frequency bands are possible intentionally or unintentionally. Table 2.1 shows different classifications of EEG based on the frequency content of the observed signal[13].

A visualised description of these frequency bands is given in figure 2.2. Each frequency band can be related to a state of mind. The amplitude of activities in a given band can be altered by external experiences such as excitation or pleasure. Also brain abnormalities caused by diseases affect the content of the EEG. Alzheimer's disease typically results

TABLE 2.1: Frequency bands of free running EEG and their classification

	Frequency	Amplitude	State of Mind
Delta	0.5-3.5 Hz	20-100 μ V	Deep Sleep
Theta	4-7 Hz	20-100 μ V	Pleasure
Alpha	8-13 Hz	20-60 μ V	Eye Closed/Relaxation
Beta	14-30 Hz	2-20 μ V	Excitation
Gamma	36-44 Hz	5-10 μ V	Response to sensory stimuli

in reduction in the frequency of the Alpha band. Brain tumours show their presence in the form of a reduction in the low frequency activity in the vicinity of the region of the tumour[6]. The effects of epilepsy on brain activity have long been documented and used in the diagnosis and management of patients affected by seizures. Typically a seizure, shown in part (b) of figure 2.2, is accompanied by a sudden sharp rise in amplitude of low frequency activity of the 3 Hz spike wave [15].

Patterns of brain activity of an individual can also change based on their age. Theta waves, which occur at about 4 to 7 Hz, are reported to be more common in recordings of EEG for children in comparison to adults. Amplitudes of 100 μ V are reported in infants experiencing a pleasurable event [13].

2.3.2 ERPs

Brain activity observed in spontaneous EEG is caused by hundreds of aggregated neural sources. As a result, EEG provides an overall picture of brain activities, therefore, it lacks precision in the sense that a specific neural reaction to a certain cognitive, motor and sensory event cannot be segregated. Nevertheless, if averaging techniques are applied to the EEG, different signals can be extracted from the background EEG that illustrates brain's responses to certain events. These responses form the second category of brain

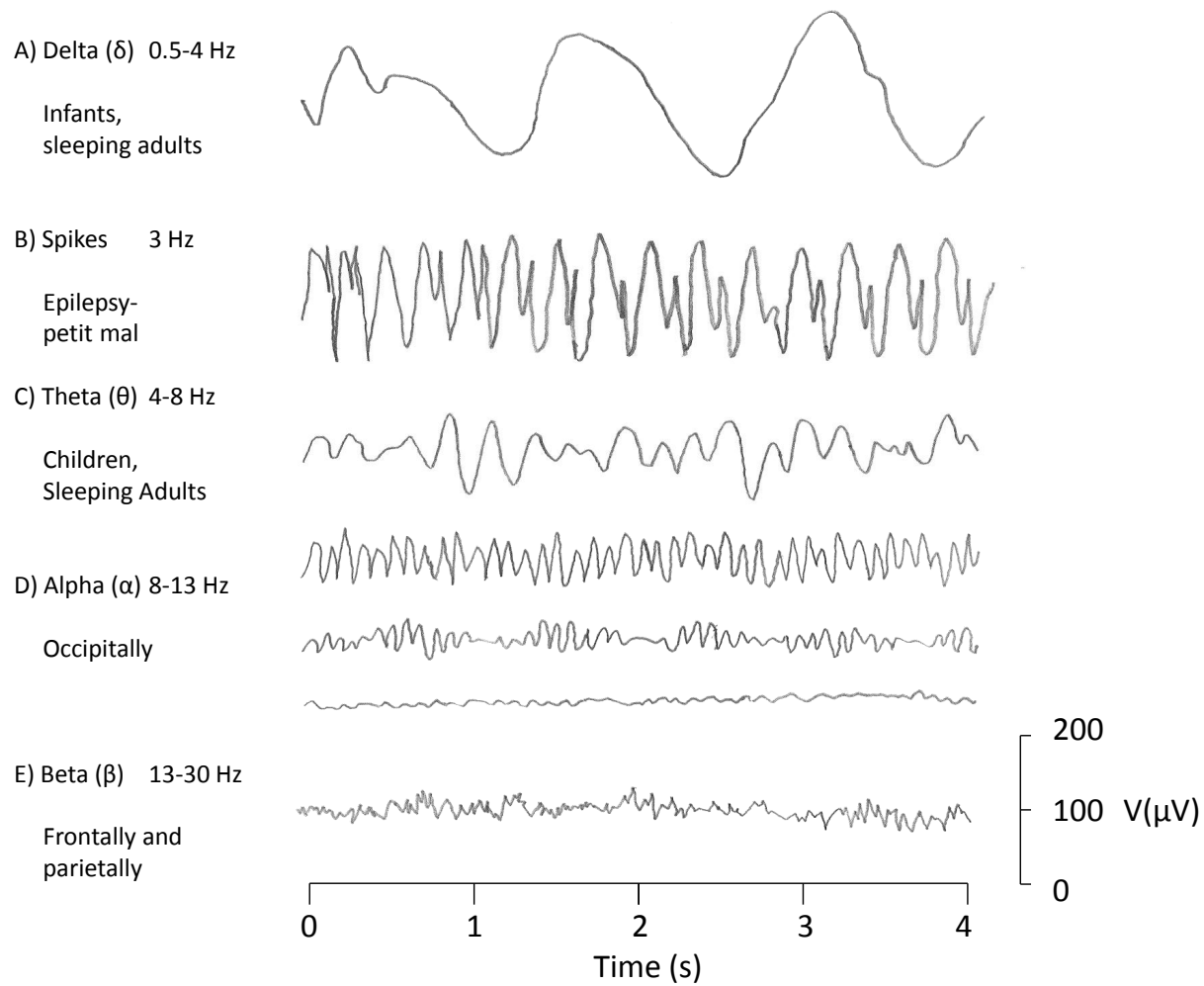


FIGURE 2.2: Different Signals in free running EEG, with extended information on brain region and age group. [5]

activities. As these activities are phenomena in direct relation to a specific event they are called event related potentials (ERPs)[14].

ERPs themselves can be divided into two major groups based on the set of events that lead to observation of these signals. While the brain signals are being recorded a volunteer can be asked to observe an event passively or show a reaction to specific events. Certain ERPs such as visually evoked potentials (VEP) are an example of the first type of the ERP where the volunteer is merely a passive observer of an event. In this type of experiments a stimulus is provided repeatedly with a specific rhythm with the purpose of stimulating sensory parts of the brain[13]. Thus the term sensory ERP is used for these signals[14].

The second type of ERPs is called cognitive ERP[14]. The origin of this signal is thought to be the reaction shown by a volunteer to a specific event. When stimuli are presented to the volunteer, he or she is asked to perform a task if a specific event has occurred and to passively observe the rest of the events.

2.3.3 Source Localisation

By collecting ERPs it is also possible to investigate the source of a signal arising from a cognitive or sensory event. The standard 10-20 placement system currently involves the placement of 21 electrodes approximately 6 cm apart. Within the last decade the popularity of high density electroencephalography (hd-EEG) set-ups has increased (128-256 electrodes) [16] with the aim of localizing sources that drive the scalp recorded EEG signals. While the problem of volume conductance has been widely cited as a critical issue preventing this goal, the fact remains that the scalp recorded EEG does exhibit distinct spatial characteristics, which are not represented with low density EEG recordings [17][18]. This has led researchers to investigate the number of electrodes necessary to adequately capture the spatial pattern of scalp recorded EEG. Estimates range from electrode spacing of 2-3 cm [19] to 0.5–1 cm [20]. Odabae et al., (2013) found that that sensor distances of between 6-10 mm are required to capture the full spatial texture of the raw EEG signal on a neonatal scalp. Petrov et al., (2014) found strong variations in EEG signals (VEPs) at the scale of 1cm when using an ultra-dense electroencephalography (ud-EEG) sensor array. They found that the use of this array led to a two-fold increase in the signal to noise ratio compared to a hd-EEG system. The studies mentioned above did not record ud-EEG over the entire head, due to the technical challenges involved, but used a small dense array of electrodes (e.g. 16 electrodes [18]) placed over a small region of the scalp.

2.3.4 Brain Computer Interface

Brain computer interface (BCI) is an area in which researchers and industry are becoming increasingly interested. A number of products are currently available which allow the user to control or manipulate an activity performed on a computer through their mind [21][22]. Researchers have been exploring BCI with aim of assisting disabled people and improving user experience for able-bodied individuals[23]. Chi et al., (2012) demonstrates a system for communicating with mobile phones to perform various tasks such as entering a number. Other researchers have used motor-sensory information from the brain to control external devices. A study was conducted with five participants in which they were asked to navigate a quadcopter through a course, using EEG[24]. The successful outcome of such studies demonstrates the possibilities for further integration of such systems for paralysed individuals to assist their interactions with their surrounding environment[25].

2.4 Methods of measuring EEG

Various types of sensors have been used to investigate recording of EEG in both humans and animals. Currently the most common method is to form a low impedance contact with the surface of skin using wet (gel) electrodes. However, other methods exist that do not rely on low resistance contact with body. Dry and insulated sensors rely on active circuitry to provide a high input impedance needed to compensate for the lack of a low ohmic path between the electrode and the measuring surface.

2.4.1 Wet (Gel) Electrode

Traditional methods of acquiring EEG signals rely on the use of silver/silver chloride (Ag/AgCl) transducing electrodes, which have not changed significantly since their first

use by Hans Berger in 1929. This type of electrode converts ionic current on the surface of the scalp to electronic current for amplification and subsequent signal processing[26]. Such electrodes are cheap, and in clinical applications disposable, but require the use of a conducting gel between the electrode and the skin, since they rely on maintaining a low electrical resistance contact [27]. When applying gel electrodes a low impedance path of approximately less than $10^4 \Omega$ is usually achieved by abrading the scalp. This is then followed by an acquisition system with a typical input impedance of 10^6 to $10^7 \Omega$. Although this ratio seems high, it still causes distortion of the very surface potentials it is trying to measure. Since the electrical potentials that are attempted to be recorded are caused by the flow of current in the body, any device that requires a real charge current to flow through it in order to make a measurement distorts the source of that potential. A model for gel electrode connection with the surface of the skin is shown in Figure 2.3[28].

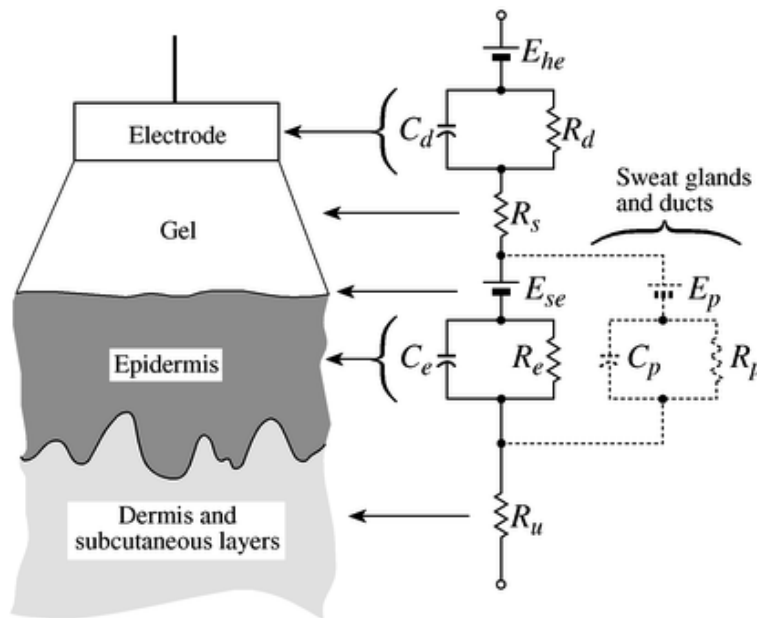


FIGURE 2.3: Gel electrode model in contact with skin. The Epidermis layer is removed by abrading the skin to form a low impedance path for the gel electrodes.[29]

Both in clinical and research fields the acquisition of clean EEG data requires skilled personnel to setup, as the application of EEG electrodes needs to be carried out in a precise manner and involves the abrasion of the scalp. In addition, the conducting gel

may cause skin irritation and discomfort, tends to dry out after a period of time, and needs to be washed out of the hair upon completion, meaning that wet electrodes are unsuited for long term clinical monitoring applications [30]. The gel may also lead to cross coupling or bridging between electrodes in an array if great care is not taken during placement, and this problem is enhanced by the use of high-density EEG arrays.

In the setup of conventional gel electrodes a connection between the scalp and metal conductor is achieved through the use of an electrolyte solution. The electrical properties of this interface, known as half-cell potential, is governed by the electrochemical reactions between the two layers [28]. The electrochemical reactions produce fluctuations in the metal-electrolyte potential that can cause an increase in noise levels of up to 10 μV peak-to-peak for Ag/AgCl electrodes [31].

2.4.2 Dry Electrode

Dry conducting electrodes have the potential to provide a more user friendly approach, with the electrodes making resistive contact with the skin. This overcomes some of the problems caused by the wet gel electrodes, but introduces an additional variable: the variation in contact resistance due to perspiration, skin creams etc. and their susceptibility to movement artefacts. For these reasons they tend to produce noisier signal measurements than wet electrodes. In the absence of a specific electrolyte to transduce ionic currents, the dry resistive sensors rely on the presence of moisture on the skin such as sweat; thus a half cell potential is developed in the same way as for wet gel electrodes[28].

In recording the EEG, dry electrodes have the added problem of the presence of hair that stops them from forming a reliable contact with the skin surface. A number of interfaces have been used by researchers such as stainless steel[22]. However in order to circumvent

the problems of hair and dead skin layer researchers have used different conductive materials. Other passive electrode designs have been used to lower the skin electrode impedance. These designs include conductive rubber [32], metal-coated polymer bristles [33], comb-like structures that would penetrate the epidermis layer [34], and conductive fabric [35]. A novel hydrogel-based electrode was introduced by [36] where polyacrylate swells up when immersed in electrolyte over 12 hours. The sample is cut to an electrode size of 10 mm in diameter and 3 mm thickness, and a AgCl coated cable is inserted. A low impedance contact was reported compared to commercial gel electrodes when applied on unprepared forearm skin and scalp hair, furthermore this low impedance was maintained for 8 hours. In most instances of dry and insulated electrodes an active electrode structure is used with high impedance amplification [37][38], as this minimizes the noise due to cabling and the transmission of the signal.

A recent approach by Baek, et al., (2012) has used conductive polymer foam in front of an insulated electrode to produce a more reliable contact with the surface of the head. This shows successful recording of alpha signals. The constructed electrode has a diameter of 38 mm [39]. This can limit the number of electrodes that can populate the head, compared to the conventional electrode size of 5 to 10 mm. No information on the reference signal was provided in this case.

2.4.3 Insulated Electrode

An alternative approach to recording electrical activity from the brain is to dispense with the conventional resistive contact approach and instead couple capacitively through an insulating layer. With this method the signal fidelity no longer relies on skin resistance, reducing the variation in signal. However, these electrodes are also susceptible to movement artefacts and charge sensitivity.

Taheri, et al., (1994) has shown a version where they record EEG through hair. A stainless steel electrode was coated with 200 nm thick silicon nitride, connected to a buffer amplifier. Power was provided using a battery which was mounted on the sensor. The reference signal was provided by an Ag/AgCl electrode. Excessive motion artefact was reported due to the bulkiness of the design [40].

Harland, et al, (2002) reported recording of Alpha and Beta waves with an air gap of 3 mm between the sensor plate and scalp hair. They used a pair of electric potential sensors (EPS) positioned to measure a differential recording of P3-O1. Alpha blocking phenomenon was successfully demonstrated [41]. It should be noted however that the recording was performed within a screened room.

The capacitive electrode sensors reported have generally used a high resistance at the input pin of the amplifier to provide a input bias current for their sensor[26]. Although amplifiers with extremely low input bias current of 3 fA exist, such as 1NA116 instrumentation amplifier, if this small current is not provided the high-impedance positive input pin of these amplifiers will be forced toward the supply rails[42]. Due to this high input impedance, insulated electrodes are prone to interference from power lines[43]. A technique known as active electrode is used to reduce this effect, where the front end electronics are placed within the electrode structure[38]. Sullivan, et al., (2007) have taken a different approach by using a reset circuit consisting of two transistors connected to the positive input pin of an 1NA116 instrumentation amplifier. They report a bandpass characteristic of 1 to 100 Hz. Their published frequency response however shows a non flat gain between 1 and 100 Hz with a variation of approximately 20 dB[42]. This leads to the integration of the signal for the lower frequencies, specifically in the 1 to 10 Hz region. They have demonstrated recording of alpha waves, where one sensor was positioned on the back of the head and one behind the ear to provide a reference.

By using an insulated electrode the DC response of a sensors is compromised[28]. This along with a high value resistor creates a high pass filter in front of the signal source. Depending on the values of R and C this will impose a settling time on the sensor, varying the time it takes for the sensor to settle to its baseline value in case of railing[38]. A secondary settling issue exists that relates to all electrode type. Once an electrode is positioned on the skin surface the impedance of the skin layer changes as perspiration occurs. This effect is studied by Searle, (2000) in an experiment where the above three electrode types are placed on the forearm with a solenoid placed on top of them to provide a reproducible motion. RMS output voltage for all the electrodes were measures for 15 minutes. The results showed a lower RMS value fo Wet electrode compared to the others at the beginning. However, after 15 minutes bot dry and insulating electrodes show similar or lower lower values to Wet electrode[27].

Chi, et al., have introduced a number of capacitive electrode-active sensor designs based on op-amps [28] and more recently a custom IC sensor by VLSI design [44]. In [28] a recording of Alpha signals was reported, however it was mentioned that the sensor was connected to the head using a very tight headband. In their recent paper [44] a comparison was made between their custom IC designed capacitive sensor and a wet gel electrode using a steady state visual evoked potential (SSVEP) study. The signals were recorded through hair but the recording positions were not mentioned. Cross correlation was used to compare the signals from the capacitive and wet gel electrode and this resulted in a value of higher than 0.8 for half the subjects tested. Two points should be noted about this comparison. Firstly, the cross correlation was only measured with the signals band passed between 8 and 13 Hz. Secondly, in the preparation for the wet electrodes it is mentioned that no conditioning such as skin abrasion was performed. This could have affected the results obtained from the wet gel electrodes as they rely on a low impedance contact of less

than $5\text{ k}\Omega$ as standard practice in collecting EEG[7]. Perhaps if the band width was not drastically limited and the wet gel electrode was prepared as standard practice suggests a much lower cross correlation value would have been achieved.

A number of capacitive sensors have been introduced for EEG. However, many have shown limited scope in comparing their sensors to wet gel electrodes in terms of various signals that need to be recorded by an EEG sensor, such as ERP studies limiting the signal collection to alpha recording only.

2.4.4 Quasi-Dry Electrode

More recent advances have focused on an approach where the sensor is based between the concept of wet and dry. The first aim is to eliminate the draw backs of a dry electrode, such as electrode movement artefacts and non-secure contact, but have the added benefit of quick preparation. Gel electrodes provide reliable measurement but the preparation procedure and application of gel takes a considerable amount of time. Moreover, the use of gel is damaging to hair and can be irritating to the skin [27].

Quasi-dry electrodes are designed to work based on a localized skin hydration effect provided by a very small amount (micro litres) of moisturising agent. Mota, et al. (2013) have developed a polymer based electrode made from polyurethane that releases $30\ \mu\text{l}$ of gel when pressed on to a surface from an inbuilt reservoir[1]. The electrode is first coated with silver and later a layer of AgCl is applied through anodization. An additional advantage of this method is removing the effect of bridging between the sensors in a high density recording because of the small amount of gel applied.

Furthermore, in the case of capacitive sensors, hair when in contact with the electrode exchanges static charge with the sensor this causes alteration of the DC level on the input

of the sensor, and acts as an external source of noise. In addition, the hair creates an uneven surface for the electrode to couple to the head. To counter the problem of static charge build-up on the hair, a small quantity of less than 100 μl water based gel is applied to surface of the electrode to remove the static charge and stabilise the sensor output. The use of a small quantity of gel takes away some advantages of a dry electrode, but it helps with two major issues. Firstly, it forms an even surface for the half capacitor plate of the sensor to couple with the scalp surface. That surface acts as the second capacitor plate for the sensor. Secondly unlike the conventional electrodes, where the metal electrolyte interface causes an offset voltage, no half-cell potential is developed between the gel and the oxide layer. This is the case for the Electric Potential Sensor (described below) as the electrolyte does not come into contact with the electrode, eliminating this source of noise.

2.5 Electric Potential Sensor

The Electric Potential Sensor (EPS) is a generic electric field measurement technology with many applications including biopotential recording. The EPS has already demonstrated that the difficulties faced by conventional electrodes, such as use of gel and noise levels, can be addressed for Electrocardiogram (ECG) data acquisition[45], where the inherent DC stability and short settling time of the sensors is advantageous compared to other insulated electrode implementations. This approach also dispenses with the distortion of the signal cause by standard electrodes as the EPS does not require a real charge current to flow through it in order to make a measurement[26]. Figure 2.4 shows a generic design for the EPS[4]. The ECG is often recorded with a bandwidth of 0.5 to 40 Hz in monitoring mode and 0.05 to 150 Hz for diagnostic mode[46]. However, the low frequency noise performance required for accurate EEG data acquisition (amplitude of 0.1 to 100 μV) is considerably

more demanding than for ECG; which has a amplitude of around 1-2 mV collected from electrodes placed on chest[47].

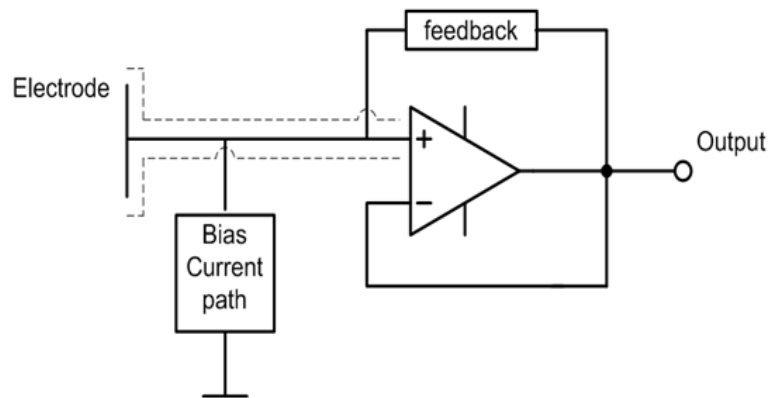


FIGURE 2.4: Generic EPS sensor design.

2.5.1 EPS Design for EEG Recording

The EPS can operate in contact and remote modes. The remote mode of operation records the signal with an air gap between the electrode and signal source. This mode forms a coupling capacitance of typically 0.4 pF. The contact mode is demonstrated in Figure 2.5 where an insulation layer is formed in front of the electrode which is in direct contact with the signal source. Here the coupling capacitance may be as high as 1nF[26].

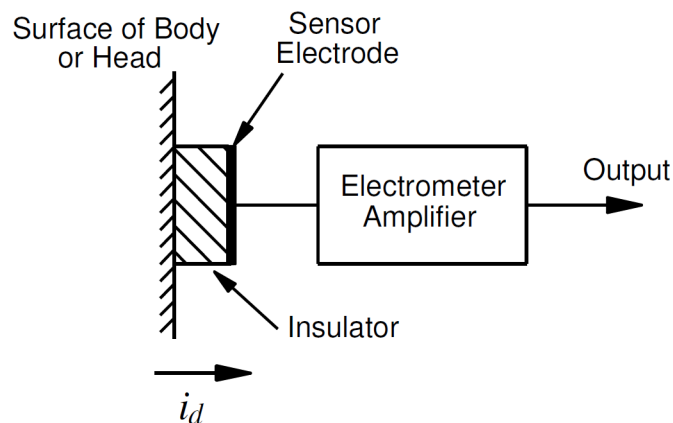


FIGURE 2.5: EPS strongly coupled to signal source in contact

A review of sensor developments for healthcare[26] discusses the low frequency noise performance of a number of active sensors and characterizes them in terms of the noise spectral density at 1 Hz. This is a useful indicator of the performance for EEG use and gives values ranging from $2\ \mu\text{V}/\sqrt{\text{Hz}}$ to $10\ \mu\text{V}/\sqrt{\text{Hz}}$; however these values will increase at lower frequencies due to $1/f$ noise.

The contact mode of operation for EPS provides a high coupling capacitance between the sensor and the source. Provided this value is in the region of hundreds of pF, the output noise of an amplifier will be dominated by its voltage noise[38]. Thus the low frequency noise performance was identified as the key indicator in determining the signal to noise ratio of the sensor when used to acquire EEG signals. For this reason the prototype Sussex EPS device for this project is based on an auto-zero operational amplifier, chosen to give the lowest possible low frequency noise. The absence of $1/f$ noise in these devices makes them ideal for use with signal frequencies of 10 Hz or less. This operational amplifier (OpAmp) has an input capacitance of 8 pF.

One of the goals of the design for this sensor is for it to be integrated into a portable system (demonstrated in chapter 6). Therefore, it is important that the supply voltage is low enough for the sensors to be battery powered, with low power consumption. The AD8629 has a supply range of 2.7-5 V which can be configured as single or dual mode, with a typical supply current of 1 mA. Furthermore, the input and output can swing fully from rail to rail. The output of the sensor was set to be fed into an analogue to digital converter (A/D). This required the amplitude of the output signal to be high enough to be detectable by the A/D. A voltage gain of 50 (the exact value is 49.49) was implemented for each sensor as it would provide a typical output voltage of 0.5 mV (the amplitude range of EEG as mentioned before is 0.1 to 100 μV). If a further gain stage is necessary it can be provided in later stages by an amplifier, this is discussed in more detail in the next

chapter. This gain was distributed into two stages of x5 (x4.9) and x10 (x10.1) in order to avoid railing the sensors if a high DC offset is present at the input of the sensor. The sensor bandwidth was limited to 0.1 Hz to 78 Hz in order to cover the range of frequencies required for recording EEG signals.

2.5.2 Noise

The gain and operational bandwidth of the sensors was confirmed using a standard spectrum analyser. The most significant parameter for the specification of the sensor in this particular application is the voltage noise referred to the input. This was measured by placing the sensor in a screened environment and recording the spectral noise density over a 1 kHz bandwidth using a HP3562A[48] spectrum analyser. The input to the capacitive electrode was shorted to ground, and the noise output noise referred to the input with a gain of x49.49.

The results obtained from these measurements are: $30 \text{ nV}/\sqrt{\text{Hz}}$ at 1 Hz and $0.5 \mu\text{V}_{\text{p-p}}$ from 0.1 to 10 Hz. The noise plot for the EPS is given in Figure 2.6. The absence of 1/f noise in this data confirms that the auto-zero amplifier used in the sensor is performing as expected.

By limiting the input bandwidth of the sensor it is possible to reduce the noise present at frequencies outside of the region of interest[2]. The amplifier used in this design eliminates the 1/f noise by combining auto-zeroing and chopping techniques. The chopping frequency is set at 15 kHz[49]. Limiting the bandwidth of the sensor would reduce this out of band noise source by 20 dB. The filtering at lower frequencies would further help with elimination of baseline variation at the output of the sensor. This effect is compared in Figure 2.7 for a signal recorded by a Ag/AgCl electrode 2.7(a) and the EPS 2.7(b). The recording

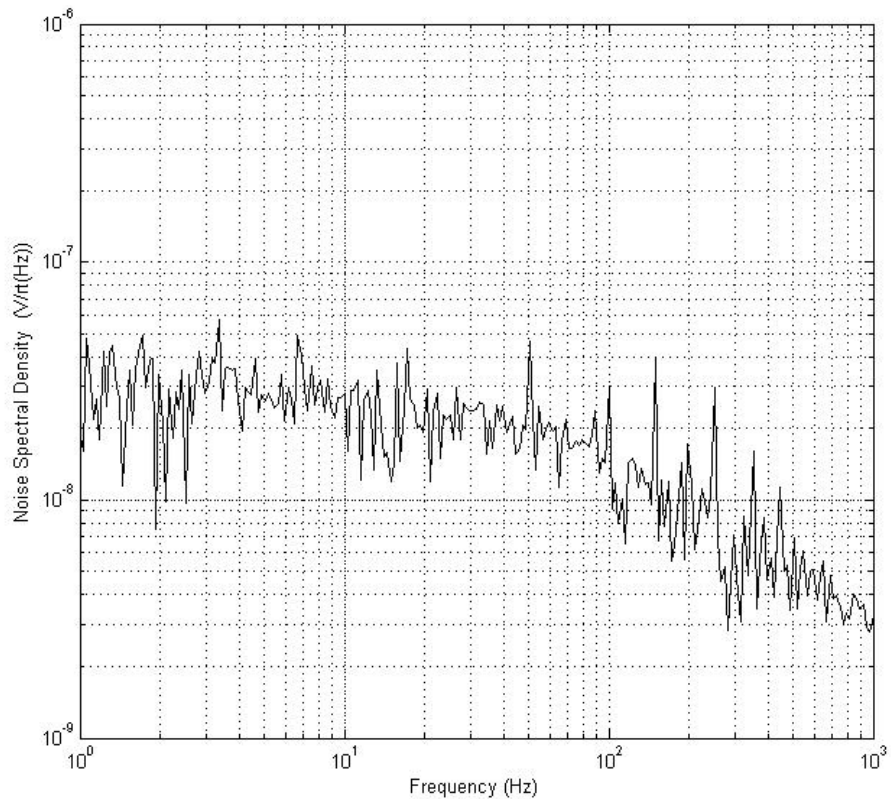
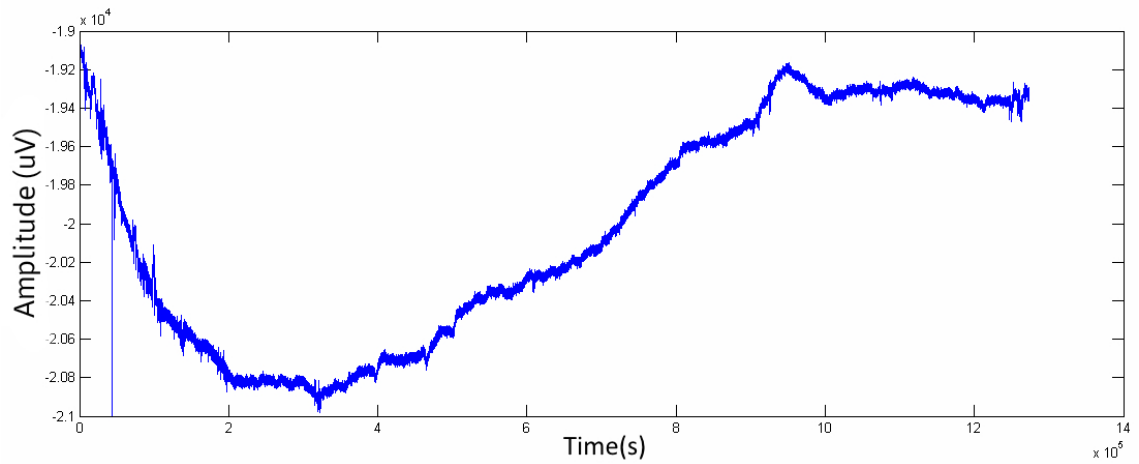


FIGURE 2.6: Noise spectral density plot for prototype EPS with auto-zero amplifier eliminating the $1/f$ noise of a typical input stage of the acquisition system.

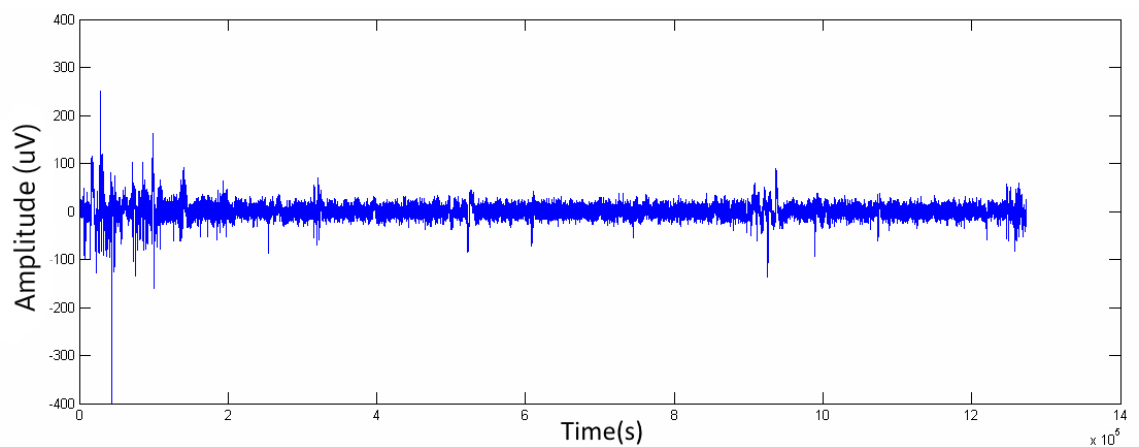
represents a differential measurement of two sensors, for each the EPS and the Ag/AgCl electrode, place on the scalp. The variation in figure (a) is contributed to by a number of effects, including the noise added by the half cell nature of the Ag/AgCl electrode.

2.5.2.1 Noise Coupling Through USB Cable

As mentioned before the noise of the sensor was measured using a spectrum analyser. This device was initially connected to a Laptop via a USB cable to export the data from the spectrum analyser. During noise measurements it was noticed that connecting the spectrum analyser to a computer using a USB cable would introduce extra noise to the system. Figure 2.8(b) is the noise plot of the sensor and figure 2.8(a) shows the effect of having the measurement device connected to a laptop by USB connection. As the noise



(a) AgCl Drift



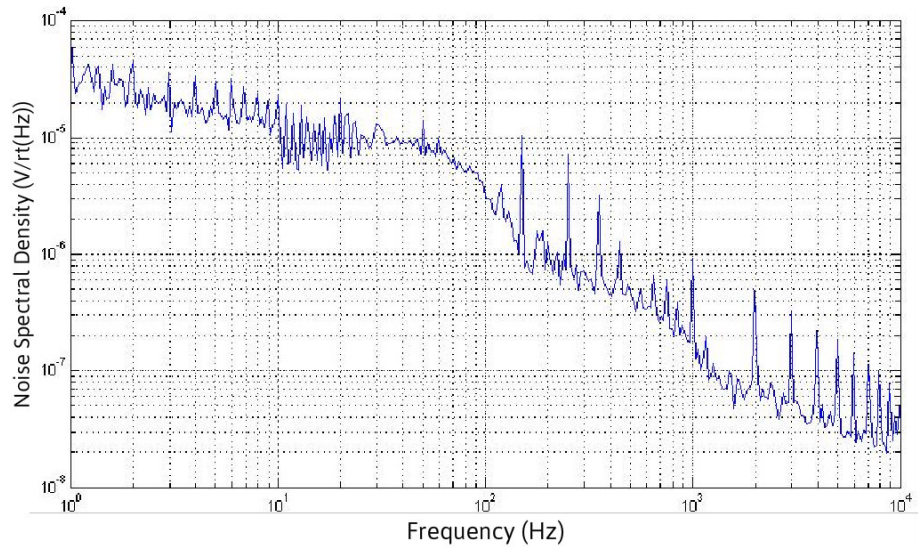
(b) EPS Drift

FIGURE 2.7: Drifts in a simultaneous recording of (a) a Ag/AgCl and (b) the EPS

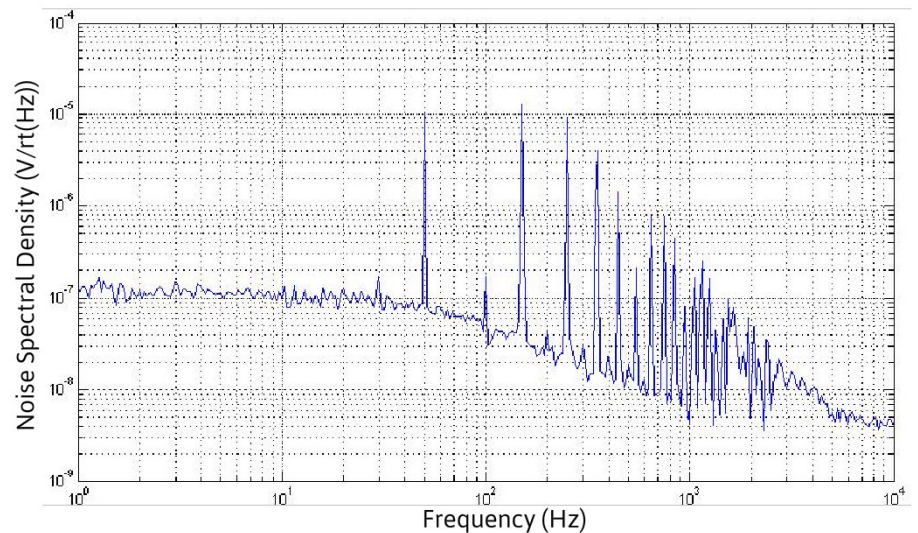
originates from the laptop's power supply, it was possible to eliminate this source of noise by disconnecting the USB cable while the measurement was in progress.

2.5.2.2 EEG Artefacts

Apart from intrinsic noise sources of electronic equipment, the human body generates other electrical signals that can be recognized as the noise in the case of an EEG recording. These signals arise from following activities or sources: Electromyogram (EMG) caused by facial muscles and activities such as teeth clenching. Electrocardiogram (ECG) which can be picked up on the neck and head. Furthermore, movement of the person, which leads



(a) Noise with a USB connection in measurement system



(b) Noise in absence of USB

FIGURE 2.8: Effect of noise generated from a USB connection in noise measurement system, part (b) shows same measurement as in part (a) in absence of USB connection showing the high noise content increase in low frequencies.

to cable movement and potential displacement of the electrode on the head, can lead to high voltage drifts on the output of the sensor[13]. This will be explored in more detail in later chapters. Searle et al., (2000) found that both Dry and Insulating electrodes are more susceptible to movement artefacts than capacitive sensors. However, after the sensors were allowed to settle for approximately 15 minutes, they showed lower levels of movement artefacts compared to standard wet electrodes [27]. These artefact will be explored in more detail in later chapters.

2.5.2.3 Shielded Room

Shielded enclosures are often used to reduce the presence of noise in experiments that require low levels of external noise[50]. Many experiments in psychology are performed in a screened room to reduce the effect of mains on the recorded signals[14]. The total noise reduction by a screened room is made up of absorption loss (A) and reflection loss (R). Equation 2.1 provides a simple method to calculate Shielding Effectiveness (S) of a screened room against electric field.

$$S = A + R \quad (2.1)$$

These values depend on the electrical and magnetic properties of the material used for building the screened room and also the thickness of that material. The absorption loss is defined by equation 2.2 and the reflection loss can be calculated using equation 2.3.

$$A = 3.344t\sqrt{f\mu_r\sigma_r} \quad (2.2)$$

$$R = 322 + 10\log\left(\frac{\sigma_r}{\mu_r f^3 (0.0254r)^2}\right) \quad (2.3)$$

Where (t) is the thickness of the shielding material and (r) is the distance of the source from shield, both in meters[50]. The symbol f is the frequency of interest. The relative conductivity is denoted by σ_r , and the relative permeability is μ_r .

If these values are calculate for a shielded room that is built from steel ($\sigma_r = 0.1$, $\mu_r = 1000$) with thickness of 2 mm then at 0.1 Hz the total shield effectiveness is 300 dB and at 100 Hz it is 222 dB. These numbers are typical of a screened room commonly used for psychology experiments. The data recorded in this work is focused at recording EEG

outside of a screened room. However, some of the experiments were conducted inside a screen room, to facilitate simultaneous measurement with conventional electrodes. These experiments are mentioned in later chapters.

2.5.3 EPS Configuration

The relation between voltage and capacitance based on the amount of charge on the capacitor in simple form is given by equation 2.4.

$$V = Q/C \tag{2.4}$$

This indicates the sensitivity of a capacitive sensor to static charge as a small amount of charge can produce a high voltage on the input of the sensor if the coupling capacitance is low. When the sensors are placed on hair, addition of hair and an uneven skin surface results in an inhomogeneous dielectric layer which is not only defined by the oxide layer of the electrode, but also by the gaps cause by hair strands between the sensor and skin surface, reducing the coupling capacitance and increasing the noise. Furthermore, simply increasing the size of electrode increases the capacitance according to equation 2.5. A higher coupling capacitance in turn reduces voltage noise[38].

$$C = \frac{\epsilon A}{d} \tag{2.5}$$

The EPS electrodes are electrically insulated (anodized). The sensors were housed in inert stainless steel machined housings with the electronics fabricated in surface mount on a PCB compatible with epoxy potting compounds. Potted sensors are designed to be immersed in alcohol for sterilisation purposes. To decide on the contact size and ground configuration

of the electrode a study was designed to accommodate five different combinations. Eight participants were tested, where for each participant the alpha signal was recorded (The process of recording alpha signal itself will be discussed in more detail in next chapter). Table 2.2 demonstrates all five combinations and whether detection of alpha signal was possible based on that configuration.

Two different electrode sizes were used in this study, 12 mm and 18 mm diameter, to enable reliable contact to be made to different parts of the scalp and mastoids. Figure 2.9 shows the EP sensor with two different electrode sizes of 12 and 18 mm. The sensors are powered through a shielded four wire cable that carries the output signal and the ground connection. The shield is connected to the case covering the electronics attached to the electrode. The shield and the ground are connected to each other in a star configuration once the sensor is connected to an amplifier (the amplifier configuration will be explored more in later chapters). The shield is used to prevent the noise from entering sensitive parts of a circuit. If the shield and the ground are connected in more than one point in the over all system it results in a ground loop which further add to the noise picked up by the sensor[51]. Each sensor was tested with and without a Kapton[52] tape covering the case shielding the sensor. This has the effect of removing the ground connection on the head from the locality of the electrode. The Kapton was used due to its thinness, as it would not act as spacer between the electrode and head. A tick represents the condition where it was possible to record alpha blocking from a person and a cross when it was not possible. This enables a decision to be made on how to connect the sensors to the head where the skin is covered with hair.

As can be seen from the table 2.2 the two sensor configurations where the casing was covered with Kapton, proved to be functioning for the majority of the participants. Therefore, this modification was made for all the tests performed in the work presented here. The

TABLE 2.2: Size and ground connection effects on recording alpha signal

Participant	Electrode Configuration				
	12mm	12mm+Kapton	18mm	18mm+Spacer Ring	18mm+Kapton
One	X	✓	X	X	✓
Two	X	X	X	X	X
Three	✓	✓	✓	✓	✓
Four	X	✓	✓	✓	✓
Five	X	✓	X	X	✓
Six	X	✓	X	X	✓
Seven	✓	✓	✓	✓	✓
Eight	X	✓	X	X	✓



FIGURE 2.9: Two electrode sizes of 12mm and 18mm was examined with various ground configurations.

results from sensor configuration showed less success for participants with higher hair density. Therefore, variations between the signals recorded from individual participants could be further investigated by categorising participants based on their hair density.

2.5.3.1 Present Design

To achieve the low noise performance demands of an EEG sensor and for it to be implemented into a portable system, as described in the previous sections, the following factors were implemented in the design of this EPS:

- Based on AD8629, Auto-zero OpAmp with C_{in} of 8 pF
- 0.1 Hz to 78 Hz sensor bandwidth

- Sensor voltage gain of x49.49, in two stages of x4.9 and x10.1
- Bias Resistor of 1 G Ω
- Insulated anodized electrode sizes of 12 mm and 18 mm diameter
- Supply rails of ± 2.5 V

2.5.3.2 Different EPS Designs

Apart from variations in electrode size, different sensor designs were tested in order to find the best combination. The input impedance of an amplifier could reduce as a result of the stray capacitance between the amplifier input pin and the surrounding circuit[38]. Careful attention to the design of guarding and shielding can assist in avoiding stray capacitance in the circuitry. If guarding is applied the input node is enclosed by a driven guard which is connected to a low impedance output node in the circuit thus bringing both nodes up to an equal potential[38]. Eliminating this stray capacitance is also possible by removing the excess copper from the input PCB plate connected to the insulated electrode. Both methods were implemented, by measuring the input capacitance (C_{in}) of the amplifier it was found that for this design both methods succeeded in reducing the stray capacitance. The input capacitance was calculated by feeding a known signal to the amplifier through a known capacitor forming a capacitive divider with the C_{in} of the amplifier. The output voltage is related to the input capacitance through this capacitive divider configuration. The present design maintains the idea of a DC bias path but has not included guarding. It was important to find whether inclusion of other techniques such as guarding would overcome the problem of static charge, when the sensor is in contact with hair. The result of testing these different EPS versions was that all the sensors did require use of a method

to remove the static charge from the hair, by means of applying a small amount of water based gel.

2.6 Discussion

For optimal EEG signal acquisition, evidence suggests that smaller, lighter sensors with a higher array density are required in order to reduce movement artefacts and to allow for measurement redundancy [40]. A comprehensive review of wet, dry and insulating electrode technologies concluded that insulated active electrodes offer the most promising solution to reduce these issues for future clinical applications [27]. A standardised comparison of concurrent measurements with wet and dry EEG electrodes concludes that there is a high degree of correlation between the two and that dry electrodes offer better long term performance [32]. A new approach has been the use of quasi-dry electrodes for recording EEG. This provides a local hydration, for the sensor, that both eliminates the static charge build up under the sensor and forms a homogeneous layer between the electrode and skin surface in the presence of hair.

The low noise performance of an EEG sensor is the key indicator in determining the signal to noise ratio. Operational amplifiers have an intrinsic $1/f$ noise that increases at lower frequencies, leading to higher noise in the 0.1 to 10Hz region. By using an auto-zero amplifier it was possible to remove the $1/f$ noise effect. Different EPS configurations were studied for connection of the EPS to the head, based on the outcome it was decided to cover the case with an insulation layer (provided by Kapton[52] tape) when the sensor is in contact with areas of the head where hair covers the skin.

The EPS prototype has many advantages over conventional EEG sensors, including setup time, elimination of sensor cross-coupling, lack of a ground electrode and the distortion of electrical potentials encountered when using standard gel electrodes.

Chapter 3

Spontaneous EEG

3.1 Introduction

This chapter focuses on discussing alpha rhythm and in particular alpha blocking phenomenon. This covers experiments conducted on the recording of spontaneous EEG using EPS. In these experiments, the sensors are interfaced with a commercial EEG data acquisition system for compatibility with a direct comparison of recorded signals with conventional Ag/AgCl electrodes. The spontaneous, or free running EEG, is shown by recording alpha signals. Furthermore, information is provided on the interfacing of the EPS to external amplifiers for further processing and signal acquisition.

3.2 Alpha Rhythm

Table 2.1 in chapter 2 showed the different activities that can be present in the normal EEG of a healthy adult, in combination or alone. The most common of these activities is the alpha rhythm which presents unique attributes in terms of frequency, distribution and responsiveness.

The exact frequency of alpha rhythm varies in different subjects but it ranges from 8 to 13 Hz. In a given subject this frequency is fairly constant and changes merely by 1 Hz in case of drowsiness. A higher variation is abnormal. The frequency of alpha rhythm should be constant in both hemispheres, although the phase relation can be different. The highest amplitude for alpha is recorded over the parietal and occipital lobes. Presence of alpha signals, with same amplitude as on parietal lobe, in recordings from frontal regions can be a sign of an abnormality. The Alpha rhythm does not have a constant amplitude and often varies from one hemisphere to another during a recording session. This signal has its maximum amplitude in childhood and its value depreciates with age [53].

The alpha signal is found in 95% of healthy adults [6], yet its significance and origin are unknown. This signal presents itself as a rise in the activity of the alpha band of EEG caused by various reactivity cues. It can also be tested by the reduction observed in its amplitude caused by certain manoeuvres. The observed effect is thought of as an accumulation of responses from different events triggered by a lack of specific input to the visual system. Blocking of this signal by eye opening, mental concentration, and attention to a presented stimulus is possible [53].

3.2.1 Alpha Blocking

A number of events can cause this reduction, even complete blocking, of the alpha wave. Figure 3.1 demonstrates the alpha blocking phenomenon due to eyes opening. As shown in part (a) sensors are positioned close to the occipital region to record alpha signals with the maximum amplitude. The effects of closing and opening the eyes is demonstrated in part (b). With opening of eyes the higher amplitude signal is blocked. These changes in the alpha waves varies from person to person and alters based on time in an individual.

However, a constant lack of reduction in the amplitude of the alpha rhythm signals an abnormality in the brain [53].

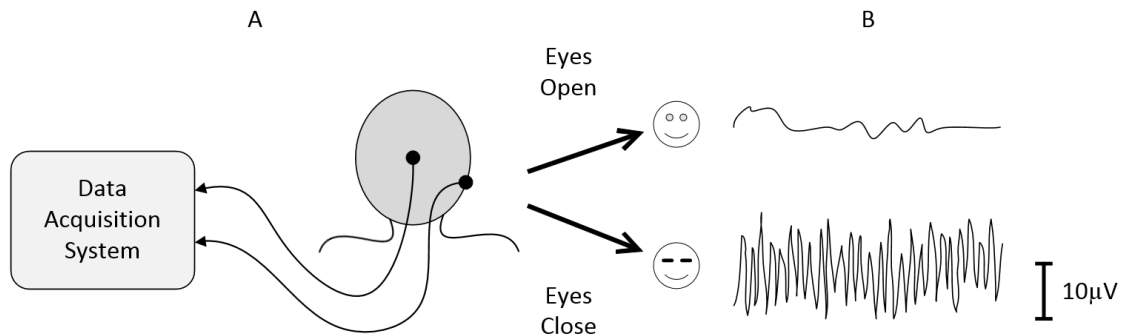


FIGURE 3.1: Alpha blocking phenomenon can be observed by noting the differences in shape of the EEG signal recorded, most notably with sensors positioned on the occipital region and a mastoid. Part (a) indicates the sensor locations for the maximal signal on back of the head, and part (b) shows the differences on the EEG signals observed with eyes open and closed. A rise in amplitude of the region between 8 to 13 Hz of EEG signal is an indication of alpha activity.

3.3 Alpha Detection using EPS

This effect of alpha blocking is observable both in the frequency and the time domains. It is also a signal that can be controlled voluntarily by an individual. The fact that the overall activity of this frequency band can easily be controlled by closing or opening the eyes provides a valuable tool for testing an EEG sensor. This signal is present in most humans and its amplitude always rises with closing the eyes. Therefore if this signal is not observed by an EEG system the conclusion could be drawn that the overall noise of the system is not low enough to show these changes in the amplitude of the alpha band. The first experiment was designed so that it could answer this question of noise regarding EPS.

3.3.1 Methodology

For this measurement a total of two sensors were used. A sensor was positioned on a mastoid to form a reference signal and the second sensor was positioned at Oz, shown in figure 2.1, to record the alpha signal. There is not a single position on the head that would not show an EEG signal, thus a point can be chosen as a point providing a reference signal. This point can be at a region on the head that has less brain activity associated with it such as the tip of the nose or the mastoids [53]. For this experiment the right mastoid was chosen as opposed to the tip of the nose as it would provide a more stable connection between the sensor and the head. Furthermore the Oz position is the central location for occipital lobe on the scalp, which produces the highest amplitude for the alpha band compare to the other regions of the brain [53]. The two sensors were connected to an external differential amplifier, for post processing of the signals, and to a power supply. The sensors are connected with a shielded four wire cable to the amplifier. A seven pin connector was used with pin outs shown in figure 3.2. The cable carries positive and negative supply lines of ± 15 volts, ground connection wire, output and shield. The active parts of the sensor used a supply of ± 2.5 V, and they are provided by using Zener diode regulator at the power inputs of each sensor. The higher supply rails allow for extra gain to be implemented after the gain stage of the sensor. Unlike conventional EEG systems, a dedicated ground electrode, which is usually positioned between Fz and Fpz, is not used in a recording with EPS. This allows for floating measurement of EEG with a battery powered device. A block diagram of the sensor is shown in figure 3.3.

The amplifier rack shown in figure 3.4 provides battery power for four sensors. The buffered output of each individual sensor and the differential signal from pair of sensors are all accessible as outputs from the rack. The input from the sensors can be buffered with DC or AC coupling of 0.5 Hz.

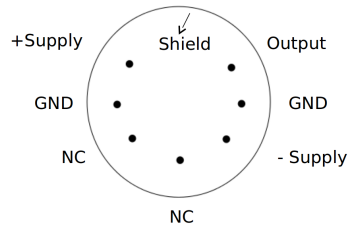


FIGURE 3.2: Din plug connector used for EPS.

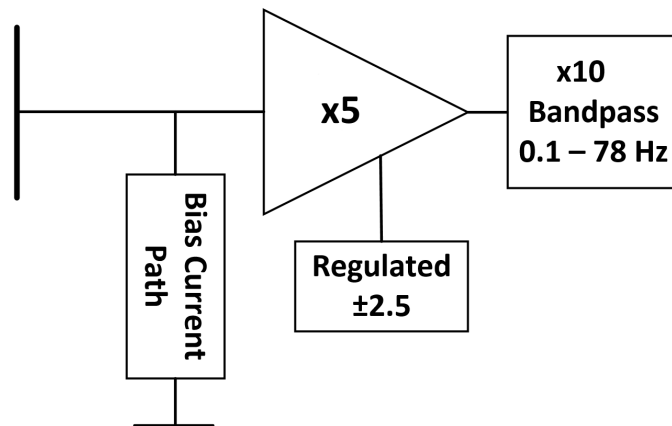
FIGURE 3.3: The EPS block diagram. The vertical line represents the input electrode. The voltage regulation is provided by Zener diode regulator providing ± 2.5 V.

FIGURE 3.4: Amplifier and power box for EPS, providing power to the active sensors and a buffered output for each sensor. Further signal conditioning such as adjustable gain of x1 to x100, notch filter for 50 Hz signal, and high-pass filter is implemented.

The rack used allows for adding extra modules if needed such as a notch filter at 50 Hz or extra filtering and signal processing. Finally the output of the box was connected to an oscilloscope for displaying and recording of the signal. Two different electrode sizes of 12 and 18 mm diameter were used to enable reliable contact to be made to different parts of the body. The sensor with the smaller electrode size of 12 mm was positioned on the right mastoid and the 18 mm electrode was placed on Oz. It is shown that in animals, unless the recording is done with an invasive electrode, the size of the scalp electrode does not make a difference in the resolution of the recorded signal [6].

It is important to be able to make and repeat a measurement with all or the majority of its variables constant, thus if a condition has changed in a given experiment the effects can be analysed and compared to previous conditions. In EEG recording it is important to record the signal from a specific region of the brain. The 10-20 system provides a tool to find the desired location but as the body or head moves the sensors change position. Therefore, sensors need to be fixed to these locations during a recording session. A boxing cap was used initially to cover the head. This head gear shown in figure 3.5 provided a stable structure behind both ears for placing the reference electrode on the mastoid.

Usually alpha signal is at its highest amplitude over the occipital region (Oz position). However, it is possible to record the alpha signal from the front area of the head, such as at AF7 (which is positioned on the forehead), as well as the occipital region albeit with a smaller signal in terms of amplitude of the recorded alpha band being observed from that site. Using the AF7 site means that the sensor is in contact with the skin, thus providing strong coupling with the electrode. On the other hand, placing the sensor on Oz means having the addition of a layer of hair between the scalp surface and the electrode. Hair, when in contact with the electrode exchanges static charge with the sensor, which cause changes in the DC level on the input of the sensor. These changes act as an external



FIGURE 3.5: A boxing cap used for holding the sensors on the head, point (a) shows the location for the reference sensor which sits on the mastoid and point (b) is the location for the signal sensor which is on Oz

source of noise. Also, the hair creates an uneven surface for the electrode to couple to the head. To counter the problem of static charge build-up on the hair, a small quantity of water based gel is applied to surface of the electrode that removes the static charge and stabilises the sensor output.

Figure 3.6 shows the interfacing of hair with the EPS electrodes. The use of a small quantity of gel takes away some advantages of a dry electrode, but it helps with two major issues. Firstly, it forms an even surface for the half capacitor plate of the sensor to couple with the scalp surface. Figure 3.6b shows a condition where hair is placed between the skin and the electrode. That skin surface acts as the second capacitor plate for the sensor. However, the addition of hair and an uneven surface results in an inhomogeneous dielectric layer which is not only defined by the oxide layer of the electrode, but also by the gaps cause by the hair strands between the sensor and the skin surface. The use of gel restores a homogeneous spacer layer. Secondly, unlike the case of conventional electrodes where the metal electrolyte interface causes an offset voltage, no half-cell potential is developed

between the paste and the oxide layer of the EPS electrode, as the electrolyte does not come in to contact with the electrode, eliminating this source of noise. Thus the EPS does not suffer from this source of noise.

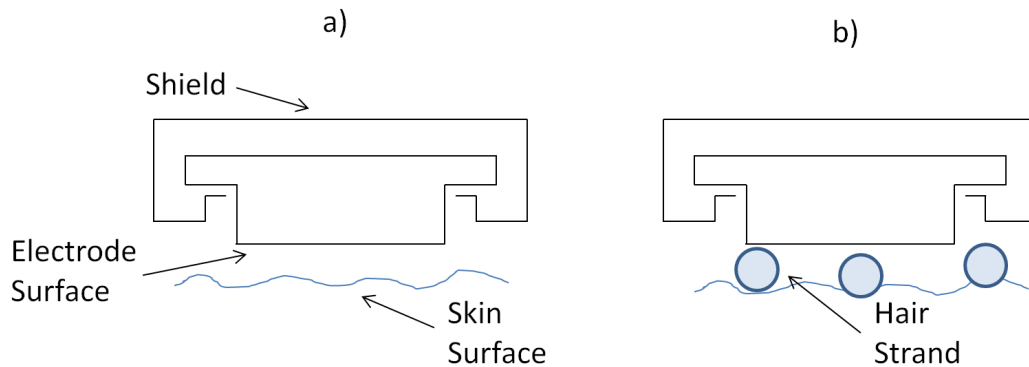


FIGURE 3.6: Interface of EPS electrode with the scalp surface. Part (a) is the case when the sensor is in direct contact with the skin. In part (b) a cross section of this connection is shown with addition of hair strands in between the two surfaces. Skin forms the second plate for the EPS's capacitive input. With inclusion of hair the capacitor formed by the two plates is defined by the air gaps between hair strands. In addition to forming an inhomogeneous layer, contact of hair with the sensor causes exchange of electrostatic charge which translates to voltage drifts at the input of amplifier.

If the sensors do not form a stable connection with the head, a strong coupling between the electrode and the surface of the scalp would not form. This would result in the output signal of the sensors to be unmatched, therefore reducing the effects of common mode rejection in a differential pair. Thus, in a bipolar recording if one of the sensors is not matched with the other, common mode rejection would not reduce the 50 Hz main signal or other common mode signals such as movement artefacts. This results in having a higher level of noise in the output signal which could mask the desired scalp potentials. If matched it will be rejected by the subtraction of two channels, otherwise it will be observed after the differential stage adding to the overall noise of the signal.

Length of an EEG recording depends on the type of experiment designed. A typical psychology study is performed over a few hours or spread into multi-hour sessions between days. Therefore, it is necessary to have a mechanism that would indicate to a user whether they have a connection that would produce results with the least amount of noise, such

connection will be considered a good connection. Two tests were performed to evaluate the quality of the signal from the EPS. The first one is to inspect the output of each individual channel on an oscilloscope and measure the amplitude of mains signal (50 Hz in England). If correctly matched, amplitude of the mains signal present at the output of all sensors should be same.

The second test is to visually inspect the output of the differential channel for signs of muscle signal in EEG. These signals can be easily picked up in the EEG as they have higher amplitude levels. Typically these signals are produced by clenching teeth or eye blink. A volunteer can be asked to clench their teeth and that should result in a high frequency and high amplitude signal being superimposed on the EEG. If the sensors are not matched then this high amplitude and frequency signal would not be detectable. Figure 3.7 demonstrates a range of signals that can be picked up by an EEG sensor from the scalp. Alpha signals can be seen in section (a), and section (b) shows the signal generated by rapid eye blink, noting that it has a higher amplitude than an alpha signal. The signal seen in section (c) shows a much higher frequency and amplitude signal compared to the other sections, it is the result of muscle signal being picked up in EEG signals (in the form of clenching teeth). Finally, section (d) shows the lowest level of activity and represents the free running EEG signal with eyes open. These effects should reduce as the volunteer relaxes their facial muscles. This change in the level of signal indicates a lower baseline noise that allows for the EMG to be observed.

3.3.2 Signal Processing

The exact frequency of an alpha signal is different for each individual. Thus a general rise in the energy of the alpha band is observed with the band being from 8 to 13 Hz [14]. In

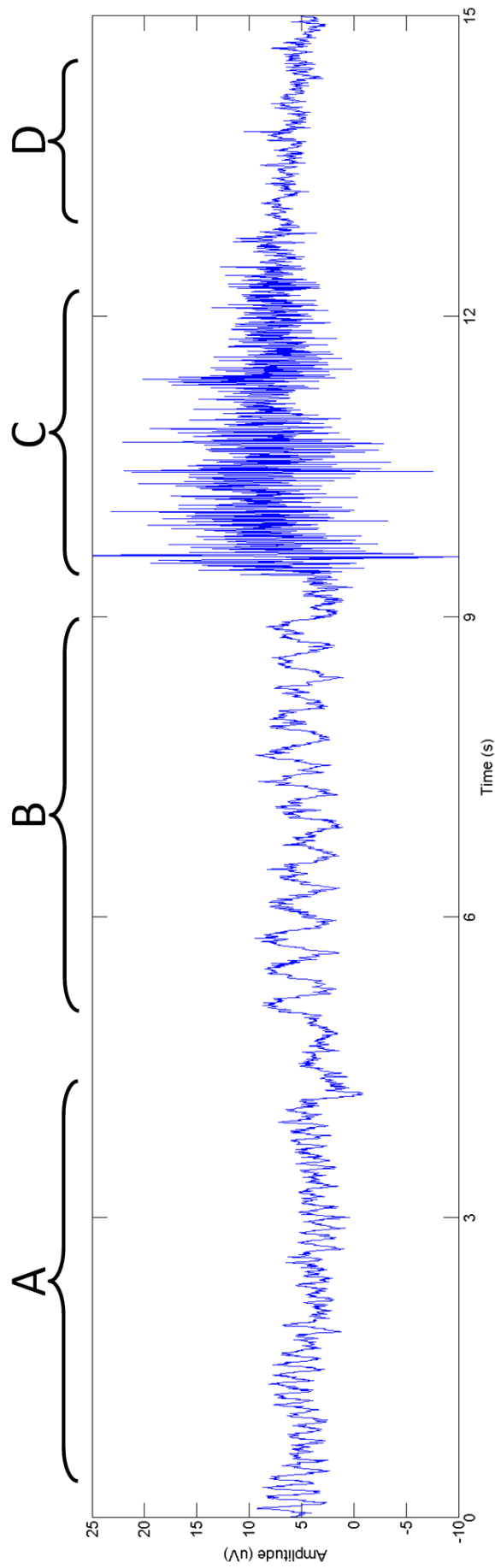


FIGURE 3.7: Apart from EEG other signals can be recorded from the scalp electrodes. Section (a) contains alpha signal with eyes closed, section (b) shows the signal generated by rapid eye blink, showing a higher amplitude than alpha signal. Signal in section (c) has the highest frequency and amplitude compare to the other sections, resulting from clenching teeth, it shows the effect of muscle signal on EEG. Section (d) represents the free running EEG signal with eyes open which has the lowest level of activity. The signal is a differential recording of MI and Cz.

the experiment described here, 60 second long sets of data are recorded to inspect their frequency content for the presence of an alpha signal.

Figure 3.8 shows the overall gain and filtering conditions in the EPS system. Recording in bipolar mode reduces much of the common mode noise such as mains frequency. A 50 Hz notch filter stage was added after this stage to further reduce the mains signal content. Also a low pass filter of 30 Hz was applied to act as an anti-aliasing filter for analogue to digital conversion, as well as reducing the effects of harmonics of 50 Hz. An extra gain of 100 was used in two stages of x10 after the input buffer, and before outputting the signal to a digitizer. Having this added gain reduces the effect of base line noise of the amplifier box on the input signal. However, if the input signal has an offset voltage it will be multiplied by that gain causing either railing of the output or high DC offset on the input of digitizer. To remove any DC offset a high pass filter of 0.5 Hz was implemented at the input stage of the amplifier box.

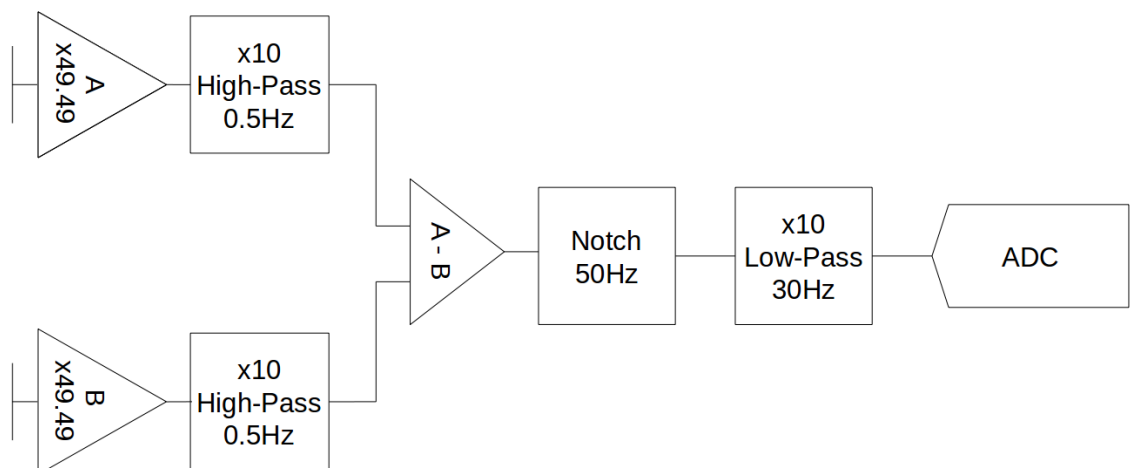


FIGURE 3.8: Block Diagram of the EPS system including the sensors, the vertical lines in front of the gain stages A and B are the half capacitor plates representing the electrodes. The gain is distributed in different stages to prevent railing of the sensors, over all gain of the system is x4949.

Signals were digitized and recorded by an oscilloscope which allowed for further processing in the software. Data were imported to MATLAB and analysed using MATLAB's inbuilt

$fft()$ function to give a visual demonstration of frequency content of recorded signal. The MATLAB mfile routine used for analysing and plotting can be found in appendix A.

Before analysing the signals recorded from the scalp it is important to consider the consequences of adding the extra filtering stages in the amplifier box. The sensor itself has a bandwidth of 0.1 to 78 Hz which covers the entire range of EEG, but with the addition of a notch filter and further high and low-pass stages this frequency band is limited. Figure 3.9 shows the compound effect that these additional stages have on the system response. The system response demonstrated sharper roll-offs with higher and lower cut-off corners for high and low pass filters respectively. Also the inclusion of a notch filter shows a sharp decline in system response for the 50Hz frequency.

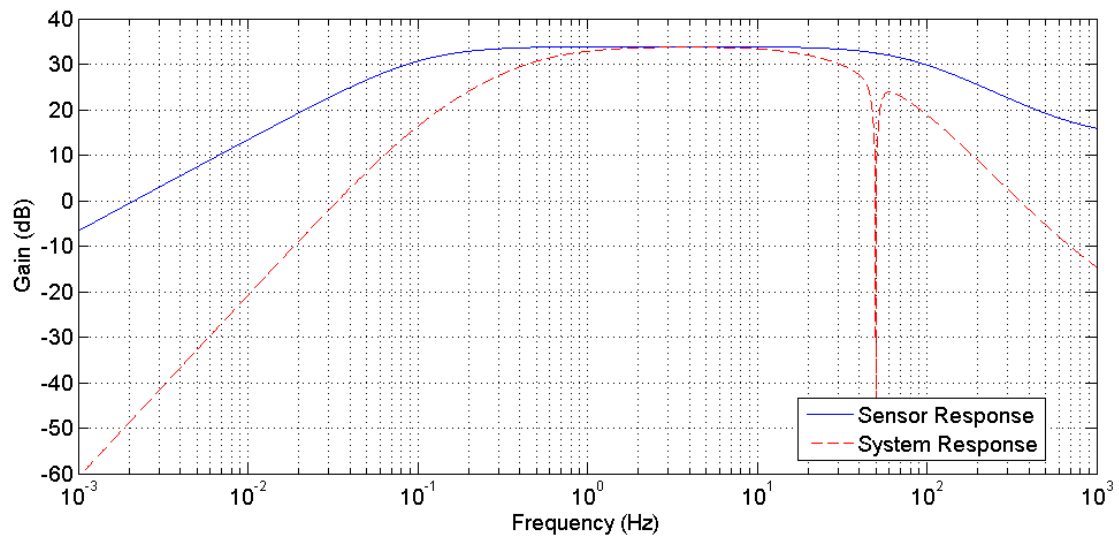


FIGURE 3.9: Frequency response of the sensors and the system from 1 mHz up to 1 kHz. The solid line represents the sensor's frequency response and the dashed line is the overall frequency response of the sensor and amplifier box. Noting it still has a flat response between the 0.5 and 30 Hz thus not affecting the alpha band. the sharp dip in the System response is the 50 Hz notch filter.

Although this limits the frequency band of final signal, it does not affect the alpha band as the response of the system is flat from 0.5 to 30 Hz. This allows for undistorted collection of signal for the alpha band which lies between 8 to 13 Hz.

3.3.3 Results

Alpha blocking is observed in time domain data. Figure 3.10 shows the EEG recorded for 6 seconds with eyes open in figure 3.10a and eyes closed in figure 3.10b. The average amplitude of the signal in figure 3.10a is $15\ \mu\text{V}$ and figure 3.10b has an amplitude of $30\ \mu\text{V}$. This shows an increase of a factor of two times in the activity recorded in figure 3.10b compared to figure 3.10a.

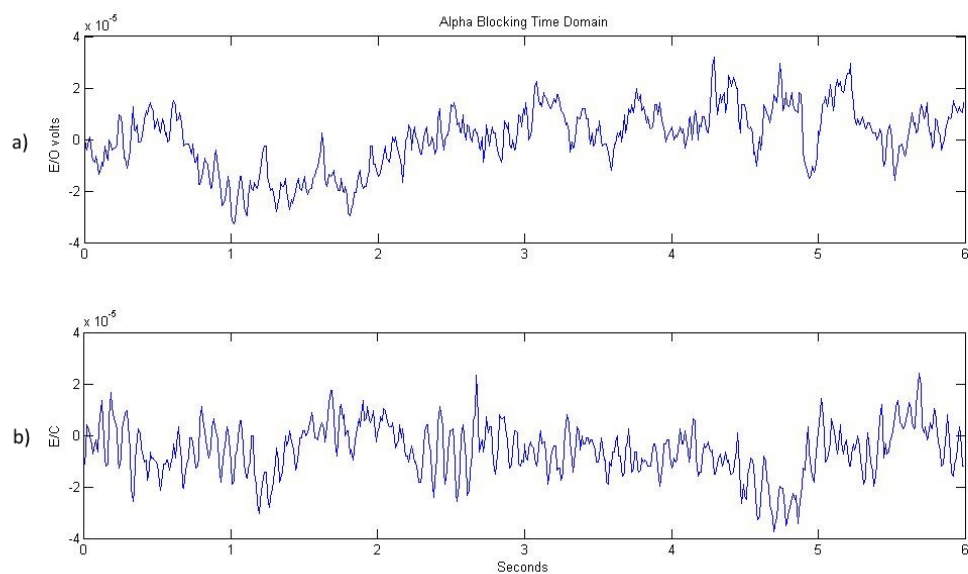


FIGURE 3.10: Alpha blocking in the time domain. Part (a) refers to the signal while eyes are open and part (b) is recorded when the eyes are shut. A rise in the amplitude of the signal in part (b) is observed compared to part (a). Average amplitude in part (b) is $30\ \mu\text{V}$ compared to an average amplitude of $15\ \mu\text{V}$ for part (a).

The exact frequency of this change is investigated by frequency domain information from this signal. Figure 3.11 is the fast Fourier transform of figure 3.10. Figure 3.11a is the frequency content of the recorded EEG while the subject's eyes are open with the base line for 10 Hz signal being $1\ \mu\text{V}$. In figure 3.11b the subject's eyes are closed and the base line amplitude of the 10 Hz signal rises to $30\ \mu\text{V}$.

Another important point to consider is the impact of correct referencing in common mode noise rejection. If the output of the sensor is not referenced to the correct reference signal

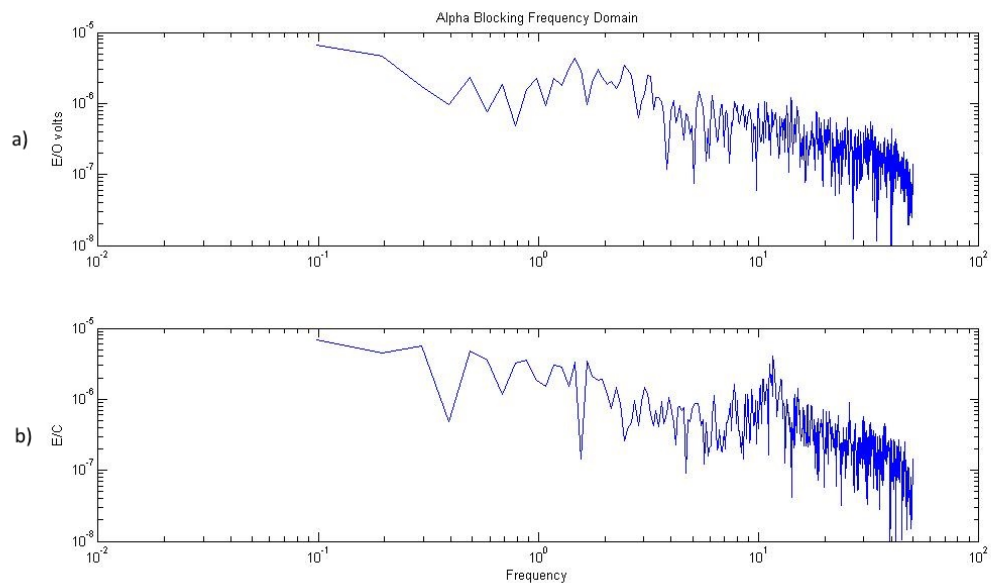


FIGURE 3.11: Alpha blocking in the frequency domain. A general change in the shape of the signal can be observed but the exact nature of this change is demonstrated by investigating the frequency content of figure 3.10. Part (b) shows an amplitude of $30 \mu\text{V}$ for the 10Hz signal as opposed to $1 \mu\text{V}$ in part (a).

additional noise will appear on the output of the system. An example of this is shown in figure 3.12, where the signal in part (b) is recorded with ground as reference compared to part (a) which is re-referenced in software to the sensor on the mastoid. Figure 3.12a and (b) are both section of the same signal where the referencing has been altered.

This is further confirmed in the frequency domain representation of the same signal in figure 3.13. In addition to removing the 50Hz signal referencing to the mastoid removes the harmonics of 50Hz.

The correct referencing not only eliminates the effects of mains, it helps with reducing the DC drift in the signal. Figure 3.14b shows offset voltages of 1mV distorting the signal between seconds 8 and 10. However in part (a) that section of the signal is recovered along with removal of mains frequencies, bringing the over all amplitude to less than $80 \mu\text{V}$. These DC drifts can be result of head movement or general body movement.

Figures 3.12, 3.13, and 3.14 contain no external signal processing other than differential

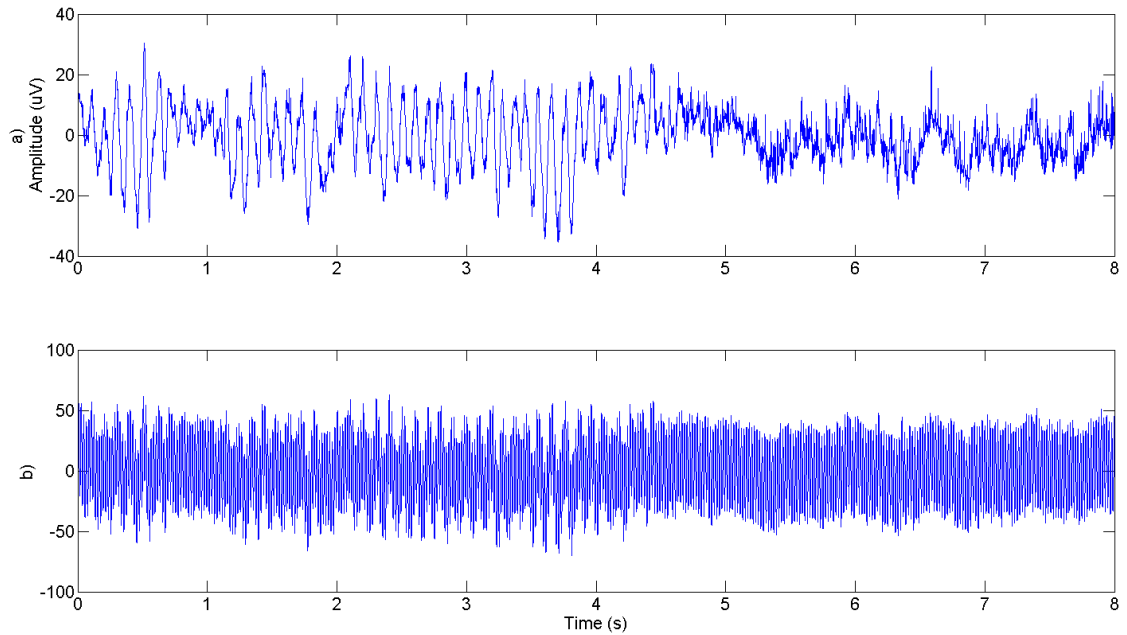


FIGURE 3.12: Correct referencing removes the common mode noise. Part (a) and (b) are representing the same signal, part (a) is O1 re-referenced in software to M1 and part (b) is O1 recorded with ground as the reference.

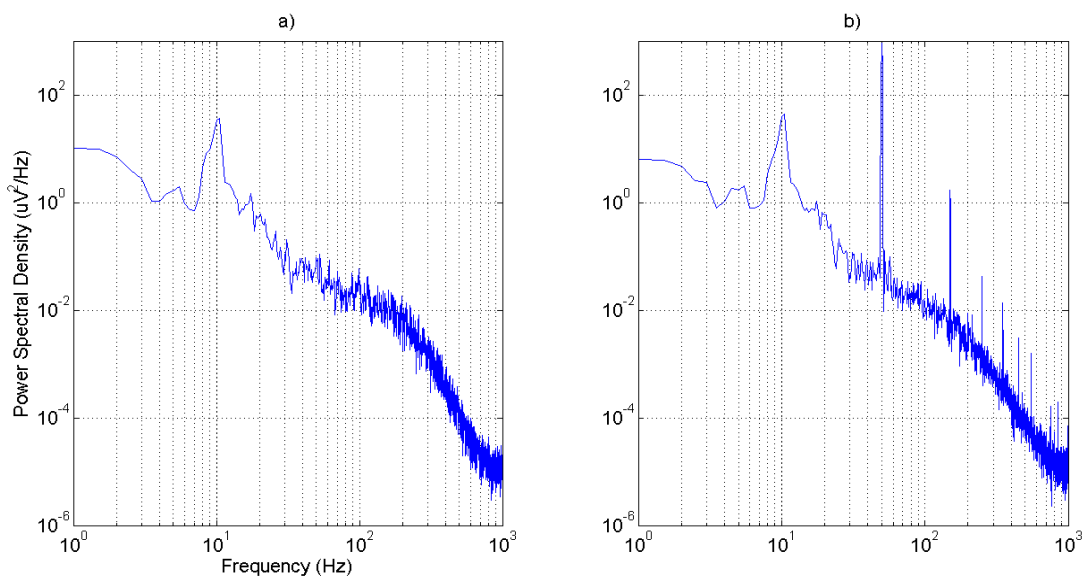


FIGURE 3.13: Removal of common mode noise shown in the power spectral density, the peak in part (b) at 50 Hz represents mains frequency, further peaks are observed which are the mains harmonics. In comparison part (a) shows a complete removal of mains frequency along with its harmonics. The signals presented are the frequency domain data extracted from figure 3.12. The data in part (b) is recorded with reference to ground, whereas the data in part (a) is re-referenced in software to the sensor positioned the mastoid

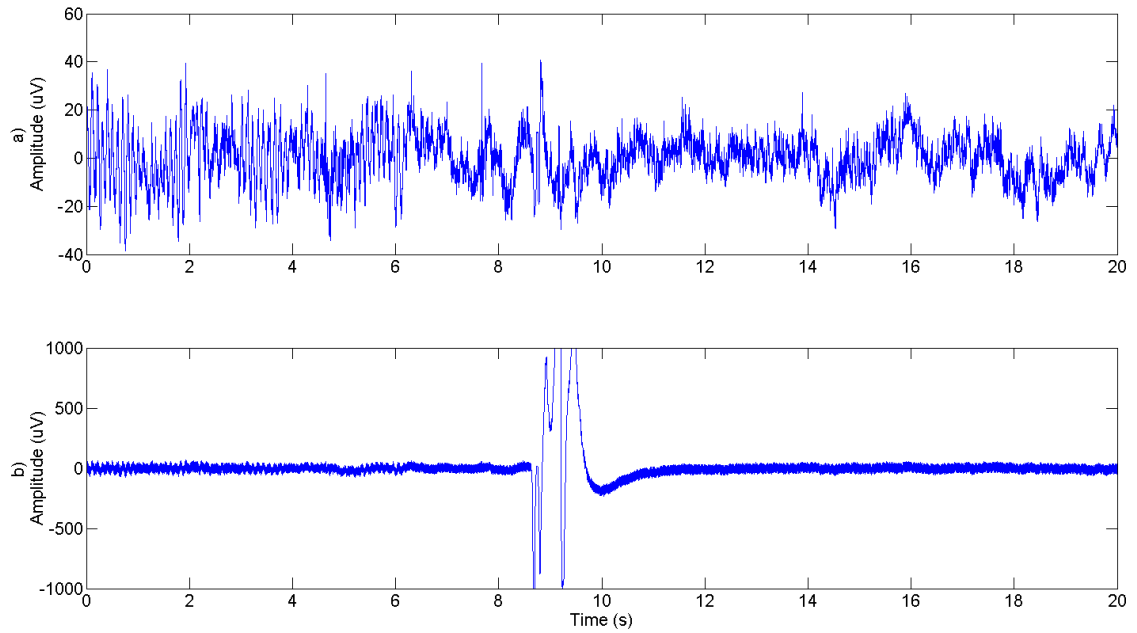


FIGURE 3.14: Correct referencing removes DC drift common to both channels. Parts (a) and (b) are presenting the same signals with (a) being referenced to M1 and (b) being the recording of O1 alone. DC drifts of higher than 1 mV are seen in part (b) which are removed after referencing in part (a). Both parts have same vertical and horizontal units.

measurement. The bandwidth of these signals was only limited to the sensor's bandwidth of 0.1 to 78 Hz.

3.4 Comparison with Conventional Sensors

The aim of this study was to investigate whether the signals produced by the EPS are comparable to an EEG recorded using standard Ag/AgCl electrodes. Previously, it has been demonstrated that the EPS sensors are sensitive to fluctuations in brain activity, such as alpha and beta activity as well as alpha blocking [41]. To expand upon these findings, alpha activity was recorded simultaneously from an EPS and a standard EEG system to enable characterising, in terms of the raw signal, frequency spectrum and similarities between the two signal measured by cross-correlation.

3.4.1 ANT EEG Monitoring System

In order to confirm that the sensor design was both suitable for high quality EEG signal acquisition, and that it was compatible with commercial systems and practice, The amplifier and power supply rack described above were replaced by an ANT[54] (model Refa8) amplifier produced by TMS International (TMSi) with 64 EEG channels. This system was also used to acquire the signals from the Ag/AgCl electrodes. All electrode cables have active shielding to reduce 50 Hz interference and cable movement artefacts. The specifications for the commercial system are as follows:

- Noise 1 μ Vrms
- Gain 26.55x
- CMRR 90 dB
- Input common mode range -2 V - +2 V
- Resolution 24 bit, 18.39 nV per bit
- AUX Sample frequency 1024 Hz, 512 Hz, 256 Hz
- High-pass none
- Low-pass digital FIR filters calculated using equation 3.1 [54]

$$\text{Corner frequency} = 0.2 * \text{sample frequency} \quad (3.1)$$

In the comparative data presented later the TMS International acquisition system and data processing were applied to both sets of data.

3.4.1.1 Methodology

Three male participants contributed data to this section. For two of the participants, data were collected in two separate blocks, one measuring EEG using the TMSi devices, one using the EPS sensors. The EEG was measured from conventional electrodes placed at O1, and at the two mastoids as reference, resulting in a total of 3 Ag/AgCl electrodes. Three EPS sensors were placed at similar positions. Participants were seated in a dim shielded room and asked to relax and stare straight ahead. A shielded room was used to reduce the background noise, and enable the comparison between the two systems based on their intrinsic noise. Recording lasted approximately 60 seconds for each block. Participants were asked to alternately close and open their eyes every time they heard an auditory signal, which came approximately every 4 seconds.

For participants 1 and 2, data were collected in two separate blocks, one measuring the EEG using a 64 channel TMSi amplifier (model Refa8), one using the EPS sensors, both at a sample rate of 2048 Hz. EEG was measured from electrode O1, plus the two mastoids, and online re-referenced to linked mastoids. The re-referencing is necessary as the commercial software provided with the Refa8 amplifier records EEG channel with reference to a mathematical average of all available channels. The linked mastoid reference in itself is a mathematical average of the signal recorded from the two sensors positioned on the mastoids. The EPS sensors were placed at similar positions, and re-referenced in the same way. Data was offline detrended and filtered using a bandpass filter between 0.1 and 80 Hz. In order to compensate for the built-in amplitude gain in the current EPS sensors, EPS data were divided by the value of 49.49 to make it commensurate with the ANT EEG data.

For participant 3, EEG and EPS data were measured simultaneously at a sample rate of

2048, as a continuation of this experiment. EEG was measured from electrode Oz, online re-referenced to electrode Fz. EPS electrodes were placed under the EEG cap between Oz and O1 and between Fz and F1, with the EPS Oz online re-referenced to Fz. The recording conditions and task were the same as for the other two participants, but overall recording duration was two minutes. The intention was to take this opportunity to make a direct comparison between the two systems with simultaneous recording.

When initially observing the data, it was noted that ocular muscle artefacts caused by opening, closing or blinking the eyes caused small amounts of drift in the data measured at Oz by both systems. Interestingly, the two systems reflected this drift to different degrees such that whilst the underlying higher-frequency signals were very similar, momentary lower-frequency differences in the range of up to 2Hz created larger-scale drifts between the two. Because these low frequency drifts are generally considered to be less important, and are usually eliminated in event-related analyses by baselining techniques, the decision was made to remove these trends by offline filtering the EEG and EPS data from participant 3 between 2 and 80Hz.

Cross-correlation was used in order to quantify similarities and time-lag between the signals recorded from the two systems. This is a similar mathematical process to convolution, where instead of forming the integral of the product of $f(t)$ with $g(-t)$, the original waveform shape $g(t)$ is used. The MATLAB function `xcorr(f,g,'coeff')` provides a normalized comparison between the two waveforms f and g . The outcome of this process exemplifies any delays between the recorded signals as well as how closely matched the two signals are[55].

3.4.1.2 Results

Figure 3.15 shows representative images of EPS and EEG data from participants 1 and 2 during 4-second periods when they transitioned from eyes-open to eyes-closed. Both participants clearly show the characteristic increase in alpha activity (10 Hz) when they closed their eyes (at approximately the 2 second mark), and this type of activity is apparent in both EPS and EEG recordings. Figure 3.16 shows power spectral density, measured by MATLAB's inbuilt FFT method with windowing, over the entire 60 second recording period. As can be seen, the spectral density patterns are quite equivalent between the ANT EEG and the EPS systems, further evidence that the EPS system measures similar underlying neural activity to the standard EEG system.

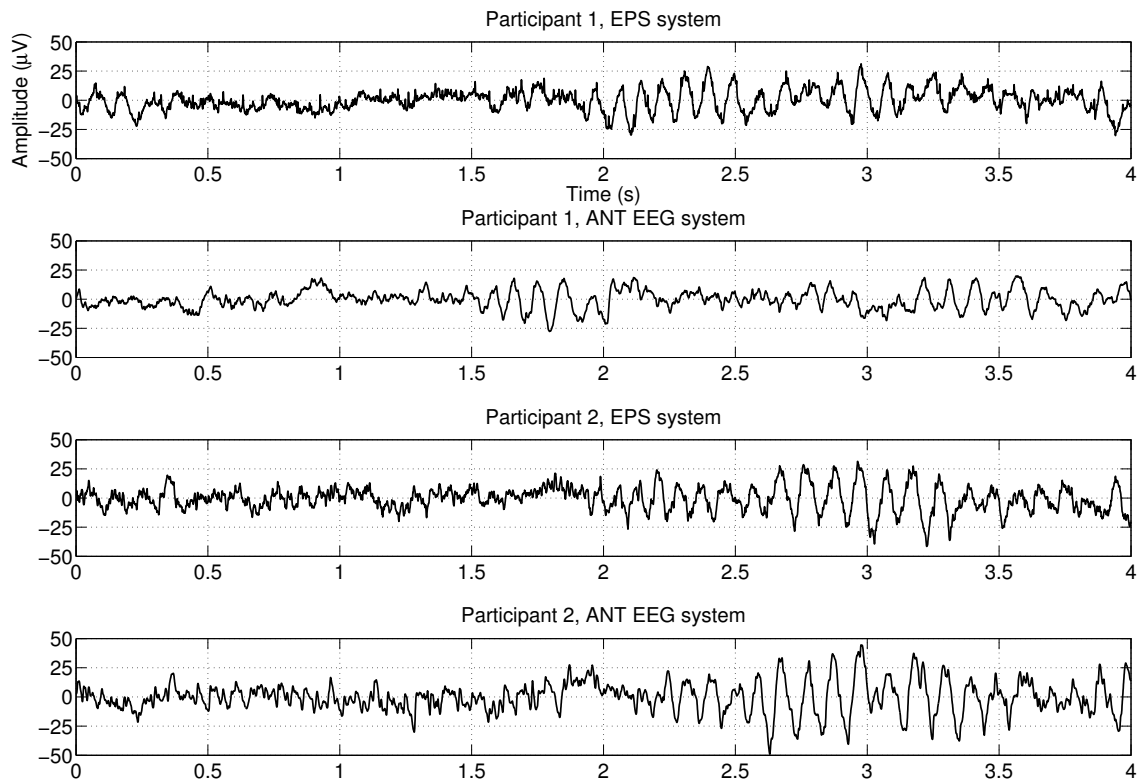


FIGURE 3.15: Representative raw data recordings from Participants 1 and 2, from both ANT-EEG and EPS systems, over 4 second periods including transitions from eyes open to closed (around 1.5 to 2.5 second mark). Note patterns of alpha band activity after eyes are closed, which appear similar for both the ANT-EEG and EPS systems. All axes have the same scale as part (a).

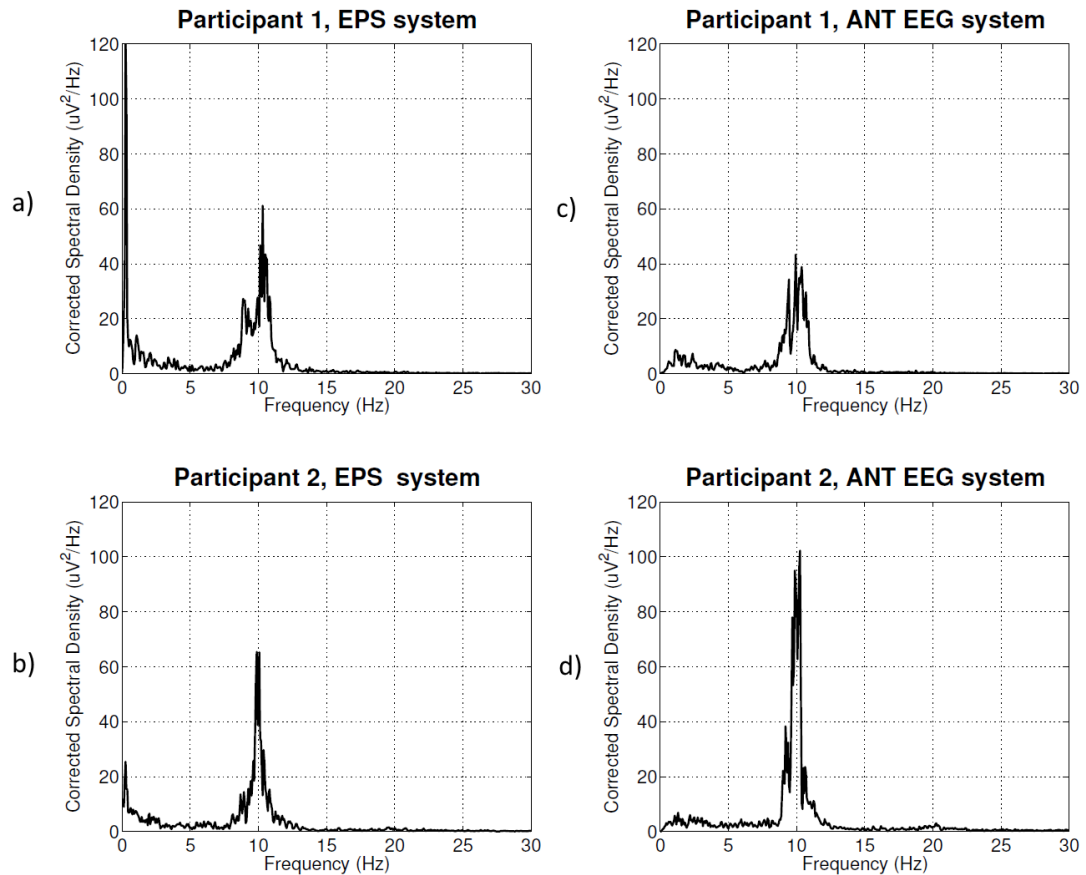


FIGURE 3.16: Frequency spectral density plots from the full 60 s recordings for participants 1 and 2, for both ANT-EEG and EPS systems.

Figure 3.17 shows results from participant 3, where we took the opportunity to collect EEG and EPS data simultaneously and from as-close-as-possible electrode locations. Figure 3.17a shows six seconds of simultaneous data from EEG and EPS systems at or around electrode Oz during a transition from eyes open to eyes closed (at around the 1 second mark). Note how remarkably similar is the activity measured by the two systems. Figures 3.17b and (c) show the frequency spectra of the two minutes' worth of recorded data from the EEG and EPS systems at the Oz location. Again the spectra are virtually identical. Figure 3.17d shows a cross-correlation between the data from the two systems over the entire 2 minute recording session. The cross-correlation value is highest around lag zero, sharply reducing to around $r = 0$ at either side. This is a strong, further evidence that the signals measured by the two systems are virtually identical, and that they are both

measuring the same underlying neural activity.

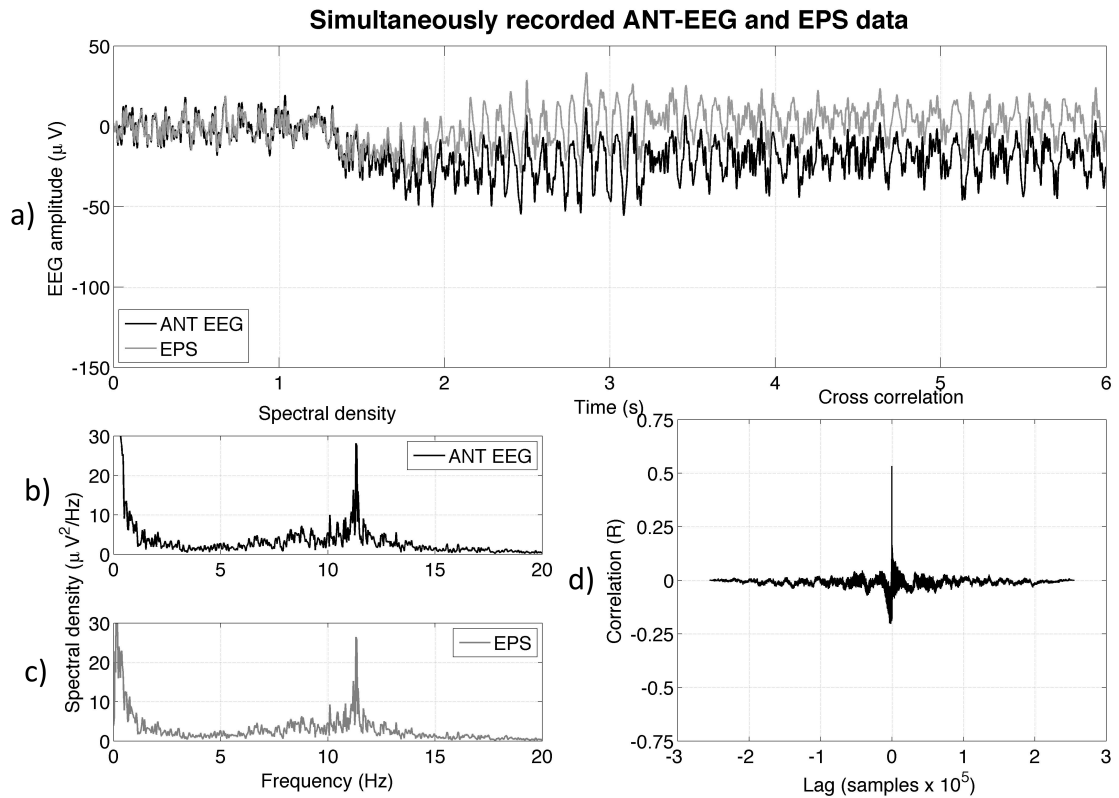


FIGURE 3.17: (a): 6 seconds of simultaneously recorded EEG and EPS data during a transition from eyes-open to eyes-closed. (b) and (c): Frequency spectra for EEG and EPS data over a 2 minute period. (d): Cross-correlation between the two systems over a two minute period.

The following are three important points to consider. Firstly, the signal in Figure 3.17a has been high pass filtered with a corner frequency of 2 Hz. Although this does not affect the frequency content of the alpha band, it does change the shape of the signal by lowering the effects of any signal picked up with a frequency of lower than 2 Hz. An example of such a signal is a DC drift that can be seen in EEG caused by eye muscles. An eye blink is observed in EEG when the reference sensor is positioned close to the front of the head (e.g. Fz). Figure 3.18 shows the same signals as figure 3.17a without the high-pass filter. A similar high frequency content is seen in both signals. The data also shows the faster return to baseline in EPS sensor compared to ANT, the signal recorded with EPS returns to baseline within 2 s where as ANT systems takes longer than 5 s for returning to baseline.

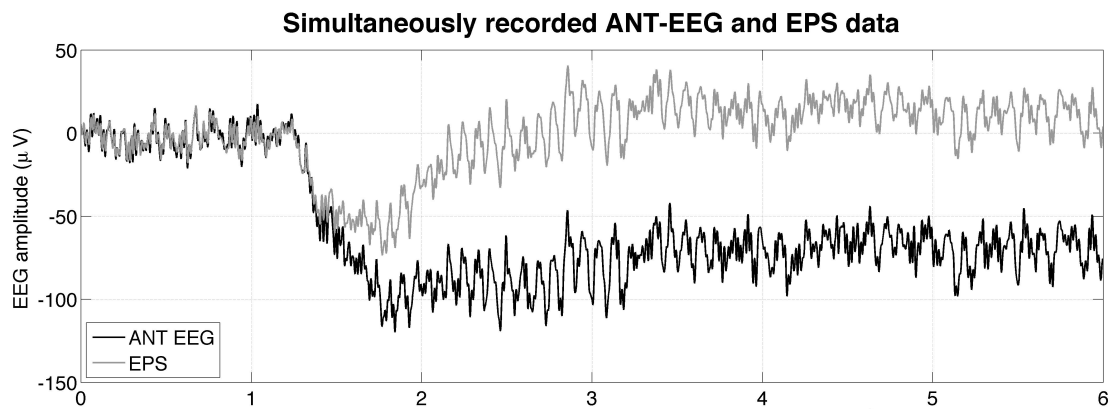


FIGURE 3.18: Effect of eye blink in terms of signal drift, caused by positioning the reference sensor on Fz. The eye muscles produce a much bigger signal than EEG which can be picked up from anywhere on the front of the head. This Figure shows the same data as in figure 3.17a with the difference being the lack of a 2 Hz high-pass filter. A much quicker return to 0 v baseline is observed, 2 s, for EPS compared with more than 5 s for the ANT. The higher frequency content has stayed unchanged.

Secondly, another consequence of the eye blink artefact is the effect on the cross-correlation values behaviour of the two signals. Figure 3.19 shows that the cross correlation at lag 0 reduces from around 50% in figure 3.17d to 20%.

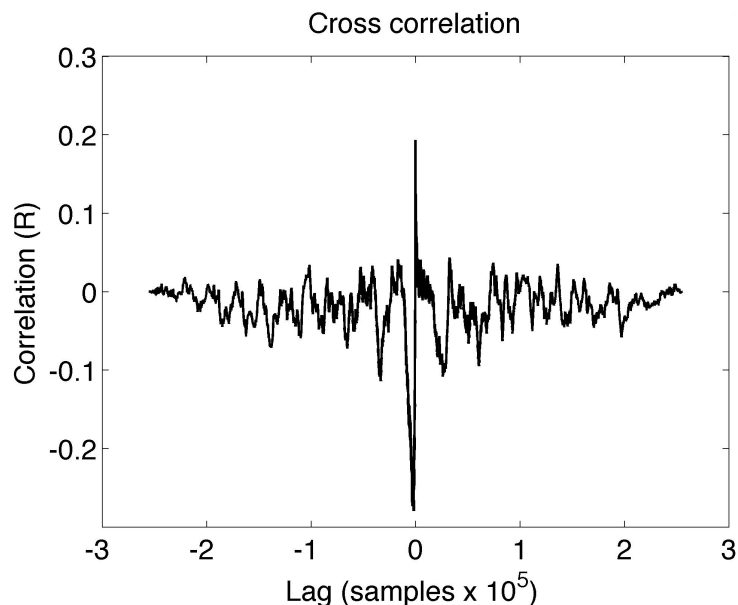


FIGURE 3.19: Effect of Drift on Cross Correlation. It has a value of 20% at lag zero, compared to a cross-correlation of more than 50% in figure 3.17d. This is the effect of inclusion of eye blink signal in EEG.

Thirdly, comparing the data for subject 3 with subjects 1 and 2 (where the signal was not collected simultaneously) a notable difference in the frequency analysis for alpha signal

is detected. Although the signal in figure 3.16a and (c) are collected from the same participant and same sensor locations for both systems, the frequency contents of the alpha band are not equal. Whereas figure 3.17b and (c) displays a much closer correlation between the two signals, although the sensors are not positioned at exactly the same locations. This shows that time causes a higher variation in the frequency content of the alpha band in comparison to sensor location.

3.4.2 g.tec EEG Monitoring System

To further investigate the accuracy of signals recorded by EPS a setup was created in which it was possible to simultaneously record from EP sensors and g.tec active sensors. The g.LADYbird active wet gel ring electrode, with sintered Ag/AgCl, was used with g.GAMMAcap[56]. This sensor with cap setup is shown in figure 3.20. The EP sensors are positioned under the cap at POz and M1.

3.4.2.1 Methodology

In g.GAMMAcap the ground electrode is positioned in front of the head and the reference electrode is connected to right ear lobe. Eight more active sensors were positioned according to 10-20 system. To be able to compare these sensors with EPS, two EP sensors were used. One is positioned on left mastoid to provide a reference and a second sensor is positioned at POz. Both sets of sensors were connected to a g.USBamp for data conversion.

A single participant was used for this experiment. He was sat in an unshielded room. The g.USBamp can be controlled using MATLAB's Simulink toolboxes. To compensate for the extra gain in the EPS sensor a software gain of 1/50 was added with a 50 Hz notch filter.

The EPS amplifier box was used for providing power to the sensors. Instead of feeding the signal from individual sensors the differential output of the box was used, supplying POz-M1 to reduce the common mode signals before feeding it into the ADC.

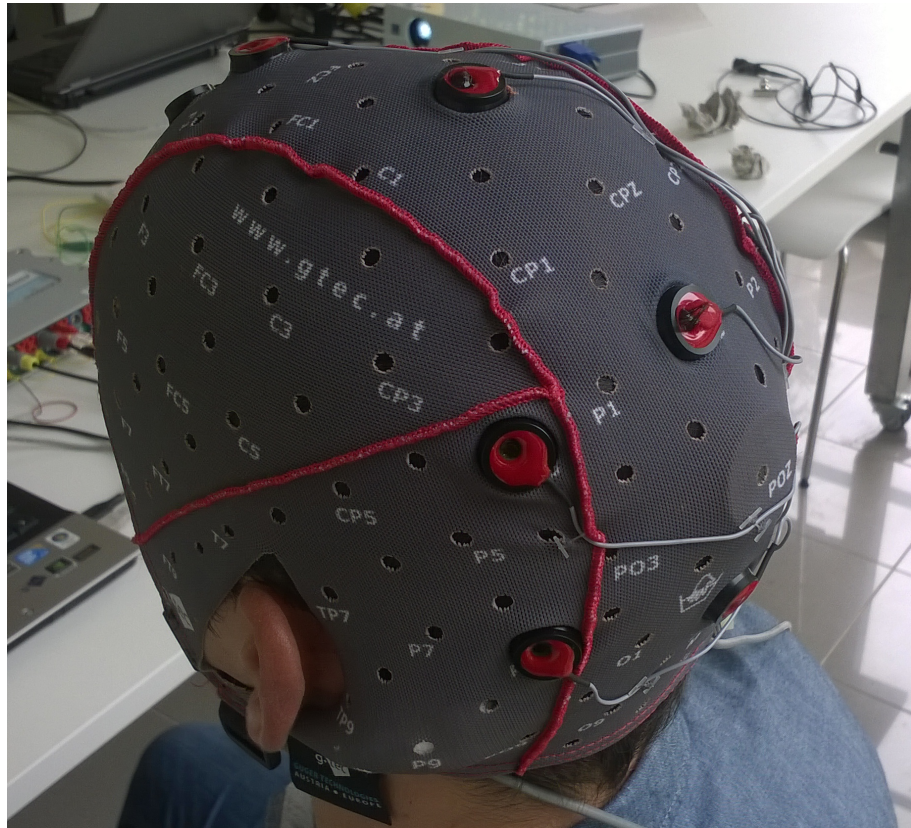


FIGURE 3.20: g.LADYbird active sensors filled with gel in g.GAMMAcap, EP sensors are positioned at POz and M1

3.4.2.2 Results

Figure 3.21 shows the frequency content of the signals recorded from the EPS and g.LADYbird sensors. The results of data recorded from EPS was compared to the results from the sensor placed on Oz. These positions were chosen as they are closest sensor positions on the head to the occipital lobe. A similar amplitude for the alpha band is observed for both 3.21a and (b), 8 and 6 μV respectively.

The data used for figure 3.21 was taken from a 60 s section of data shown in figure 3.22. Figure 3.22 shows time activity of three sensors simultaneously, a software notch filter has

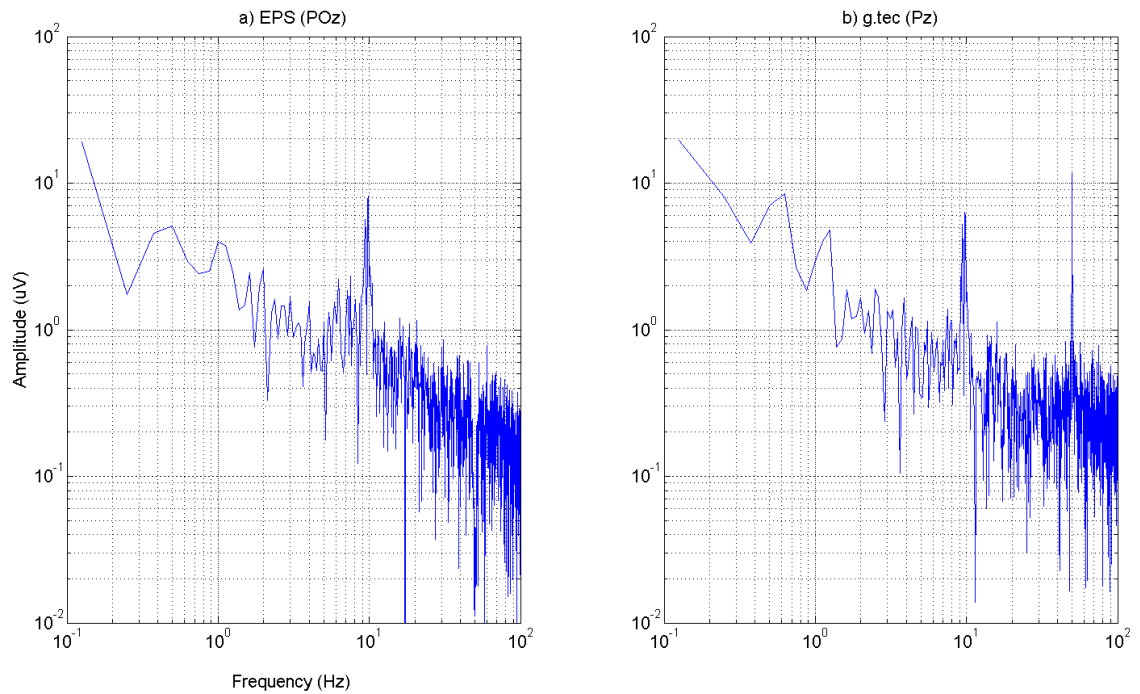


FIGURE 3.21: Alpha signal present with eyes closed in the frequency domain with part (a) showing the EPS results and part (b) the signal from g.tec sensor. Comparison between the EPS and active g.tec gel sensors show similar amplitude of $\sim 8 \mu\text{V}$ in the alpha band. Signal (b) shows a higher amplitude for 50 Hz signal where as part (a) shows a dip in the same frequency, this is the result of using notch filter in data collection for EPS and lack of it for g.tec.

been applied to all channels. The first two are g.tec sensors positioned at Fz and Oz and the third signal is the EPS placed at POz, with reference sensor for the EPS positioned on the left mastoid. The g.tec acquisition systems uses the right ear lobe as the reference point and has a dedicated ground electrode positioned according to 10-20 system, refer to figure 2.1.

The difference in the shape of signal recorded from the front of the head in figure 3.22a compared to locations closer to the occipital lobe in parts (b) and (c). A high DC drift is seen in figure 3.22a. This sensor is positioned closer to the front of the head and therefore closer to the eyes which results in picking up EOG and other muscle signals. Further results from all 9 recording channels can be found in appendix B.

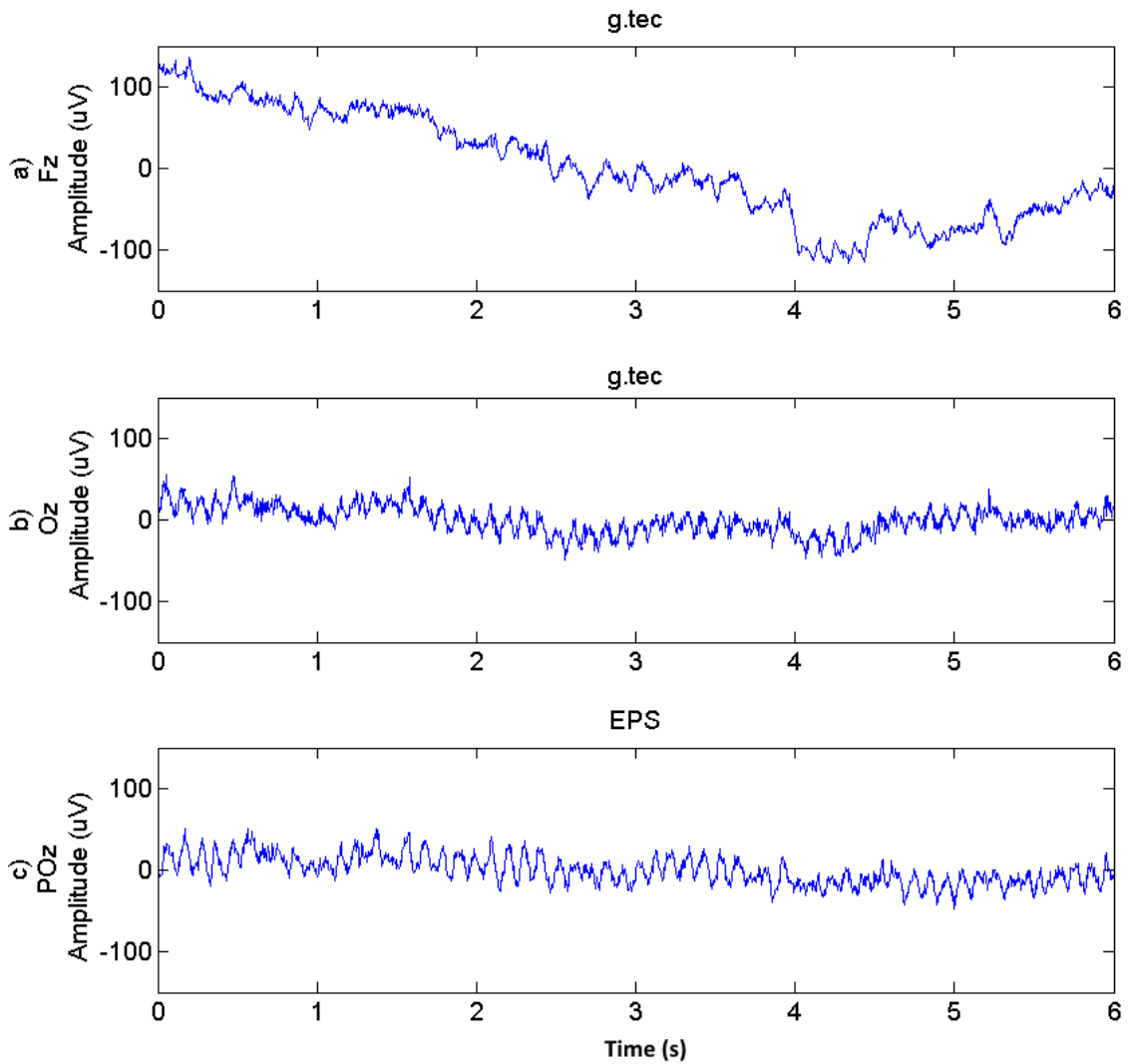


FIGURE 3.22: Alpha signal present with eyes closed in the time domain, comparison between the EPS and active g.tec gel sensors is shown for three locations of (a) Fz and (b) Oz for g.tec and (c) POz for the EPS. DC drift of $100\mu\text{V}$ is observed in part (a) compared to parts (b) and (c) due to its closer location to front of the head, resulting in picking up EOG and muscle signals.

3.5 Discussion

The alpha signal has its origins deep in the brain [13], and perhaps can best be understood as the accumulated effect of a number of events that happen when the eyes are closed or opened. What makes this signal useful for testing EEG sensors is that it could be effectively turned on or off much like a signal generator. Therefore, this signal was used to decide whether the internal noise of the EP sensor is low enough for the alpha signal to

be recorded.

At the beginning of a recording session the signal quality of the conventional electrodes is monitored by measuring the resistance between any single electrode and the ground electrode on the head. This should result in a value of less than 5 k Ω . Similarly, to insure the EPS has made a stable connection with head, two tests should be carried out after positioning the sensors on the head. The first is to inspect the amplitude of the mains signal present at the output of all sensor to be same. The second test involves inspecting for signs of muscle signal, such as eye blink or teeth clinching.

Alpha blocking phenomenon is successfully demonstrated using EP sensors. Furthermore the EPS was compared with two other commercial EEG systems that use conventional EEG electrodes; ANT Refa8 amp from TMS international with Ag/AgCl electrodes, and g.USBamp from g.tec with the g.LADYbird active ring electrode. The results showed a correlation of higher than 50% between the signals recorded by the EPS and the ANT system, demonstrating similarities in both time and frequency domains.

Chapter 4

Sensory ERPs

4.1 Introduction

This chapter will discuss sensory ERPs in more detail, with sections on how to record these signals using the EPS, and the signal processing involved in these type of experiments. These recordings are compared to other commercial systems for recording ERP. The cognitive ERPs and their signal recording are presented in the next chapter.

As discussed in chapter 2, ERPs are observed when presenting a audible or visual stimuli to the brain. This gives rise to activities in neurons which alters the potentials recorded on the scalp, creating event related potentials. These potentials are observable given the information about the stimulus trigger.

4.2 Sensory ERP

Historically sensory ERP, also known as evoked potential (EP), refers to a signal that represents an event that actuates one of the sensory regions of the brain. An example

of this phenomenon can be observed in recordings after the presentation of an audible stimulus such as a click. A small ERP is present in the signal within 10ms of the onset of this auditory stimulus. The resulting signal can be observed in an EEG recording. ERPs have an amplitude of 0.1 to 10 μV compared to the EEG's amplitude of 10 to 100 μV [14]. Having a much smaller amplitude, by a factor of 10, compared to the background EEG signal makes it more difficult to observe as a single ERP.

Sensory ERP was first reported in 1939 in form of single trials[57]. Although a lot of attention is given to the study of single trial behaviour of ERPs[58], the majority of studies use averaging techniques. The introduction of computers allowed researchers to apply averaging routines to time locked data recorded from background EEG and extract computer averaged ERPs, the first of which was published at 1962[59]. ERPs are best described as time locked events compared to the background EEG which has relatively no variation for the duration of the stimuli. Therefore to be able to observe and study ERP's a high number of stimuli are presented to a volunteer and the response of the brain is recorded and averaged.

Different types of stimulus can be presented in an experiment and depending on the sensory function they stimulate, they are given different names. An ocular stimulus would result in visually evoked potentials (VEP) and a sonic stimulus leads to auditory evoked potential (AEP). These are all different forms of ERPs[14]. Primary sensory areas are shown in figure 4.1 representing the origin of the sensory ERP waveforms. Also, these exemplify the location that strongest ERP signals can be recorded depending on the type of stimuli. Visual stimuli cause a reaction in the occipital region of the brain which corresponds to sensor locations close to Oz in the 10-20 system. Audible stimuli can cause brain activity in T5, T6 and their surrounding regions. All the sensory information relating to muscles

all over the human body is relayed to the somatosensory region which is covered by the central lobe of the brain, a narrow band stretching from Cz to both ears.

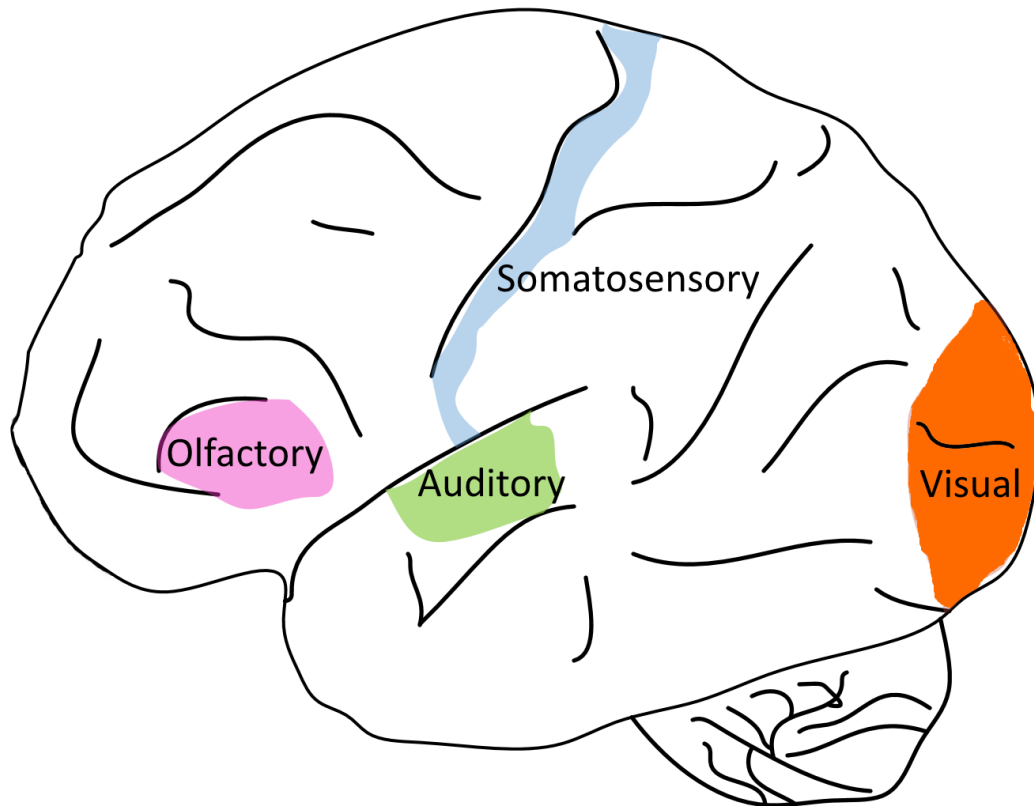


FIGURE 4.1: Primary sensory areas are shown. Sensor location close to Oz is used to cover events related to visual stimuli. AEPs can be observed over T5 and T6. A narrow band starting from Cz (centre of head) stretching to both ears can be used to observe sensory information returning from muscles[60].

4.2.1 Visually Evoked Potential

If a visual stimulus is presented to a volunteer then a recordable response is observed in the EEG of that person. The occipital region is the origin of visual sensory signals. In the 10-20 system, the locations O1, O2 and Oz cover this area. O1 and O2 present a stronger signal for stimuli that are intended for the right and left eye respectively.

The International Society for Clinical Electrophysiology of Vision (ISCEV) has defined a set of standard protocols for recording VEPs. This standard recommends three experiments that are commonplace amongst electrophysiology laboratories all over the world.

Firstly, a pattern reversal experiment using checkerboard stimuli, where checks reverse colour according to a trigger and change phase a certain number of times per second. Secondly, the pattern onset/offset experiment, for which the same checkerboard figure as the previous test is used with the difference being that this pattern is suddenly exchanged with a distorted gray image. Thirdly, there is a flashing LED experiment. This standard also advises on the recording conditions for sensors and analysis routines for exploring the recorded EEG[61]. Based on the pattern reversal and the flashing LED test, two VEP experiments were designed and conducted which will be discussed later in this chapter.

Like EEG waveforms, VEPs are age dependent. The typical waveforms described in literature is of an adult of 18-60 years old[61]. The components of a VEP signal are positive or negative deflection peaks that are described based on their latency (time from the onset of a stimulus). For example the P100 component describes a positive deflection with a latency of 100 ms and the N75 component illustrates a negative peak at 75 ms after the trigger.

The exact timing of these components can vary based on pattern size, contrast, age, mean luminance and a number of other factors. However, for a single subject this timing should show minimal variation. Thus, the P100 component represents a latency of approximately 100ms. A different convention, therefore, is used in some cases where P1 is used instead of P100 to represent the first positive peak. The same would apply to negative peaks such as N2 which point to the second negative deflection which could be positioned on either side of the 200 ms mark[14].

4.2.2 Signal Processing

A VEP occurs in the background of an EEG signal and has an amplitude 10 times smaller than EEG. Although it is still possible to observe a VEP in a single trial these signals are usually averaged more than 100 times. To be able to remove the background EEG, or to reduce its presence in the recorded signal, averaging is used. This added difficulty in recording sensory ERPs makes them a good choice for validating the results of recorded signal from the EPS.

Knowing that ERP trials are time locked to an event, it could be assumed that the background EEG does not vary during the duration of that trial. It could further be deduced that by averaging these time locked signals the ERPs are increased by a factor of square root of the number of trials compared to the background EEG. Equation 4.1 shows the effect that number of averages has on the degree that the background EEG signal is diminished[13] as a function of number of trials N . This example is done for ERPs with average amplitude of $5 \mu\text{V}$ with a background EEG activity of $20 \mu\text{V}$ with N equal to 400 trials.

$$\frac{\text{ERP amplitude} * N}{\text{EEG amplitude} * \sqrt{N}} = \frac{5 \mu\text{V} * 400}{20 \mu\text{V} * 20} = \frac{2000}{400} = 5 \quad (4.1)$$

This shows that the averaged ERP will be bigger than the background EEG. Considering the background EEG to be an incoherent signal, in relation to the time locked coherent ERPs, this result can be understood in terms of signal to noise ratio (SNR) of 5:1. The signal to noise ratio before averaging was 1:4 ($\frac{5 \mu\text{V}}{20 \mu\text{V}}$) and it has increased to 5:1. This value can further be improved by increasing the number of trials in an experiment. A ratio of 2:1 is known to produce recognisable ERPs[13].

When a stimulus is presented, a trigger signal is also recorded alongside the EEG. This timing signal is used to extract individual trials from the EEG signal. Each stimulus is presented every few 100ms, depending on the intended frequency of the signal. In order to rule out the effects of anticipation of the final result, a jitter of a few milliseconds is introduced into the timing of these stimuli. Before the averaging routine is performed a band pass filter of 0.1 to 30Hz is applied to the EEG signal. After the data for each trial are extracted, any offset voltage is removed so that it is averaged around the baseline.

4.3 Pattern Reversal Experiment

To further confirm the reliability of EEG signals obtained by EPS a comparison study was conducted between EPS and conventional gel electrodes. The ANT amp with WaveGuard cap [54] was used to record EEG signals using Ag/AgCl electrodes. Both EPS and conventional electrode outputs were recorded using ANT amp (the EPS signal was fed directly into ANT amp input).

The experiment were designed to show whether alterations in brain activity driven by perceptual change, would firstly be distinguishable by the EPS and secondly display a similar evoked profile to standard EEG measures. Evoked potential amplitudes tend to exhibit small amplitudes compared to the background of ongoing EEG activity, ranging from less than a microvolt to several microvolts, and thus in-order to resolve these low-amplitude potentials, signal averaging of large numbers of trials is required. To investigate these questions a paradigm was used that is known to elicit a robust evoked component, the visually evoked potential (VEP) response, which is commonly used to assess pathology of the visual system as it depends on the functional integrity of the visual system [61].

4.3.1 Methodology

A single participant was seated in a dimly lit electromagnetically shielded booth, 75 cm away from a LaCie Electron blue IV 22" CRT Monitor [62]. The non-dominant eye of the participant was covered using an eye-patch and their head was supported on chin rest so that their line of sight was exactly central to the screen. A standard checkerboard pattern was displayed on the screen with a red dot in the centre implemented using MATLAB and the Psychophysics Toolbox. The checkerboard consisted of a 16 x 16 array of black and white squares [61]. The array reversed (i.e., black to white and white to black) at a rate of two reversals per second. There was a total of 100 reversals in the experiment. The participant was instructed to maintain fixation on the red dot throughout the experiment. A crude illustration of the checkerboard pattern used for this experiment is show in figure 4.2. Parts (a) and (b) show the pattern reversal action. The red dot in middle of both patterns portrays a fixation point for the participant.

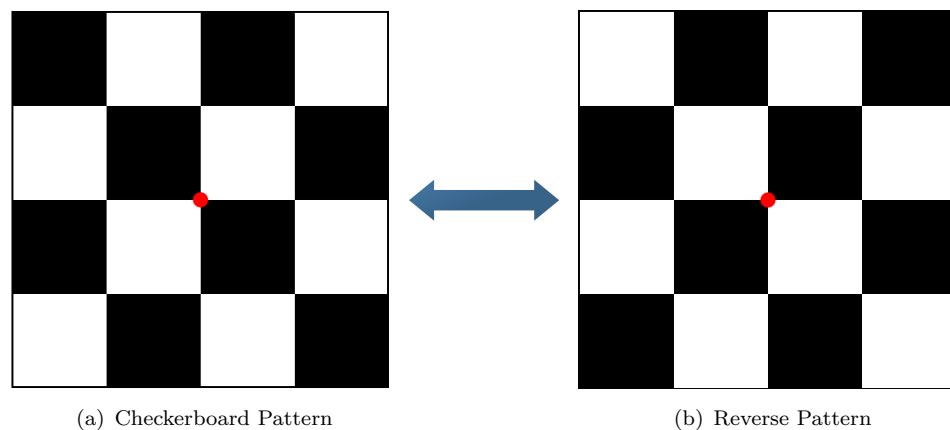


FIGURE 4.2: Checkerboard stimulus and its reverse pattern. The red dot in middle of both pattern is provides a fixation point for the participant. This is a scaled down model of the array used for this experiment, the original pattern included a 16 by 16 array. 100 reversals were presented at a rate of 2 reversals per second.

EEG and EPS data were measured simultaneously using a 64 channel ANT Neuro amplifier (Refa 8) at a sampling rate of 2048 Hz. EEG was recorded using a 64 channel wave guard cap from Oz and Fz. Data were online re-referenced to electrode Fz. EPS electrodes were

placed under the EEG cap between Oz and O1 (EPS-O1) and between Fz and F1 (EPS-Fz) and connected to the amplifier via the bipolar ExG inputs. EPS signals were measured from EPS-O1 and EPS-Fz and additionally a differential of EPS-Fz and EPS-O1 was also recorded. Two electrodes were also used to record vertical ocular artefacts. Figure 4.3 demonstrates the sensor positioning for this experiment according to the 10-20 system.

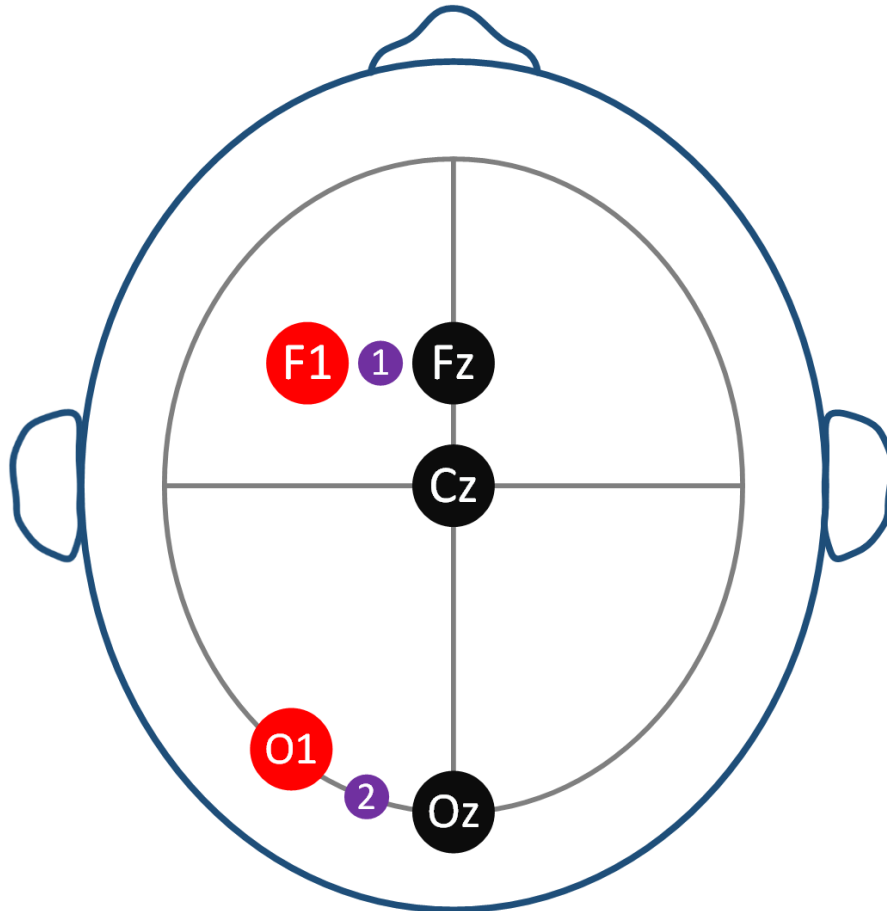


FIGURE 4.3: The positioning of the sensors according to the 10-20 system is shown. Gel electrodes are positioned at Fz and Oz. Point 1 and 2 are the positions between Fz-F1 and Oz-O1 respectively. These points were used to enable simultaneous recording for the EPS and ANT system. The new positions are called EPS-O1 and EPS-Fz. Noting that these positions are not exact and are merely provided as an approximation to the locations used

EEG data were analysed offline with EEGLAB [63] and ERPLAB Toolbox [64]. Data were band-pass filtered from 0.1 to 30 Hz with a Butterworth digital filter and target locked epochs were created. Each epoch started 100 ms before the onset of the target and ended 300 ms afterwards. Ocular artefacts were identified using a moving window peak-to-peak

threshold, with a voltage threshold of $40 \mu\text{V}$. Epochs were then baseline corrected for -100 to 0 ms before stimuli onset. Epochs were then averaged to produce VEPs. In order to compensate for the built-in amplitude gain in the current EPS sensors, EPS data was divided by the value of 49.49 to make it commensurate with the ANT EEG data.

The participant was asked to clean four sites on their head. Firstly, two sites on the right and left mastoids were cleaned with abrasive gel and alcohol wipe to form a reference point for the ANT amplifier. Secondly, above and below the left eye of the participant was cleaned using the same procedure to attach EOG electrodes.

4.3.2 Results

Figure 4.4 shows the raw signal recorded from EPS from point Oz with reference to Pz for a duration of 3.5 seconds. The red vertical lines illustrate the onset of stimuli. Finally, the rectangular boxes form the boundaries of each VEP trial, from -100 ms to 300 ms after the trigger signal.

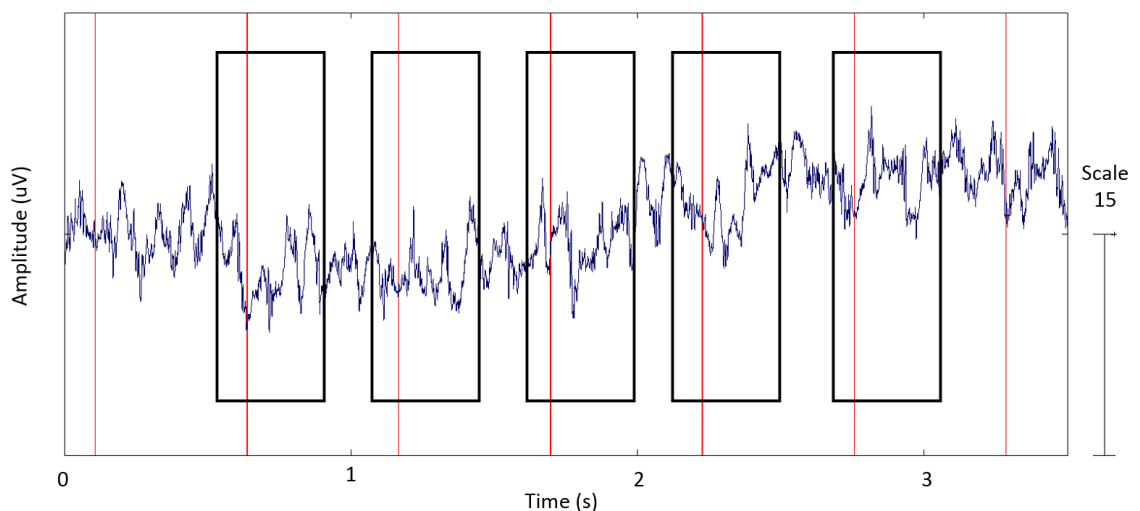


FIGURE 4.4: Raw VEP waveforms covered by background EEG. The red vertical lines indicate the stimuli trigger points. A boundary of -100 ms to 300 ms after the onset of stimuli is shown by rectangular boxes positioned around certain sections of the raw EEG.

Applying a bandpass filter of 0.1 to 30 Hz and removing the baseline offset presents a much clearer waveform. Figure 4.5 is made up of the signals from figure 4.4 where the boundaries of -100 ms to 300 ms ,after the trigger signal, is applied to all the trials and the rest of the signal is removed. It is, therefore, possible to observe single trial VEPs in the background EEG without averaging in some of the trials as shown in figure 4.5. The blue dashed lines demonstrate the lower time boundary of -100 ms for each trial, followed by the solid red lines at times zero indicate the onset of stimuli.

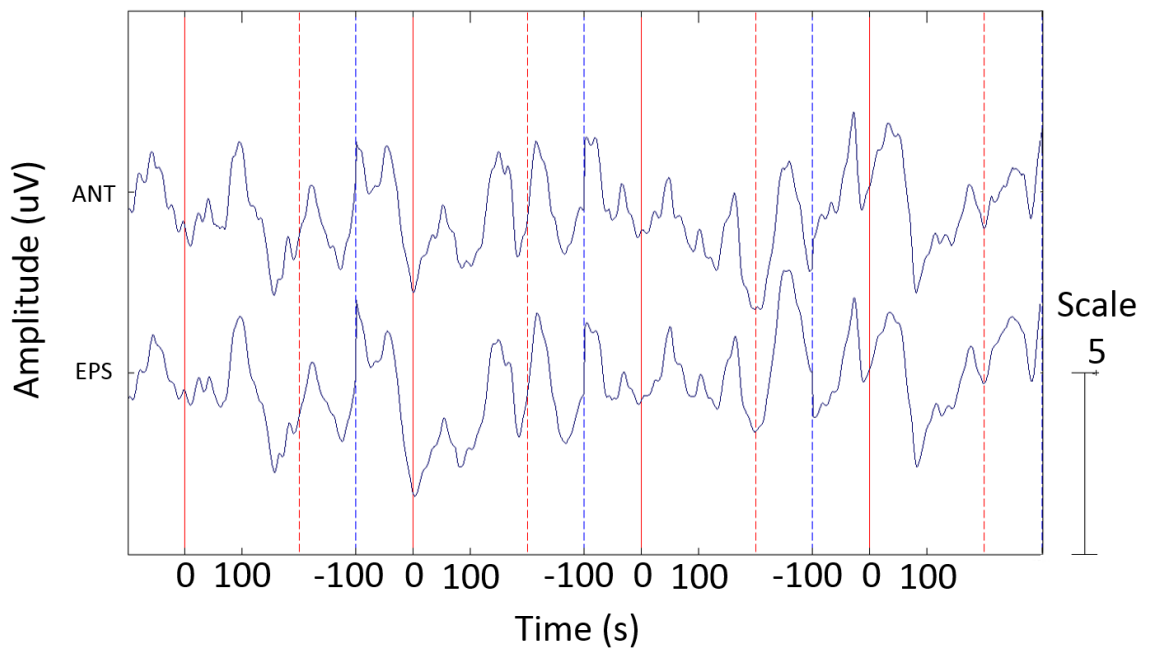


FIGURE 4.5: The waveforms here are results of applying the time boundaries of -100 ms to 300 ms to the raw EEG presented in figure 4.4, followed by bandpass filtering of 0.1 to 30 Hz. Also the DC offset of each trial is removed. Top trace is signal recorded by ANT from location Oz and the lower trace is the EPS signal from approximately same location. The dashed blue lines present the lower time boundary of -100 ms for each trial, followed by a solid red line indicating the trigger signal. Single trial VEP is observable in some of the trials.

Finally, these trials are averaged, the resulting waveform can be observed for both EEG systems in figure 4.6. As can be seen from (a) visual evoked potentials for both EPS and ANT EEG systems display a very similar pattern of evoked responses, which both display a standard evoked response for pattern reversal stimuli including the N75 and P100 components. It should be noted that the P100 component does not occur at exactly 100 ms after the trigger (zero second), as its latency is expected to be approximately 100 ms[61].

A cross-correlation value is highest around time zero, sharply reducing to around $r = 0$ at either side. Apart from the evident visual similarities in the VEPs recorded by the EPS and EEG sensors the results of the cross-correlation provides further evidence that the signals measured by the two systems are similar, and that they are both measuring the same underlying neural activity.

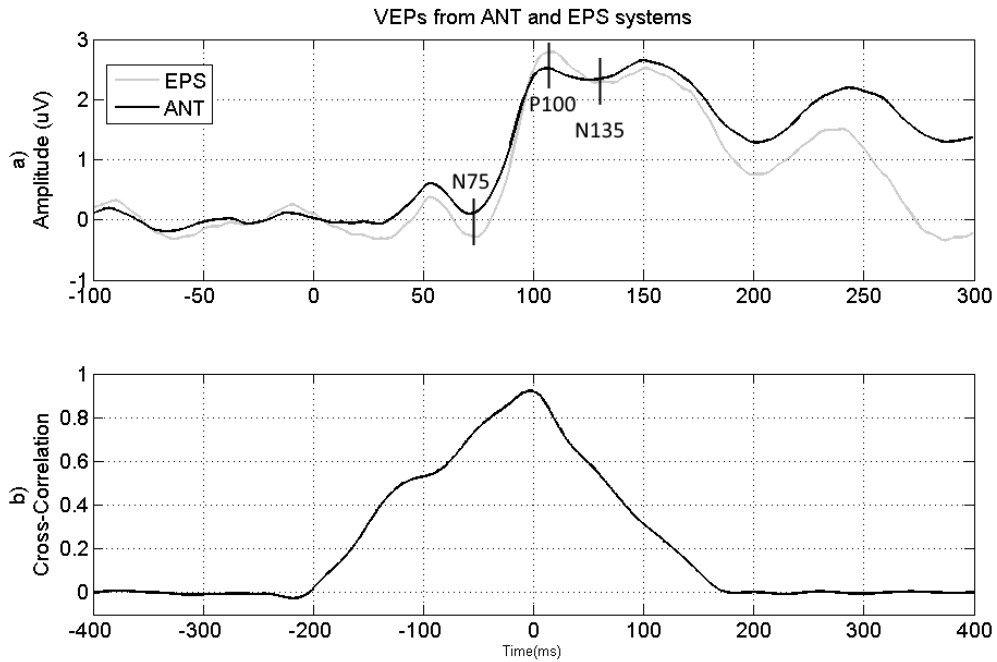


FIGURE 4.6: Comparing EPS with ANT results. (a): Averaged VEPs from pattern reversal for EEG (black line) and EPS (gray line). The VEP components of N75 and P100 can clearly be observed in both signals. (b): Cross-correlation between the two systems from -100 to 300 ms, showing maximum correlation at time zero.

4.4 Flashing LED Experiment

Based on the ISCEV standard, a second experiment was designed to study sensory ERP during a flash VEP experiment. In this study, the EPS was compared to active gel electrodes made by g.tec [56]. The sensor setup is similar to the alpha experiment in the previous chapter. VEPs are recorded and the results are compared between the two systems.

4.4.1 Experiment Design

A VEP experiment was designed where a series of LEDs are flashing with spacing of 1s between each stimulus. The device presenting the stimulus is shown in figure 4.7. The recording was conducted in a bright open environment outside of a shielded room, as is shown in figure 4.8. The sensors used are g.LADYbird active sensors [56], scattered over the frontal and occipital lobes of the brain according to the 10-20 system. The flashing LEDs were kept at an arm's length from the eyes.



FIGURE 4.7: The Flashing LED device used to provide stimuli. Each stimulus was presented as a short luminance increase, a 20 ms flash, followed by 1s of zero brightness.

Each stimulus, in this case a flash of LED, was presented every second with a duration of 20 ms. This setting provides a visual stimulus. Thus, it is expected to have the signal with the greatest amplitude appearing on the locations close to the occipital lobe. The points POz and Pz were chosen respectively for the EPS and g.tec sensors. An EP sensor was positioned on the left mastoid to form a reference signal for the EPS system and the g.tec system was referenced to the right ear lobe. The gain on the EPS was 49.49 which had to be compensated for in software. Both sets of sensors were positioned on the head using the g.cap and the recording was done simultaneously.

The g.USBamp allowed for the MATLAB SIMULINK toolboxes to control the recording of the signal. Thus, SIMULINK was used to both record the signals and present a trigger for the LED device to present each stimulus. All the signal conditioning was done in the software in two stages. The first was during signal collection, online processing that



FIGURE 4.8: The recording was done in an unshielded bright environment. Various sources of electrical noise were present in close proximity of sensors.

included a 50 Hz notch filter for the EPS signal supplemented by a gain of $1/49.49$. Secondly, after the signal collection was done offline processing was applied to the signal to extract the VEP. The signals were filtered between 0.1 and 30 Hz. A 50 Hz notch filter was applied only to g.tec sensors. The recorded EEG was divided into individual trials based on the trigger signal recorded. Two hundred stimuli were presented. Each trail began at the onset of its stimulus, covering up to a second after the trigger. The baseline of these signals were removed. Thus, each trial would have a zero mean around the baseline. Finally, all these trials are averaged for all recorded channels.

Apart from these offline analyses, an online averaging routine was also performed to visually inspect the quality of recorded signal. The online averaging also followed the same steps as the offline averaging in terms of signal processing.

4.4.2 Results

Results comparing both EEG systems are shown in figure 4.9, including the cross correlation between the two. Both signals present a very similar shape. Most importantly, similar peaks can be observed in both signals with comparable amplitudes and exact same timings. Part (a) shows the recorded VEP by g.tec sensor from the Pz location. The EP sensor was positioned at POz, the result of its VEP is presented in Part (b). Part (c) confirms the close relation between the signals recorded by both systems with a cross-correlation value of more than 0.9 at time zero.

It was possible to observe the shape of this VEP in the online averaging routine after approximately 50 averages for both EPS and g.tec systems.

Further information can be extracted, in terms of VEP components, from closer inspection of figure 4.9a & b. If a boundary of 0 to 300 ms is applied to these signals, positive and negative deflections caused by the LED flash are much more visible. Figure 4.10 is a subset of 4.9a & b with the above time boundaries implemented in the VEP signal. These specific timings are set because the earliest detectable component forms a deflection after 30ms past the onset of the stimulus with a maximum latency of up to 300 ms. Various VEP components are marked on this figure, specially N2 (the negative peak at around 90ms) and the positive P2 peak at approximately 120 ms. These two are the most robust components of a flash VEP study [61].

Further results from the others sensors placed on the head is provided in appendix B. It is interesting to observe the effects on the signals recorded as the sensor locations move further away from the occipital lobe, the section of interest, on the head.

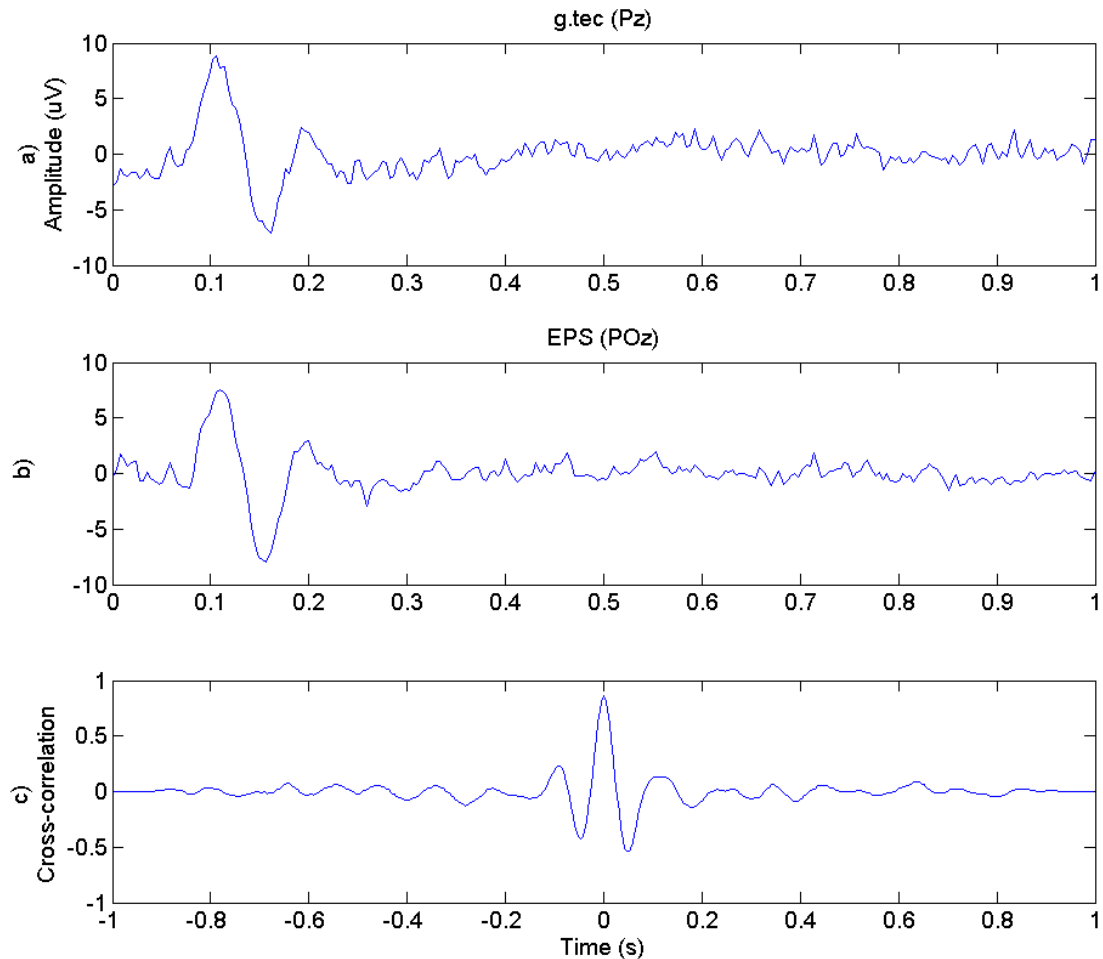


FIGURE 4.9: VEP recorded by g.tec system is shown in part(a) followed by the graph for EPS data in part (b). Both signals exhibit similar features and VEP components in terms of peaks and latency. A slight variation between the two signals is observed after 400ms. This can be explained by the variations that are expected due to the sensor location not being exactly the same on the head, POz and Pz respectively for EPS and g.tec. the graph in part (c) is the result of cross correlation between the above signals. It shows a maximum value of more than 0.9 at time zero. Noting that from 250ms onward both waveform stabilise at their baseline.

4.5 Discussion

ERPs can be studied under two conditions based on the actions required from the subject. In recording sensory ERPs the subject is asked to observe the stimuli passively. Whereas in a cognitive ERP the volunteer is asked to perform a task in response to a specific stimulus. The recorded signals are averaged according to a trigger signal, unlike the free running EEG. Online averaging is possible to visually inspect the quality of the recorded signal while running an experiment.

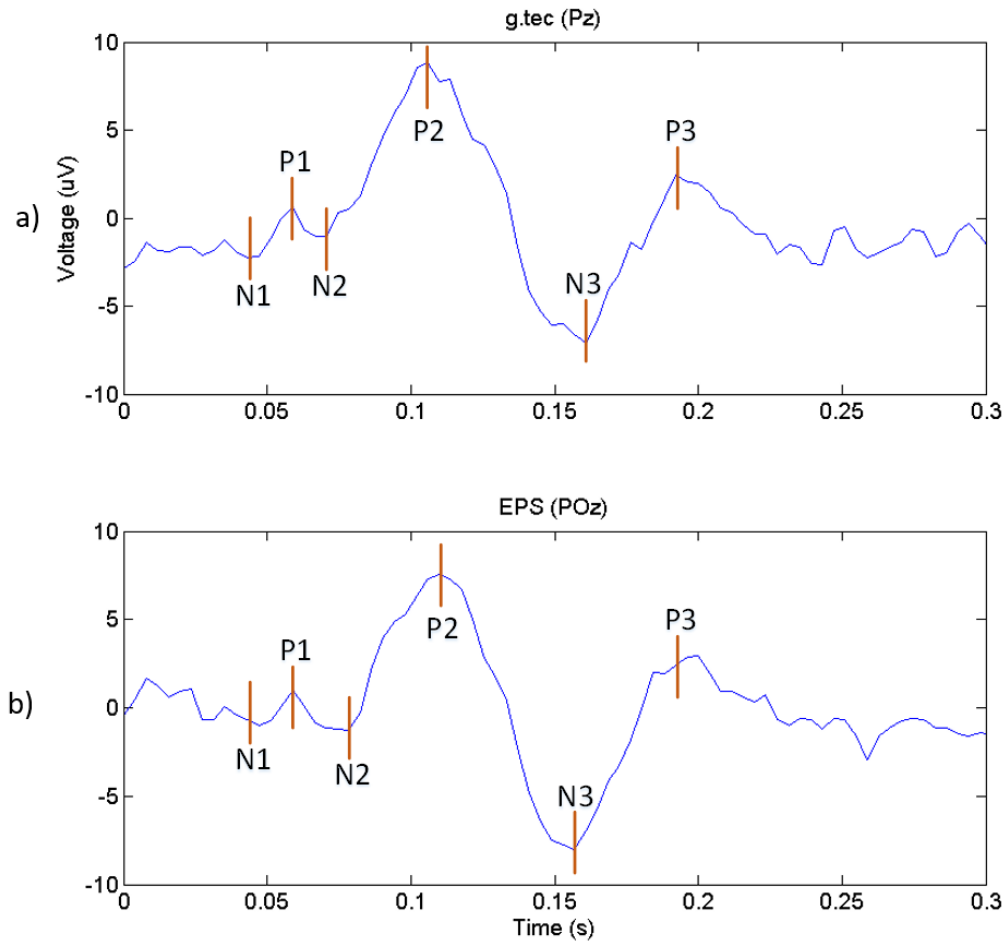


FIGURE 4.10: The first 300 ms of the signal from figure 4.9a & b are presented to facilitate a closer inspection VEP components of the recorded EPS waveform. Various element can be observed with the first negative deflection occurring at 40 ms after the trigger with N2 and P2 to follow at 90 and 120 ms respectively.

The EPS system was compared against two commercial systems to inspect the quality of signal recorded by the EP sensors. Two different VEP experiments were designed. Firstly, a checkerboard experiment was run using the ANT amplifier to record signals from both EPS and conventional gel electrodes. The results showed a closed similarity between both set of sensors with a cross-correlation of higher than 0.9. Secondly, a flashing LED experiment was conducted using g.USBamp as the recording device to compare EPS with g.LADYbird active gel sensors. A cross-correlation of more than 0.9 was observed. Different locations on the head were used for both signal and reference sensors, in the two experiments. Both showed the EPS can record VEPs through hair with results comparable to commercial systems.

Chapter 5

Cognitive ERPs

5.1 Introduction

This chapter will discuss the cognitive ERP and the techniques used to record it. The first section provides a brief overview of cognitive ERPs. This is followed by the second section where two ERP experiments are demonstrated. The first experiment is to simply record ERPs with EPS, and the second experiment provides a comparison between the signals record by the EPS and a conventional EEG system. The third section looks at the effects that artefacts have on the recorded signals and overall averages. Different types of artefacts such as movement and electrical will be discussed. Finally a brief discussion on this subject and the comparison study is provided.

5.2 Cognitive ERP

Sensory and cognitive ERP both present similar characteristics, albeit the later has more complex brain roots, in terms of voltage levels and signal components. The difference between the two is in the process of signal generation. In case of sensory ERP the volunteer

is asked to observe a stimulus while his or her EEG is recorded. Whereas in cognitive ERP the reaction of the participant to a given stimulus form certain components of the recorded signal [14].

Cognitive ERP has had a considerable impact on the field of psychology. However, recently these techniques have been used for brain computer interfacing (BCI). Motor evoked potentials (MEP) have been used for BCI. It was shown by [24] it is possible to control a quadcopter by reading the signals generated in the brain by imagining the movements of hands and feet. Further efforts have been focused on error-related potentials and their detection in single trial ERP by [65].

The experimental setup and the signal processing is also similar between the two ERP measurements, with the addition of a volunteer action from the participant in the case of cognitive ERP. This action is usually in the form of pressing a button (e.g. keyboard stroke), which involves body movement. The participants are commonly asked to remain motionless during a study in order to reduce the movement artefacts and DC drifts. Also devices used for producing stimuli can create electrical artefacts that will be present in the recorded signal (e.g. a cable carrying a high amplitude trigger signal)[14]. It is interesting to study the effects that these artefacts have on the EP sensors and to find possible steps to eliminate them.

Historically the ERPs are presented negative sign [14]. Thus the peak that is called N100 (negative 100) or N1 is presented above the zero baseline. The part 100 represent 100 ms which is the length of time it takes this peak to appear after the stimuli. This is not necessarily a strict time point and can vary from person to person, it is more an indicator of the first peak that is observed in an ERP signal.

ERPs are made up of distinguishable components, with different timings and amplitudes.

Characteristics or even presence of these component are affected by various factors such as intensity of a stimulus, its frequency, and whether that stimulus is task-relevant [66]. A distinguishing factor between sensory ERP and cognitive ERP is the presence of the P3 component (also known as P300 or P3b component) in the signal arising from a task related stimulus.

5.3 Oddball Paradigm

A simple experiment is described in this section that allows recording of ERPs. This study is based on the Oddball paradigm. It is used to show the ability of EPS in recording ERPs. Two stimuli are presented each indicating a distinct event, with a specific probability of occurring. A participant is ask to respond only to a specific event. The brain responses to all the events are recorded and averaged according to the type of event. The overall result compares the average response of the brain to both events, with the results expected to show a greater signal (ERP) to the event with lower probability of occurrence. This is the case although the participant is asked to only attend to the event with higher probability and ignore any other event.

5.3.1 Methodology

Two distinguishable stimuli are presented on a screen, each marking an event. One event is randomly chosen to occur more than the other. Using a keyboard a volunteer is asked to press the space bar only when they are presented with one of the events. This experiment was based on a similar experiment mentioned in [14]. These stimuli are formed of the letters 'X' and 'O', each one is displayed for 100 ms with a 1.4 s space between each

stimulus. The participant was asked to attend to the letter 'X' and ignore any other event.

Figure 5.1 shows the timing and shape of the stimuli that were presented to the volunteers. The letters were presented randomly on a white background, with letter 'X' being shown for 80 percent of the time and letter 'O' for 20%. The stimuli are shown at time zero. After 100 ms from the onset of a stimulus the letter is removed leaving a white screen for 1.4 s before the start of next stimulus. The total length of a trial is 1.5 s.

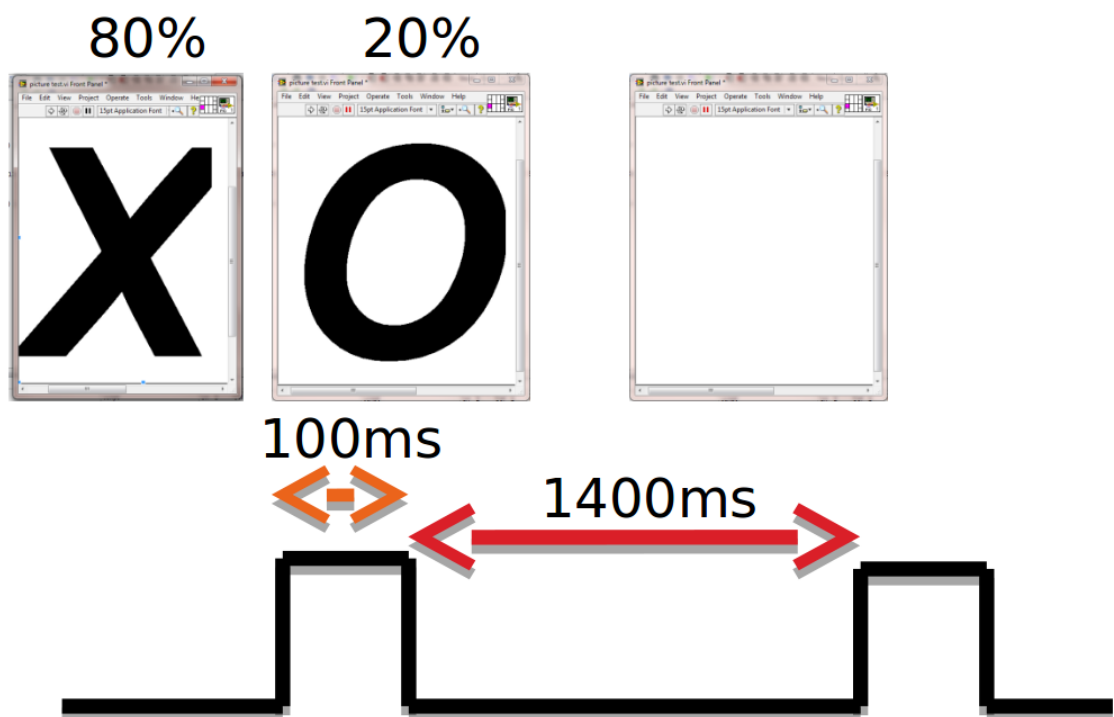


FIGURE 5.1: Oddball paradigm. Letters of 'X' and 'O' are presented on a screen for a duration of 100 ms as stimulus. After that time the image is replaced by a white screen. The letters are shown randomly with the probability of letter 'X' showing on the screen set as 80% and 20% for letter 'O'. A trigger signal is issued every 1.5 s indicating start of a trial and onset of a stimulus [14].

The measurement was taken outside of a screened room, in a noisy laboratory environment. A linked mastoid reference was used with a third sensor positioned at Pz to provide the signal. The sensors were powered using the rack described in chapter 3. The stimuli were presented using the NI LabView [67] program and the data recording was done using a Rohde & Schwarz RTO1012 [68] digital oscilloscope. In order to be able to reproduce the

timing of these stimuli a trigger signal was generated by the NI USB-6210 DAQ [69] and recorded by the scope along with the EEG signal buffered by the rack.

Three sensors were used in this experiment, one was positioned at Pz with two sensors placed on mastoids (M1 and M2) to form the reference signal. The signal from the reference sensors are mathematical averaged, thus providing a linked mastoid reference [6].

The LabView program written for this experiment can be found in the appendix A.

5.3.2 Signal Processing

A hardware bandpass filter of 0.1 to 30 Hz was applied to the output of the sensors. The low pass cut-off frequency of 30 Hz helps with reducing the high frequency noise (such as mains frequency) and also acts as an antialiasing filter for the digitizer. In addition to the internal gain of the sensors (x49.49) a variable gain of x100 was added in the amplification stage. This extra gain is implemented to compensate for possible use of low resolution ADC for digitization of the signal.

In ERP experiments the noise is commonly reduced by averaging, thus resulting in a logarithmic increase in the number of trials used to keep the noise low [13]. The digitized signal is then averaged according to the trigger signal recorded to reduce the presence of background EEG activity in the recorded signal.

5.3.3 Results

Figure 5.2 shows the results for 67 averages for an 80/20 ratio. The blue trace is the average of 53 trials for stimulus 'X'. The red trace represent the average of 14 trials for the stimulus 'O'. There is a clear time difference between the peak components of 'X'

& 'O' data as expected. The positive and negative peaks for 'O' happen later than the corresponding peaks for the 'X' and also have a greater amplitude as expected.

The P300 event is observed outside of the range of general latencies (300 ms). The ERP component may vary from person to person and the P300 in particular has been observed to be anywhere from 250 ms to 900 ms post stimulus [14].

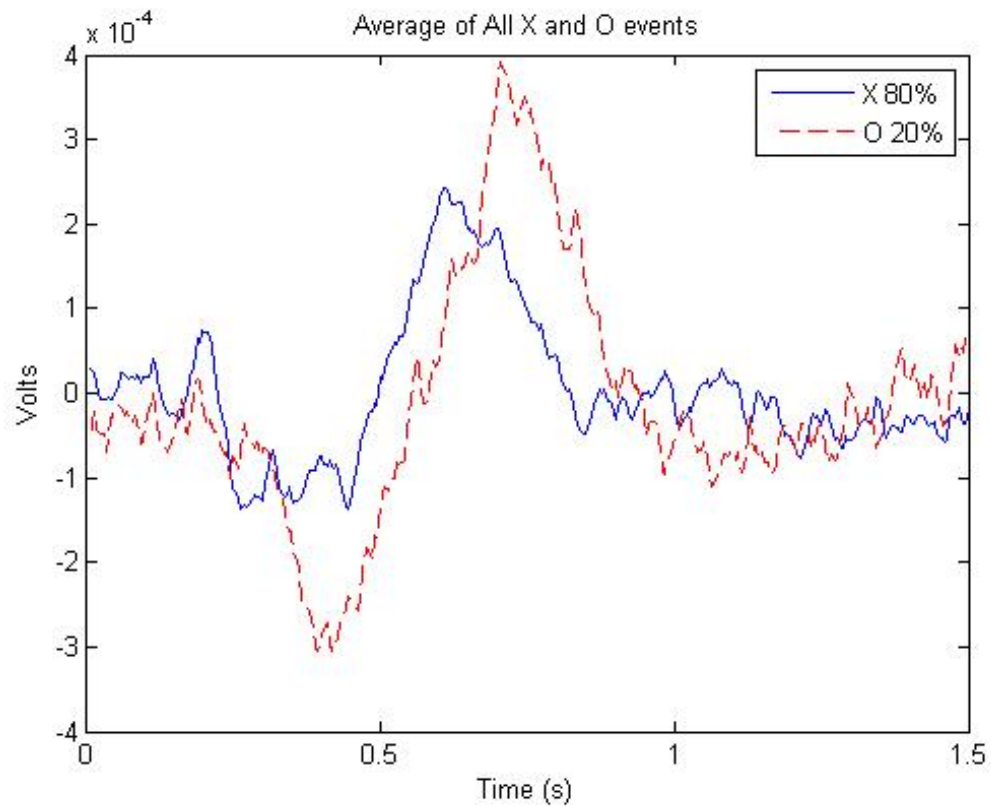


FIGURE 5.2: The averaged responses for both 'X' (attended) and 'O' (unattended) events. The blue wave is average of 53 trials for the 'X' stimulus, and the red wave is result for averaging 14 trials for the unattended event of 'O'. The latency between the corresponding positive and negative peaks of the two signals must be noted, along with higher amplitude for the red trace representing the unattended event

5.4 Face Processing Experiment

The next experiment was designed to determine if the EPS would also be sensitive to changes in the category of visual stimuli presented by using a classic face perception

paradigm known to reliably elicit early visual processing components [70]. Early event-related potentials that have been previously associated with face processing include the P1 and the N170. They are assumed to reflect, respectively, the extraction of fine/local information from a stimulus [71] and face-specific structural encoding [72]. When compared to other categories of stimuli, face stimuli consistently elicit a larger negative deflection in the ERP from around 150-200 ms after stimulus onset over occipitotemporal electrodes. Typically the N170 elicited by inverted face stimuli displays larger amplitudes over the right hemisphere and also occurs at a later time point compared to face stimuli of normal orientation [72].

5.4.1 Methodology

Four Participants were seated in a dimly lit electromagnetically shielded booth, 75 cm away from a LaCie [62] Electron blue IV 22" CRT Monitor. In the experiment subjects were shown stimuli of faces, which were presented in both upright and inverted orientations, and scrambled faces, see Figure 5.3, which were presented for 350 ms each. There were 120 stimuli in each category. Stimuli were presented using E-Prime 1.2 software (Psychology Software Tools, Pittsburgh, PA, USA). All stimuli were matched for luminance and displayed in frontal view. Scrambled faces were created by rearranging the pixels of upright face stimuli.

Participants were instructed to maintain central eye fixation and to respond as quickly as possible by pressing the space bar if the stimulus presented was an upright face. Stimuli were presented in a random order generated for each participant. A jitter of few milliseconds was introduced at the beginning of each trial so the effects of anticipation could be ruled out.

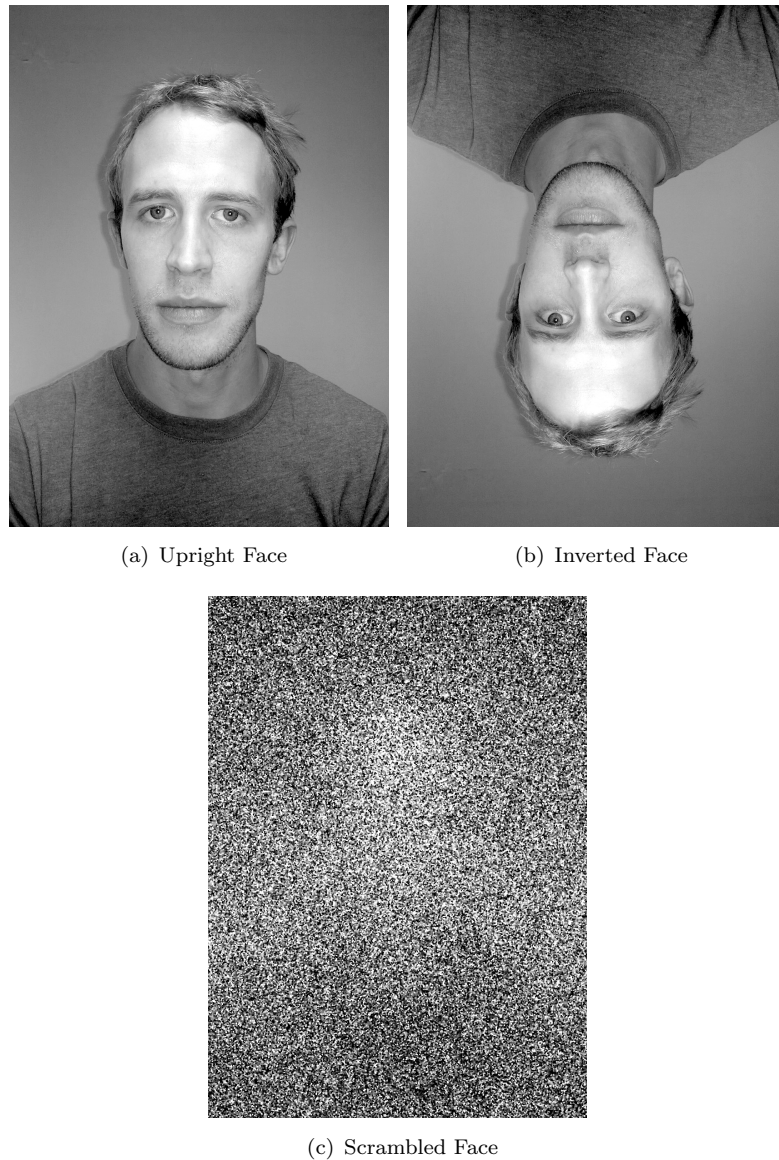


FIGURE 5.3: Examples of stimuli used in this study: (a) Upright Face, (b) Face inverted, (c) Scrambled Face.

Subjects performed the above experiment twice, first with the EPS set-up and then with standard EEG measurements. Three EPS were used placed at M1, M2 and P8 and connected to a 64 channel ANT neuro amplifier (model Refa8) [54] via the bipolar ExG inputs and data was recorded at a sampling frequency of 2048 Hz, with the left mastoid as a reference. Two vertical EOG and two horizontal EOG electrodes were used to record ocular artefacts for both EEG and EPS recordings. Conventional EEG was recorded with a waveguard 64-channel cap using the same amplifier at a sampling frequency of 2048Hz,

also with the left mastoid as a reference. To maintain consistency with the EPS setup three electrodes were used: M1, M2 and P8. All EEG/EOG electrode impedances were kept below 5 k Ω .

5.4.2 Signal Processing

EEG data was analysed offline with EEGLAB [63] and ERPLAB Toolbox [64]. Data was band-pass filtered from 0.1 to 30 Hz with a Butterworth digital filter and target locked epochs were created for each stimulus class, Face, Face Inverted and Scrambled Faces. Each epoch started 200 ms before onset of the target and ended 800 ms afterwards. Ocular artefacts were identified using a moving window peak-to-peak threshold, with a voltage threshold of 40 μ V. Epochs that exhibited excessive noise across all electrodes were manually rejected. Epochs were then baseline corrected for -200 to 0 ms before stimulus onset. Stimulus locked epochs were then created for the three conditions Face, Inverted Faces and scrambled faces and averaged across each condition. In order to compensate for the built-in amplitude gain in the current EPS sensors, EPS data was divided by the value of 49.49 to make it commensurate with the ANT EEG data.

5.4.3 Results

As can be seen from Figure 5.4 both the EEG and EPS recordings produced remarkably similar early event-related potentials and produced a standard evoked response to face stimuli. Early event-related potentials (ERPs) that have been previously associated with face processing are the P1 and N170. The results show that the EPS are sensitive to the category of stimuli presented. The finding of larger amplitudes N170 over the right hemisphere was replicated and occurs at a later time point for inverted face stimuli compared to face stimuli [72].

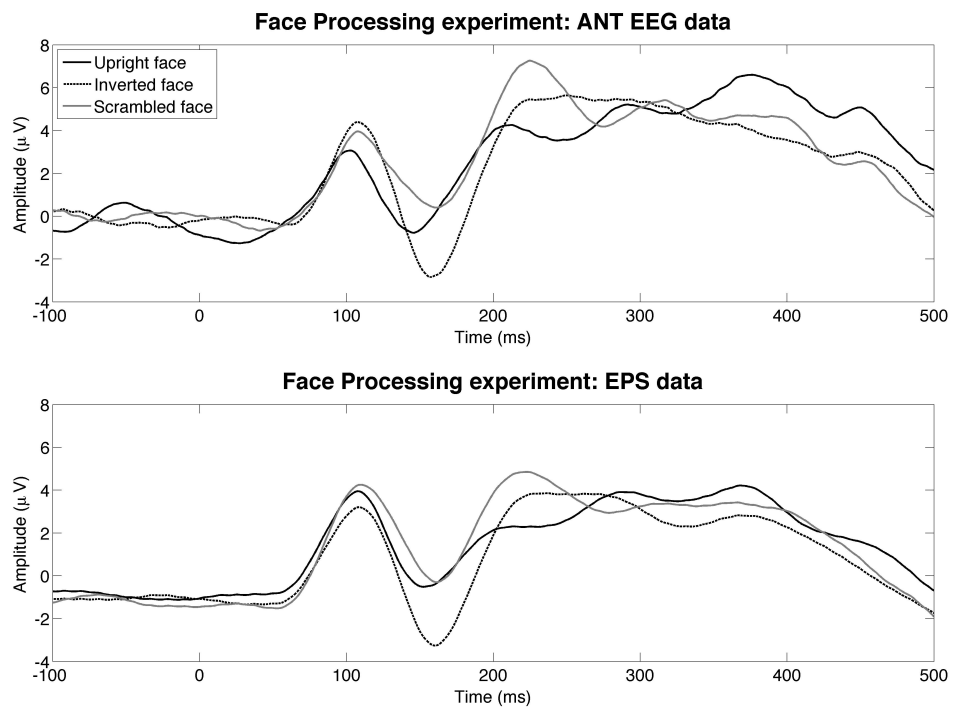


FIGURE 5.4: Grand-average ERPs ($n=4$) displayed between -100 and 500 ms for 3 categories, upright faces, inverted faces and scrambled faces over occipitotemporal electrode (P8). Note the larger N170 component for upright and inverted faces compared to scrambled faces.

5.5 Recording Artefacts

A number of different artefacts can be observed while recording ERPs. Some are directly related to the task that a participant has to perform after observing a certain stimulus, such as pressing a button. Others are indirectly related to recording ERPs such as the signal generated by a cable carrying higher amplitude (compared to EEG) trigger information.

5.5.1 Key Stroke

In cognitive ERP experiments a participant is asked to perform a certain task after he or she detects specific stimuli. In the experiments that were carried out in this chapter participants were asked to press the space bar on a keyboard. Figure 5.5 shows the EEG signal for a duration of 4 seconds, where a key stroke happens at time 1.5 s. Both figures

5.5(a)&(b) are the same time section of a EEG recording but (a) shows a high amplitude artefact at time 1.5 s compared to (b). This artefact is removed by rereferencing the raw O1 signal to M1 before performing any other postprocessing.

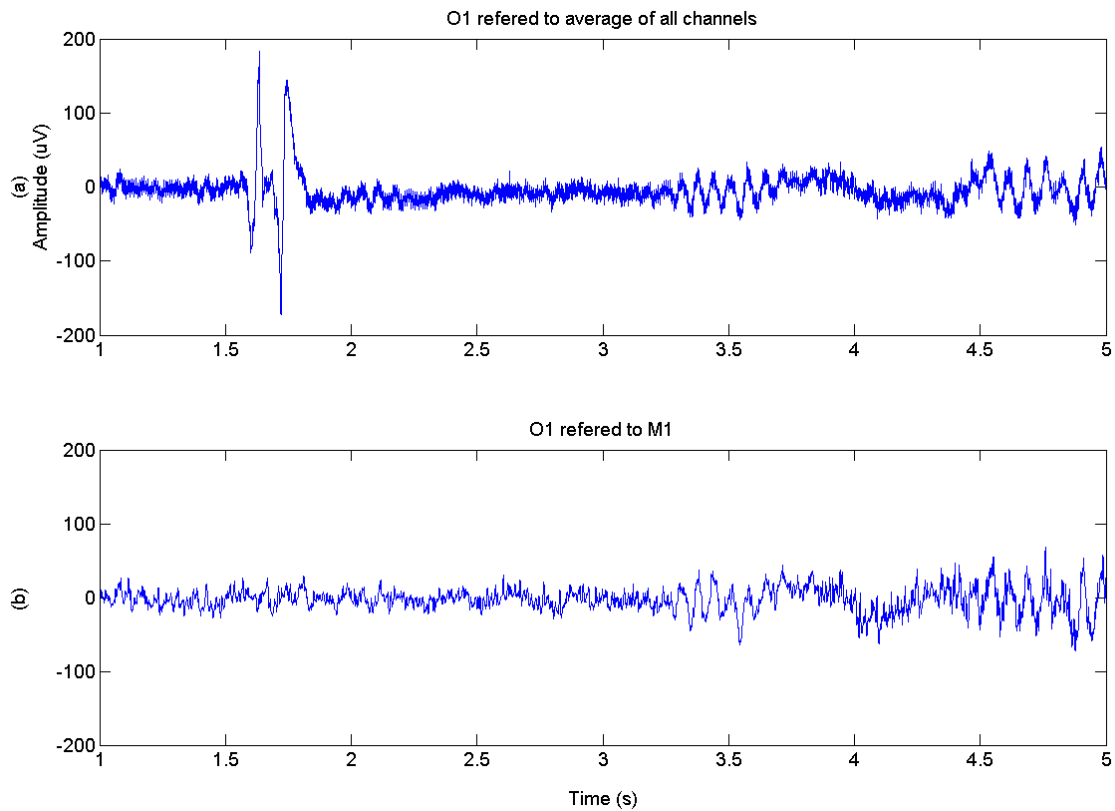


FIGURE 5.5: Noise generated due to a key stroke. Comparing part (a) and (b) a high amplitude disturbance is observed at time 1.5s in trace (a). The timing of this artefact was measured to be same as the key press data recorded from the keyboard used in that experiment. In part (a) four seconds of data are collected from location O1 on the head and the raw signal is referred to average of all channels on the head. Part (b) presents the same time section of signal as part (a) where the O1 raw data is referred to M1 instead.

5.5.2 Referencing Artefacts

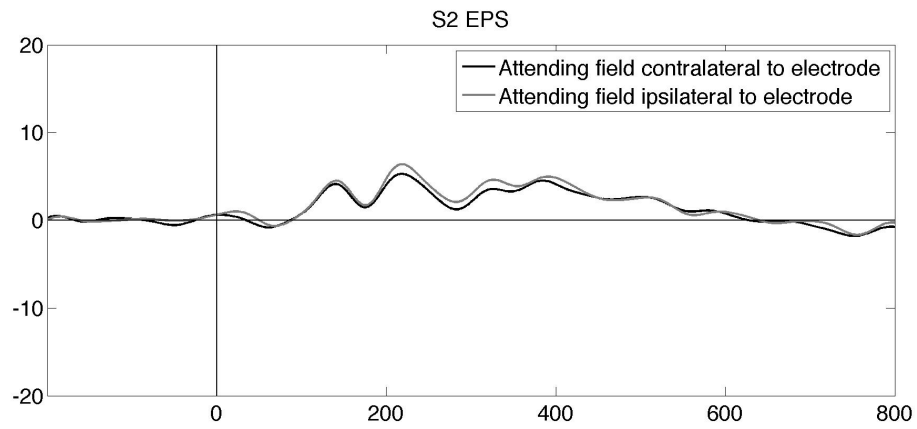
To study ERPs time locked averages of the EEG signal are produced to reduce the presence of noise and the background EEG. If more than one volunteer has participated in an experiment a grand average of all the ERPs for all the subjects is produced. In reproducing a experiment it is important to adhere to the experimental setup that is mentioned in the literature. In this section result of a study is discussed where the outcome was different

from the instated result in the literature. However, the outcome was consistent between the two systems used for running this study.

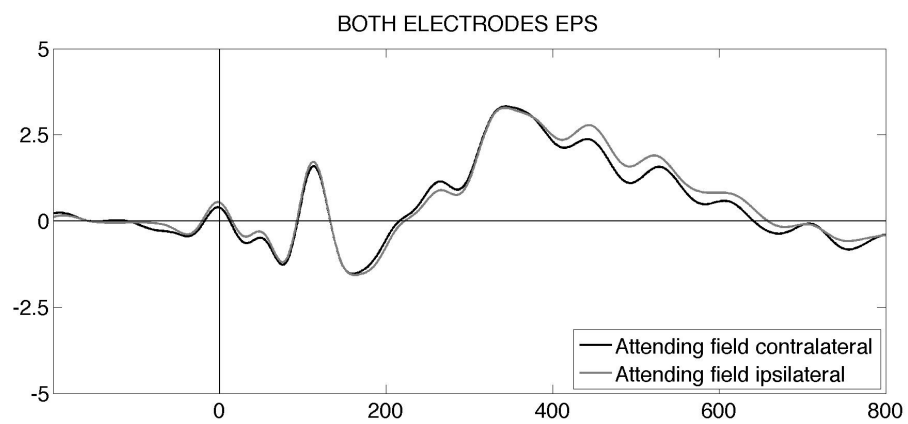
An experiment was conducted with nine participants. Specific characters were shown on the left and right side of a CRT monitor, while the participant was asked to attend to a specific field of vision at the beginning of each block of trials. This experiment was made of 10 blocks with 20 trials in each block. Each subject was asked to press the space bar on the keyboard in front of them in presence of a certain stimulus in the field of vision that they were asked to attend. Two sensors were positioned at O1 and O2 to record the response for each eye, with 2 further sensors positioned at M1 and M2 to provide reference signal. This experiment was based on the spatial awareness study performed by [73]. The same settings were applied to both the EPS and the ANT systems.

The results are shown in figure 5.6. Part (a) shows the ERP recorded by the EPS from subject two. The results shown are typical of the other 9 participants. These results did contain an ERP which was different from the expected result mentioned in the literature. Parts (b)&(c), which are the grand averages of all the participants recorded by EPS and ANT respectively, do demonstrate similar characteristics for both systems. A reason for this effect can be found in the way the referencing is done in this experiment. In the original experiment the reference was set as the average of all the 64 channels on the head where as in this case merely an average of M1 and M2 was used.

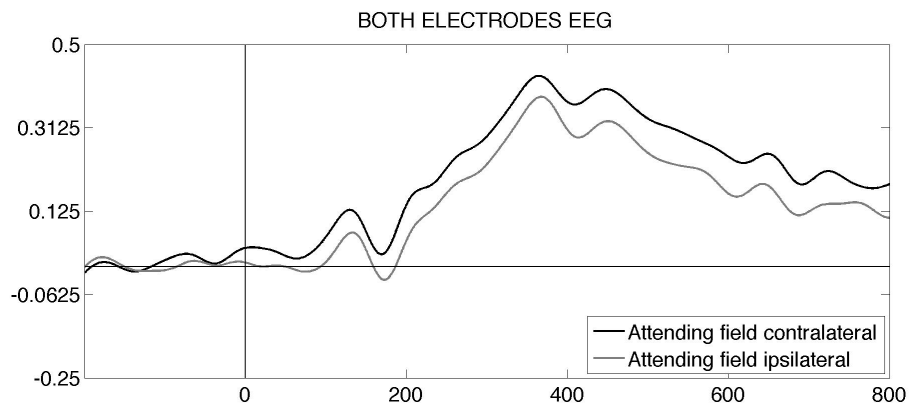
Furthermore, an extra peak is observed at time zero in figure 5.6(b). A deflection is not expected to happen at time zero as the brain processes are always delayed by a few milliseconds from the onset of a stimulus. The nature of this peak was found to be the noise pick up from the cable carrying high amplitude trigger signals. This is investigated more in the next section



(a) ERP of the second participant recorded by EPS.



(b) Grand Average of 9 participants for EPS.



(c) Grand Average of 9 participants for ANT.

FIGURE 5.6: (a) Shows the result from a single subject, The grand average result for 9 participants in (b) & (c) do show waveforms that are similar for both ANT and EPS. However, these results do not match with the expected results in the literature. Thus making these results unacceptable. One reason can be the difference replicating the original experiment, specifically in choosing a reference signal. In the original experiment the reference signal was chosen as a average of all the electrodes in the head (64 channels were used), whereas in this experiment the mathematical average of the mastoids was used for both ANT and EPS system. The rise at time zero in part (b) should be noted, it is the result of the trigger signal being picked up by the EPS and not a neural activity.

5.5.3 Trigger Signals

Commonly a trigger signal is sent to a device such as a monitor or a LED box to initiate presentation of a stimulus. These devices usually operate at higher voltages, such as 5 V, compared to the EEG signal being recorded. The field that these trigger signals generate is observed by the EPS. In the EPS data shown at figure 5.6(b), at time zero a peak is visible which is due to noise from the trigger signal being picked up in the EPS data. This was studied more closely in an experiment where a participant was asked to perform a similar task as in Spatial awareness study while his EEG was recorded. The only difference was the trigger signal that was used to operate the monitor was set at 5 different logic levels of 1 to 5 volts. The result is shown in higher detail in figure 5.7. Recorded signals are averaged based on the value of their corresponding trigger signal. A negative peak at time zero is observed for both sensors positions P7, figure 5.7(a), and P8, figure 5.7(b). The amplitudes of these peaks are proportional to the voltage levels of their corresponding trigger signal. Altering the trigger signals and setting them all to the same voltage resolved the issue as it was removed by common mode rejection.

5.5.4 Movement Artefact

The final artefact observed while conducting ERP experiments is a general movement artefact. As the participant is asked to perform some tasks a minimal movement is necessary which introduces an artefact into the recorded signal. Figure 5.8 demonstrates such artefacts recorded by the EPS. A base line signal is shown from time 0 to 1.5s, this is when the subject is seated and has no movements. From 1.5 to 6s the participant is instructed to make hand and head movement while remaining seated. Although this does not disturb the baseline much the effects are still noticeable. However, when the participant is asked

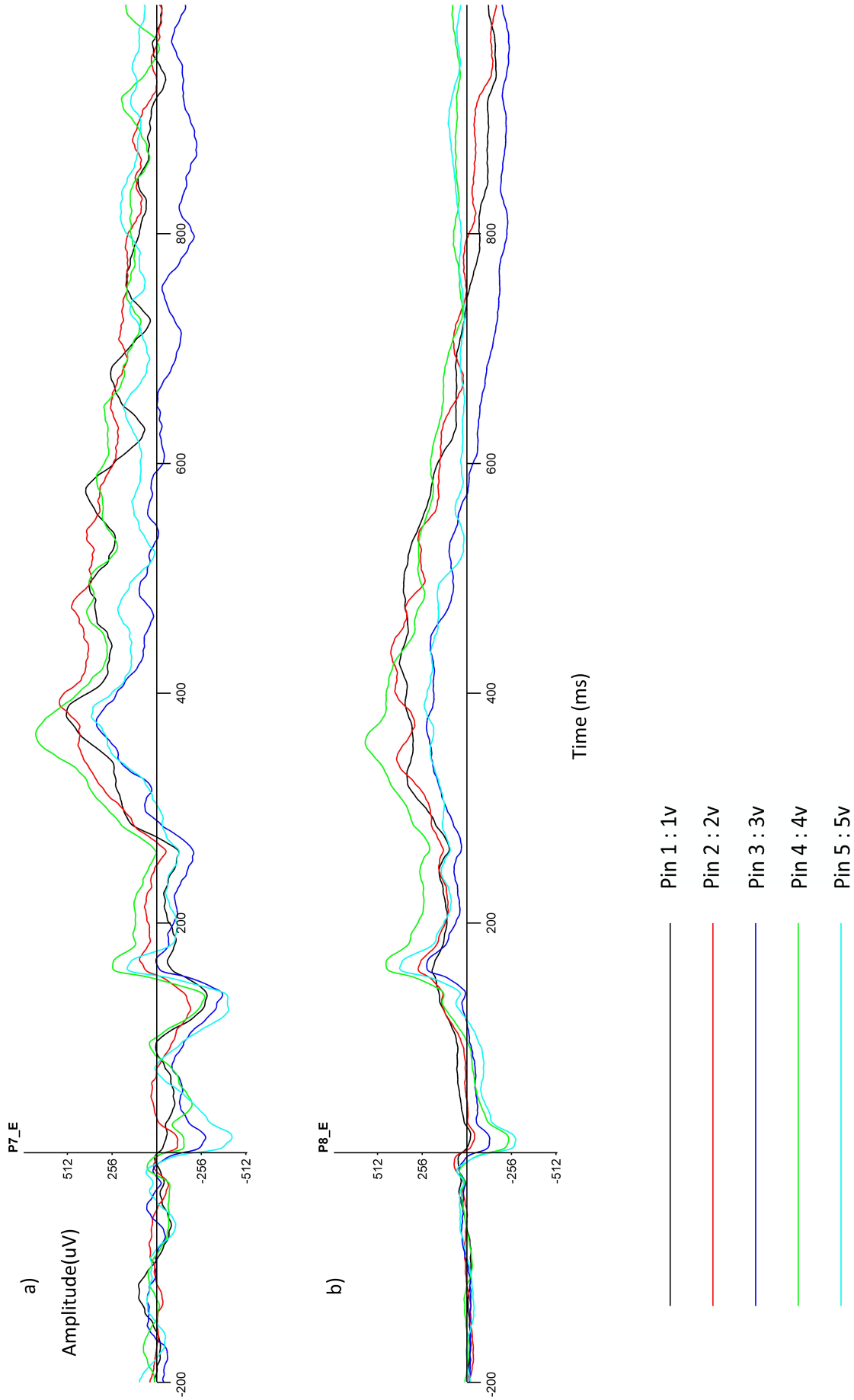


FIGURE 5.7: Noise generated due to parallel cable used for sending the trigger information. A participant was asked to perform a similar task as the Spatial awareness study. The difference in the recording conditions was that the trigger signals were set to five increasing logic levels of 1 to 5 V. The effects can be observed for two sensors positioned at P7 and P8 in parts (a) and (b). A negative deflection proportionate to the value of the trigger signal is observed at time zero.

to stand up from his seat the recorded signal is highly disturbed. This can be seen in the data in figure 5.8 from 6 to 7 s where deflections of more than half a millivolt is observed.

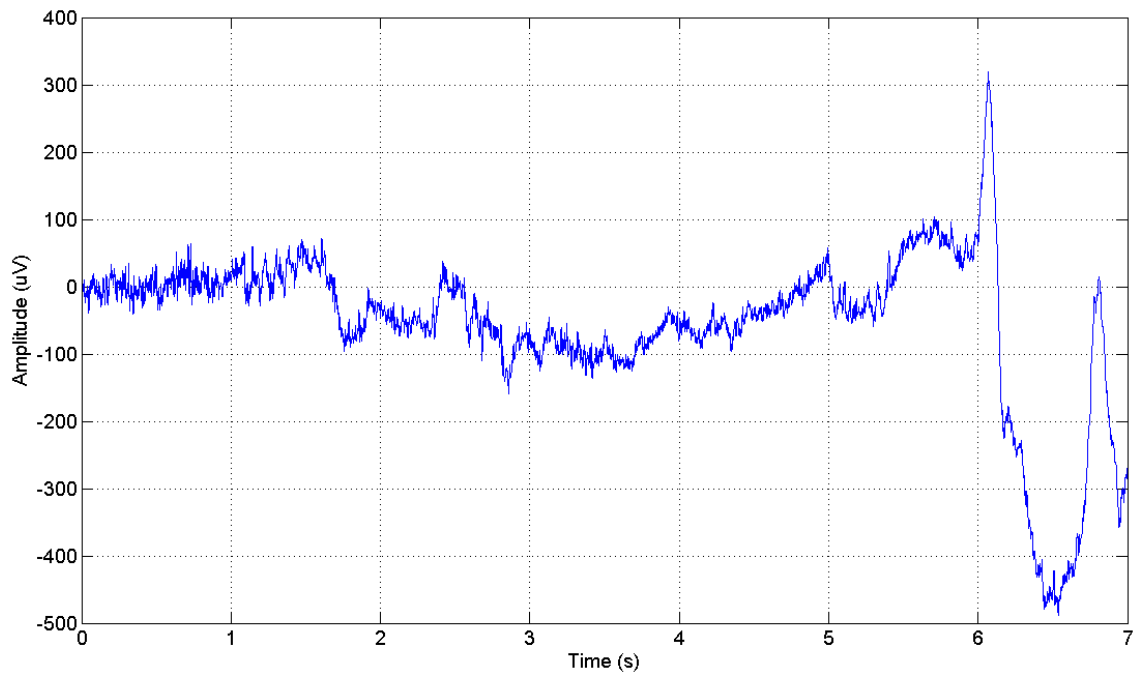


FIGURE 5.8: Noise generated due to movement artefacts recorded by the EPS. From time 0 to 1.5s the participant is asked to remain seated with no movements. This shows the subjects baseline at rest. The participant is then asked to perform hand and head movement while remaining seated, the result can be seen as small deflection starting from 1.5 to 6s. Finally drifts of more than 0.5 mV is observed from 6 to 7s where the participant is asked to stand up.

These deflection can be divided into three categories. The first is the noise caused by cable movement. Long cables are connecting the EP sensors to the amplifier box. This acts as an antenna for any external signal source, coupling noise into the output signal. Shielding the cable as shown in chapter 3 reduces this antenna effect[50]. Another issue with using cables is the fact that as the person moves the cable is flexed and vibrated. This generates triboelectric noise as a result of friction between the conductor and its insulator[74]. A possible solution is to use a wireless interface to remove the cables.

The second category is the noise created by the changes in surface potential of a participant relative to the floor. If the participant rubs his leg on the floor this introduces charge to his body surface. The solution is to place a conducting mat (connected to the system

ground) on the floor where the participant is positioned to reduce the DC offset caused by the changes in the body surface potential when the participant is lifting their foot from the floor.

The third source of deflection is motion artefact picked up from other bodies present around a participant. Presence of an external body changes the local electric field surrounding the sensor, specifically as the bodies move this becomes a varying electric field. The EPS does display a higher sensitivity to this motion artefact from surrounding environment compared to standard EEG recordings. When the EPS is in contact with skin the case enclosing the sensor is also placed on skin, thus shielding the input electrode from other external sources. However, when used on the head there is a layer of hair separating the skin from the case, which in return reduces the shielding effect of the case for blocking external noise sources such as movement from another person[75].

5.6 Discussion

The waveform of a cognitive ERP bears similar characteristics to a sensory ERP. The difference arises in recording of these signals where the participant is required to perform an action as opposed to being a passive observer. A simple Oddball paradigm was presented with the results demonstrating an ERP recorded with a very low number of averages (14) for the signal recorded by the EPS in an open noisy unshielded environment. Furthermore, a comparison study was conducted using EPS and ANT systems to record ERPs based on a face processing experiment. The results showed consistency between the two systems between four different participants.

Different movement and electrical artefacts were studied with a view to how their presence would effect ERPs recorded by EPS. Most of the artefacts are found to be removed by

using correct referencing for the signals. A key stroke was shown to be removed by means of referencing the raw data. Electrical noise was shown to have an effect on the recorded ERPs, introducing an additional peak at time zero, due to trigger signal level. Careful design of a study that kept all the trigger signals at the same voltage level proved to eradicate this deflection. However, certain signals such as movement could not be successfully removed. Another solution in terms of wireless interfacing will be introduced in the next chapter.

Chapter 6

Wireless Connectivity

6.1 Introduction

In recording EEG it is common place, for medical or research purposes, for the subject to be seated with electrodes connected to their head with wires to an amplifier. Often the participants are asked to make minimum movement while the measurement is conducted. These practices imposed by the limitation of the current wearable EEG technology forces measurements to be conducted in a laboratory environment[76]. If the device is to be worn for many hours or days, for example in case of epilepsy monitoring, three main factors exist that limit the usability of a wireless EEG system. Firstly, the power consumption is a key factor, most recent advances show a usage of one day for a limited channel system. Dias et al. (2012) presents a system that can last for about 25 h for a system with 6 electrodes[77]. Secondly, EEG can be captured using 200 samples per second per electrode [78]. However, as a high number of electrodes is necessary in monitoring patients, and to avoid spatial aliasing which could require up to 600 sensors[79], this would point

to a much higher required bandwidth. Last but not least, movement artefacts associated with contemporary wearable electrodes effect the signal quality.

The above issues could be decreased by integrating the EPS within a wireless setup. This chapter explores to combine portability with ease of use and long term functionality.

6.2 Wireless Standards

A number of wireless standards have been developed for different data rates and applications, such as IEEE 802.11 (Wireless LAN) [80] and Bluetooth[81] and IEEE 802.15.4[82], all operating at 2.4 GHz . Both IEEE 802.11 and Bluetooth (up to version 3) are designed for high data rate communication with data rates of higher than 54 Mbit/s and 2 Mbit/s respectively[80][81]. These standards are designed for high data rates and continues transmission, which in turn reduces the battery life and increases their system resources (more than 1 MB for IEEE 802.11 and more than 250 KB for Bluetooth[83]). The alternative is to use lower data rates which is implemented in IEEE 802.15.4 standard and more recently in Bluetooth Low Energy. The relative low complexity of these standards allows for a much simpler system to be used as the required resources are less (The code size of a network based on IEEE 802.15.4, depending on its implementation, can be from 4 KB to 32 KB)[83].

6.2.1 IEEE 802.15.4 Design

The IEEE 802.15.4 is designed to support data communication with data rates of up to 250 kbps. This standard defines the Medium Access Control (MAC) and Physical Layer (PHY). Three frequency bands of 2.4 GHz, 915 MHz, and 868 MHz are used with the corresponding data rates of 250 kbps, 40 kbps, and 20 kbps[84]. The protocol is

designed to maintain communication within line of sight with a distance of 30 to 100 m. The IEEE 802.15.4 only defines the lower layers of a communication protocol, thus a network layer should be implemented to facilitate the interaction between the applications and the communication radio. Zigbee alliance[83] has defined a network topology which has been implemented to take advantage of the MAC and PHY designed for low rate communication. The IEEE 802.15.4 allows for a data rate of 250 kbps, however, when the Zigbee network layer is implemented a trade off is made to accommodate for security and addressing defined by the Zigbee. This has resulted in a reduction of throughput down to 46 kbps[85]. This allow only a fifth of the bandwidth to be effectively available to application layer. This is fine in lower data rate applications such as temperature monitoring were the rate of change of data is very low (minutes or hours), or in usages were latency is not critical. However, the case can be different were the data rate needs to be higher, which in return results in the radio to be on a high duty cycle and thus consuming a higher power.

In case of a device that is designed to collect EEG from a differential measurement, thus producing a single data channel, a sample rate of at least 200 samples per second is necessary as mentioned earlier. The following shows the calculation for finding the bandwidth required by such a device:

$$200\text{Samples} * 16\text{bits} = 3200\text{bits}$$

$$3.2\text{kb}/46\text{kbps} = 70\text{ms}$$

It should be noted that although 70 ms for transmission of 200 samples is not a long time, the system defined is a very simple design with only two nodes (a sensor node and a coordinator). It has been shown that further improvement to the network layer can increase

the throughput of a Zigbee network. Simulations for Zigbee in network simulator software NS2[86] and hardware specific implementations of Zigbee network allows for higher data rate of 110 kbps [87]. Improvements in throughput, however, can be added to by reductions in code size. The Zigbee stack developed by Flexipanel (based on a design by Microchip)[88] is 50 KB for a sensor node. This could be reduced to a much smaller size (for the design proposed in this work ,including both the network and application layer, it mounts to 9 KB) therefore allowing for less resource to be tied up to the network topology and more space for complex applications (e.g. data compression) or storage.

The system designed in this work is shown in Figure 6.1. It is based on a low power microcontroller from Microchip, PIC18LF2520[89]. The chips operated on 1.8 to 3.3 V. The communication radio is implemented using a CC2420 designed by Texas Instruments. Both chips comes as an off the shelf product combined with an on board PCB antenna designed by FlexiPanel. A board was designed to condition the analogue signal from the sensors and feed it to the internal analogue to digital converter of a microcontroller. This microcontroller has a 10 bit digitizer with a input range of V_{ss} to V_{dd} , with an option to define a reference for the higher limit. Two sensors were connected to the board allowing for a bipolar recording with one used as a reference and the second sensor for recording EEG. The board powers the sensors and the output signal of the sensors are fed into a differential amplifier. A programmable gain amplifier is added after this stage with gain settings of 1, 2, 5, and 10. The variable gain could be used for changing the input range of the sensor to suit different number of biopotential such as ECG and EOG as well as EEG. More detailed board design can be found in appendix C.

A simple network and application layer was designed to facilitate the data conversion and transmission task. A simplified implementation of the Network layer is shown in Figure 6.2. This shows the requests exchanged between a sensor node and a coordinator. The

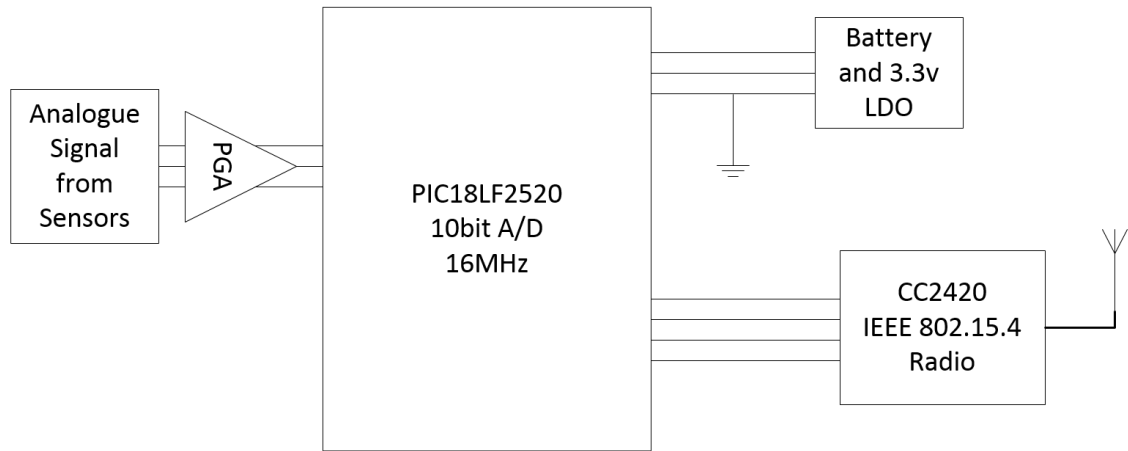


FIGURE 6.1: Wireless System Design based on CC2420 radio chip which has MAC and PHY layer hardware implemented. The network and application layer are programmed on a low power 8 bit PIC microcontroller. The analogue signal from the sensors is filtered. The gain of the input signal to the A/D can be controlled through a PGA which can be remotely configured from 1 to 10.

coordinator acts as a bridge between the wireless data and a computer. The sensor node collects the data from the sensors and digitizes them so they could be transmitted. Each device is issued a unique address. The coordinator first transmits an availability request to a specific sensor node. If an acknowledgement is received then the coordinator can request further functions such as start of data transmission or specific hardware changes (e.g. gain). This resembles a simple point to point communication link, but as the coordinator is allowed to broadcast messages and the sensor nodes are only permitted to talk to the coordinator this could be expanded based on a star topology.

The coordinator is often implemented as a more powerful device running on a higher clock frequency than a sensor node. The coordinator is often powered by mains or connected to a computer. This allows it to be always on[90]. In this work the Coordinator is implemented in hardware using a PIC18LF4620 with the addition of a UART to USB converter, schematic design can be found in appendix C. The UART converter allows the coordinator to communicate with a USB port on a computer to interact with software such as LabView for recording and analysis of the incoming data. The LabView interface

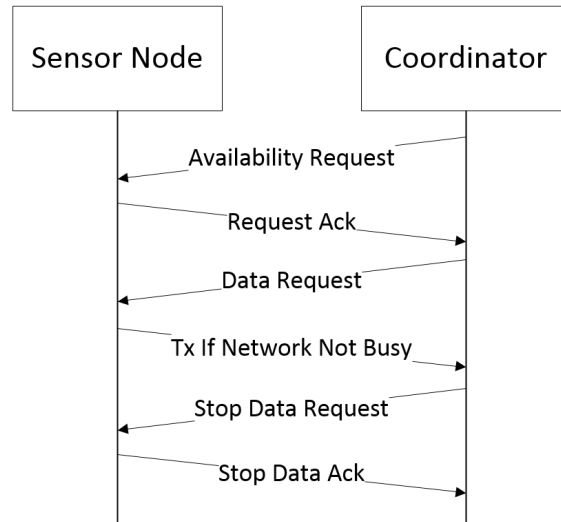


FIGURE 6.2: Network Protocol; the availability of a sensor node is firstly check by sending a request using the allocated unique address. If it is present the other actions can be requested such as start of data transmission or hardware changes such as varying gain.

designed for this work can be seen in figure 6.3. The complete LabView block diagram is presented in appendix A.

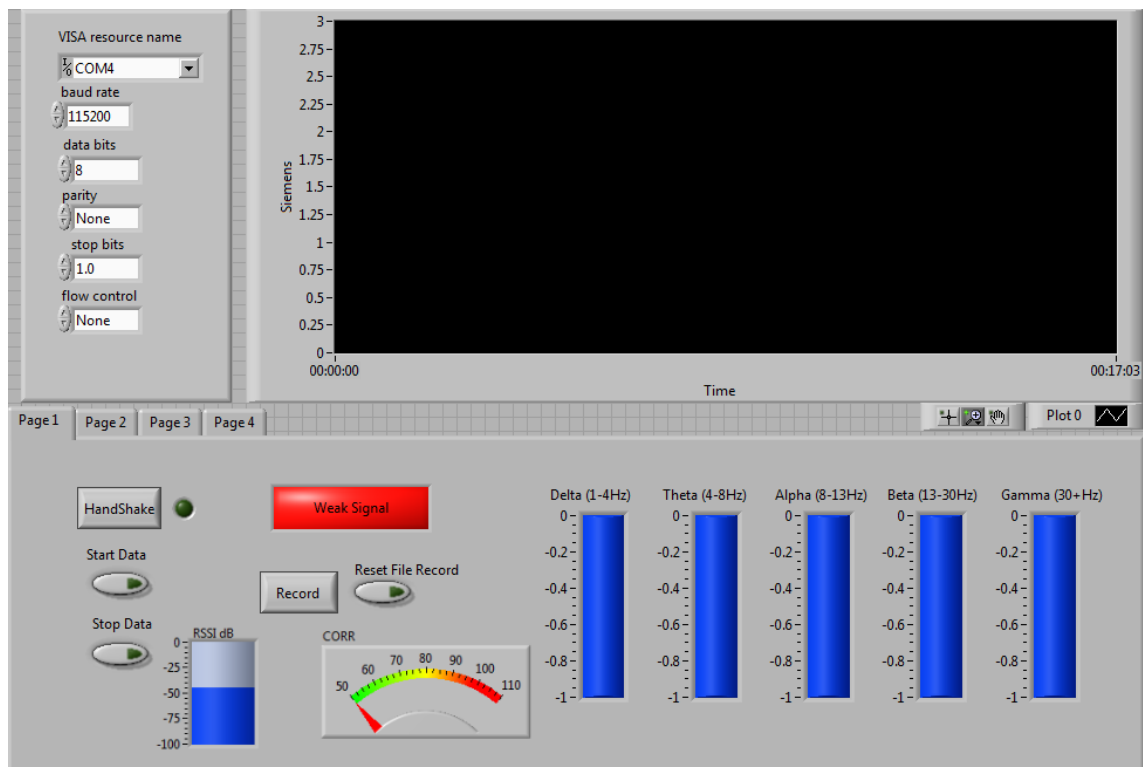


FIGURE 6.3: LabView interface front panel.

The sensor node is required to run on battery power and is to function for extended periods of time[90]. To achieve longer battery life consideration on both software and hardware

side should be made. The microcontroller chosen is a low powered PIC18LF2520 running at 16 MHz from an external oscillator. The supply voltage can be 2.1 to 3.6 V. The supply current was measured at 4 mA which can decrease to less than 1 mA in idle mode and 1 μ A in sleep mode[89]. The current consumption of the whole design rises to 23 mA in either transmitting or receiving mode when adding the power consumed by the radio chip. In order to calculate the overall power consumption, the current taken by analogue part is also measured to be 22 mA supplied from 5 V. This brings up the total power consumption to 179 mW. The data is collected continuously but is transmitted in lumps of 25 samples. Therefore, it is possible to further reduce the power consumption by decreasing the time that the radio chip is on either transmit or receive mode. The radio is measured to transmit a packet of 25 samples (the packet includes 50 bytes of data and 11 bytes of addressing and other overheads) in 3.24 ms. If the sampling rate is set to 250 samples per second then it would take 32.4 ms to transmit one second's data. For rest of the time the radio could be switched into a idle state to conserve power. When recording 250 samples per second, a sample is digitized every 4 ms. This does not provide enough time for the analogue circuitry to be switched on and off and settle in time in order to make further reductions in power. The break down of the transmission time measured for a single packet of 25 data samples is as follows:

- 940 μ s Setting up the transmitter and filling the Tx Buffer
- 300 μ s Preamble Sequence
- 2 ms Data transfer
- 3.24 ms Total transfer time

Data transfer time and Preamble sequence are limited by the speed of IEEE 802.15.4 standard. However, the set up time at the beginning is limited by the resources of the

micro controller used. Much of the 940 μs spent is used up for copying the data from A/D buffer to the Tx buffer in the radio chip. If a microcontroller with DMA was used then this time could have been used by the micro controller to perform other task. Newer chips such as nRF51822 by Nordic Semiconductor[91] use what is called an EasyDMA. The nRF51822 is a system on chip (SoC) which both include a microcontroller and a radio transceiver on a single chip. The EasyDMA allows for copying the data from A/D buffer to the Tx buffer without CPU intervention, thus reducing the overall cost of transmission time.

Dias et al. (2012) reported a power consumption of 107mW per channel with a design based on IEEE 802.15.4[77]. Chi et al. (2010), have developed a system using Bluetooth communication scheme which draws 300 mW per channel[92]. Obeid et al. (2004) designed a module based in the IEEE 802.11b standard, their design consumed 330 mW per EEG channel [93].

6.3 Data measurements

The following section presents the data collected using the developed wireless module. It contains comparison with a wired version of the same analogue sensors. The EPS sensors are powered by the wireless board. The analogue front end of the board is similar to figure 3.8 mentioned in chapter 3 with omission of the on-board notch and low pass filters.

6.3.1 ECG

The first data to be measured was ECG, as shown in Figure 6.4 and 6.5 for both time and frequency domain respectively. Both figures compare the data recorded when the system, both wireless board and the sensors, is powered by a laboratory bench power supply in

part (a) and by battery in part (b). The presence of mains frequency, 50 Hz, and its harmonic, 100 Hz, should be noted in part (a), where as it is absent in part (b) when the system is solely powered on batteries.

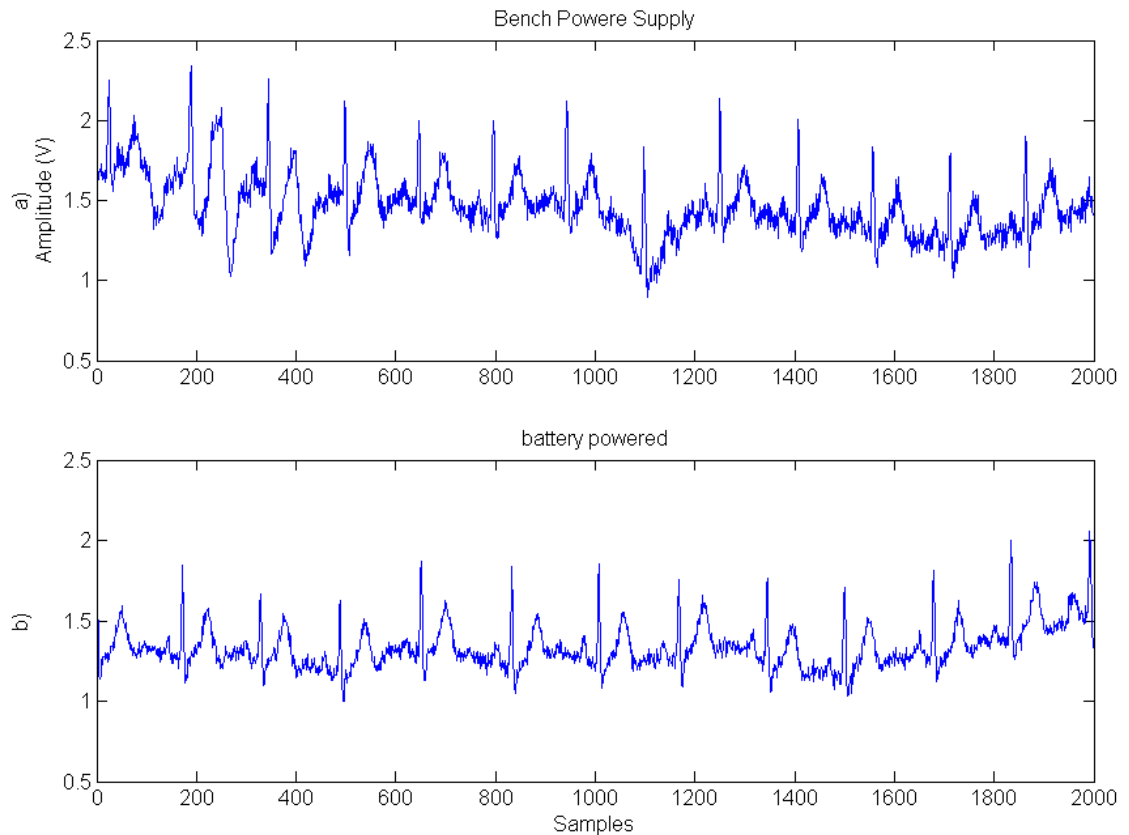


FIGURE 6.4: Time domain wireless ECG, comparing (b) battery powered with (a) bench supply noise

6.3.2 EEG

The alpha signal is observed when the eyes are closed or relaxed and is characterised by an increase in amplitude of 8-13 Hz EEG signal. Alpha activity is not normally observed when the eyes are open. The signal may be seen in real time in the time domain, as shown in figure 6.6, where the alpha blocking caused by opening the eyes may be seen clearly. Alternatively, if the time series data is Fourier transformed we see a broad peak in the frequency domain data. This is illustrated in figure 6.7 where a 40 s section of time series alpha data has been Fourier transformed to show a clear 10 Hz peak. A residual

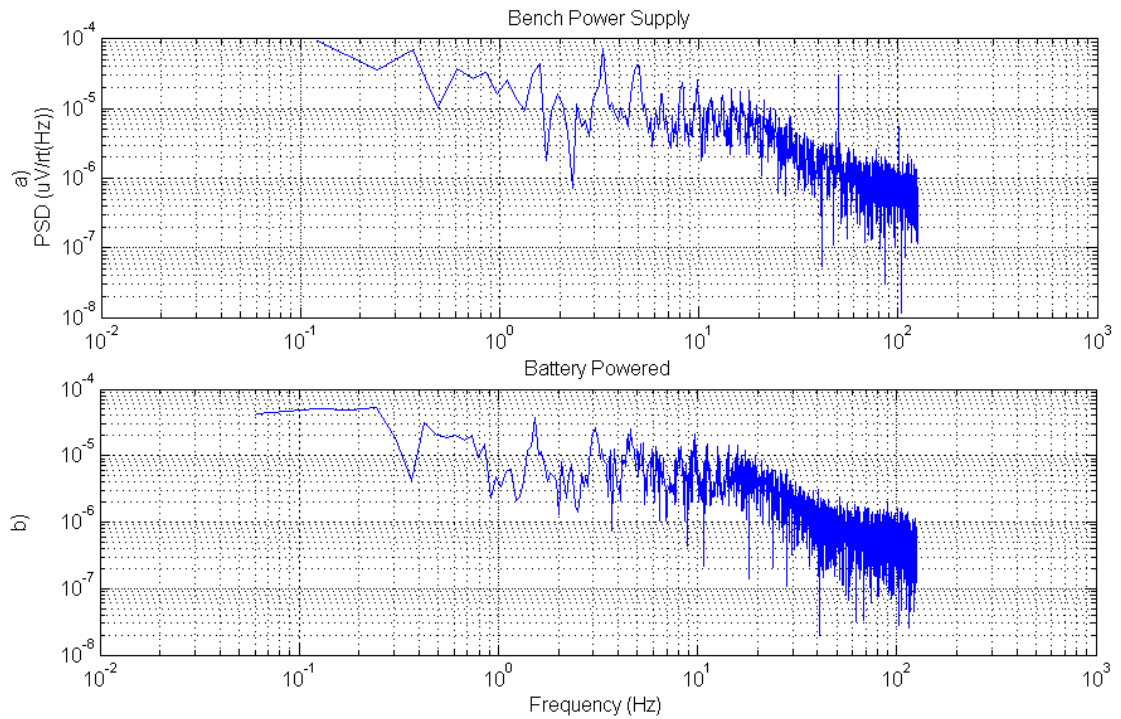


FIGURE 6.5: Frequency domain wireless ECG, comparing the ECG signal recorded while the system is battery powered in (b) and with (a) powered using bench supply. The presence of mains frequency and its harmonic, 50 Hz and the 100 Hz, is reduced in part (b) compared to part (a).

50 Hz mains interference signal may also be seen, however the CMRR is sufficient to have reduced the amplitude to be comparable to the measured signal.

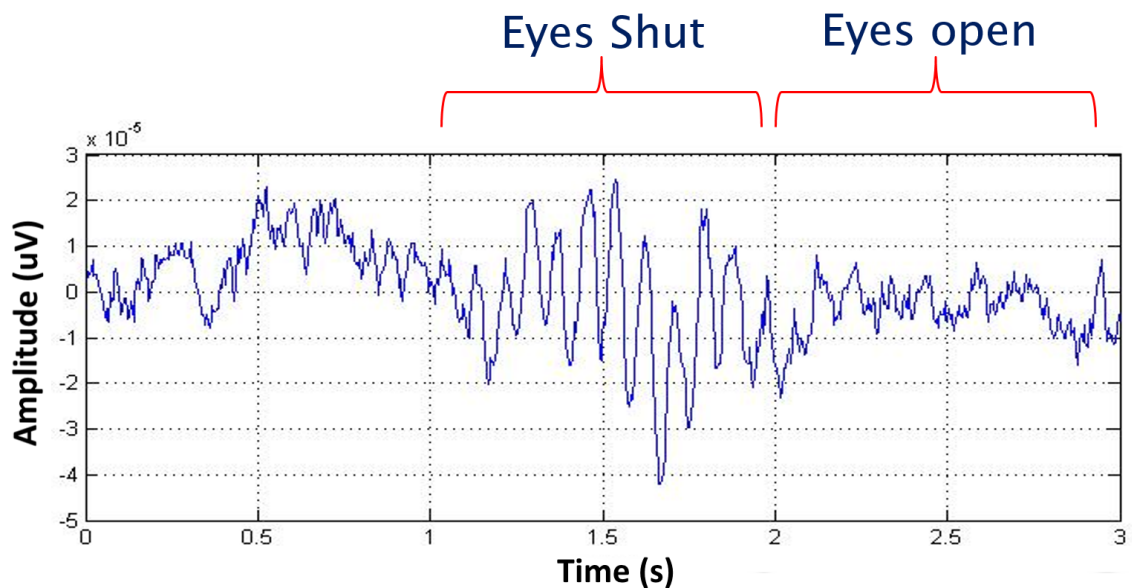


FIGURE 6.6: Alpha signal recorded using wireless sensors. Alpha signal can be observed as the rise in amplitude of 10 Hz from seconds 1 to 2 and it is blocked before second 1 and after second 2.

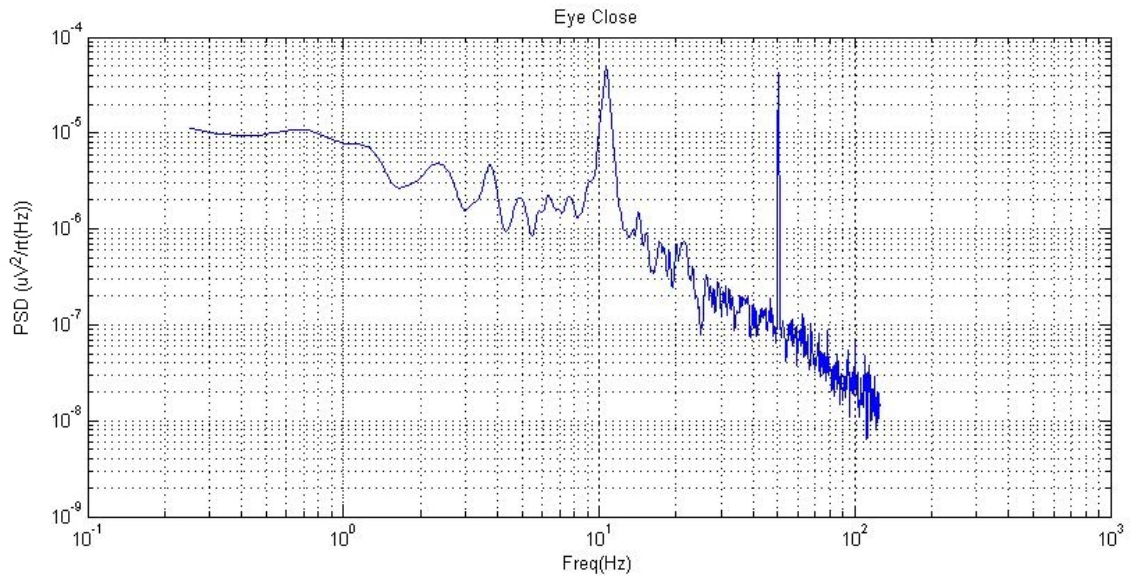


FIGURE 6.7: Alpha Wireless Frequency Domain.

Comparing Alpha signal recorded with wired and wireless versions of this system shows no difference in low frequency content. However, a reduction in amplitude of the 50 Hz present in the recorded signal should be noted. Figure 6.8a shows the data record with a wired system in comparison to part (b) when the data is transmitted wireless.

6.3.3 Frequency Bands

In this work the display of EEG has been based on providing time or frequency domain representations of the recorded data. Another useful format for presentation of the EEG data is to divide it into bins displaying averaged frequency band powers. This is produced using *bandpower()* function from MATLAB. Applying this function to the data transmitted wireless results in figure 6.9. Part (a) shows a rise in frequency band centring 10 Hz in comparison to part (b), this rise point to the attention level of the participant. The participant was asked to take part in a study that required them to pay attention to an event on a screen for a specific length of time and to rest in between the events. Part (a) demonstrates the frequency analysis of when they are asked to pay attention and part

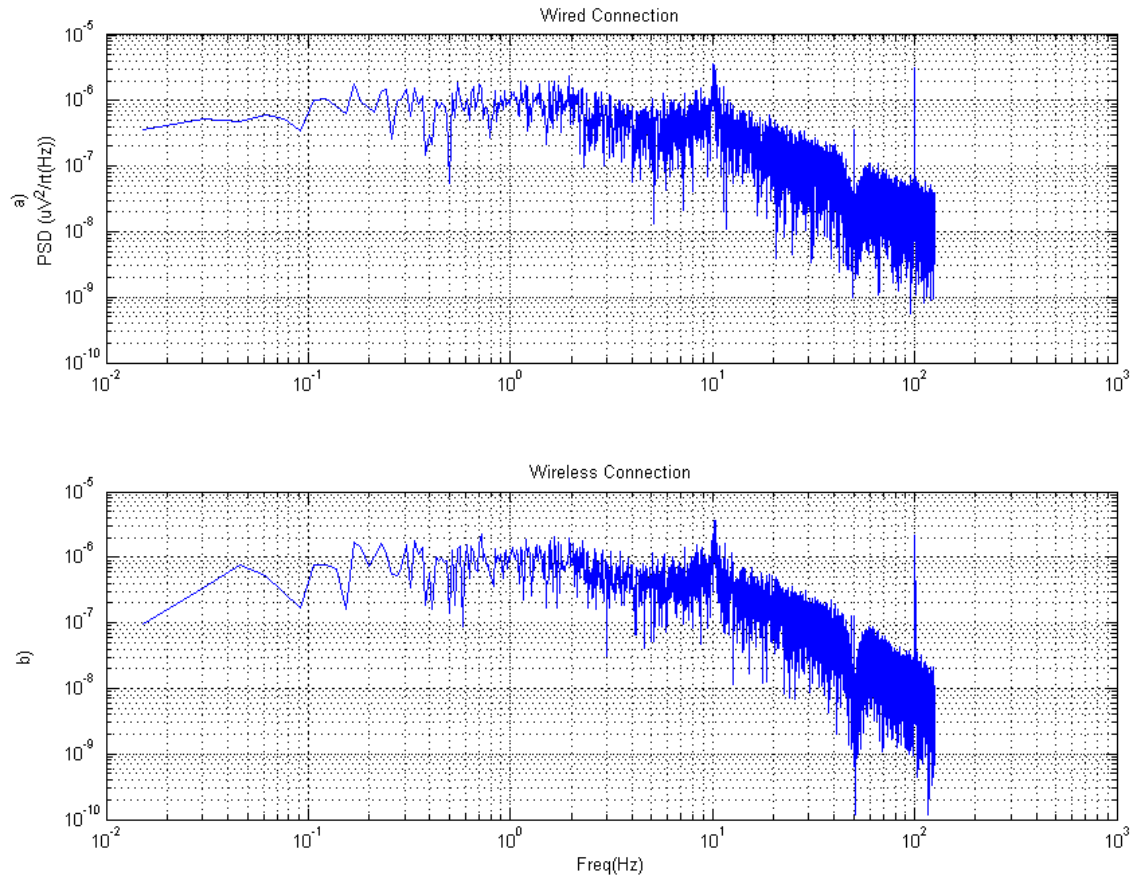


FIGURE 6.8: A frequency domain comparison of the wireless EEG data transmission (b) and data collected from a wired system (a).

(b) show the resting time. A similar presentation is included in the LabView program designed for interfacing with the wireless module demonstrated in figure 6.3.

6.4 Mobility Data

The aim with development of a wireless sensor system is to enable the user to perform their daily tasks without the interference caused by being tied to an acquisition system. Therefore it is important to monitor the data recorded while a person is walking in a room performing different tasks. Figure 6.10 shows an 80 s recording of a participant wearing the EEG electrodes on his head, along with the wireless module, and he is asked to walk in a room. Part 6.10(a) shows the raw data collected with the accompanying signal strength

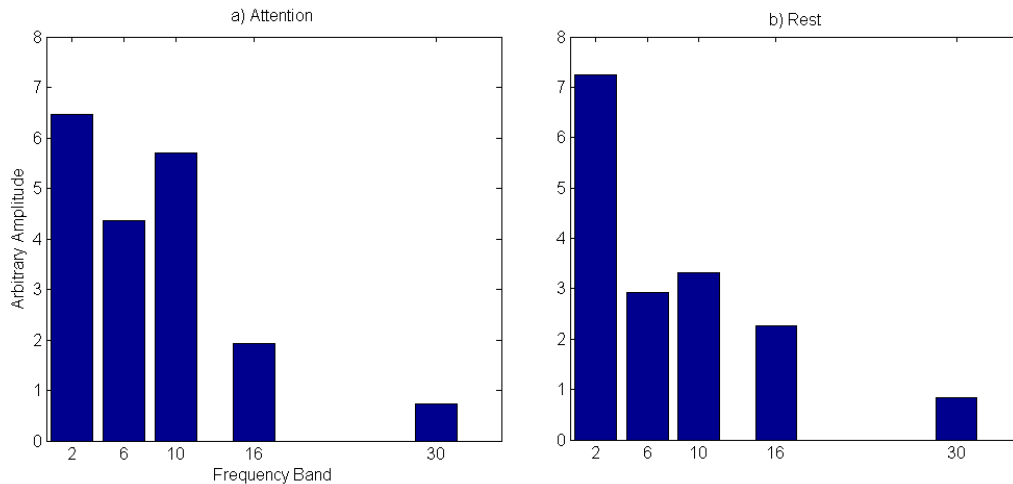


FIGURE 6.9: Frequency band power, (a) the participant is asked to pay attention to a specific event. (b) the participant is in rest state. A decrease can be seen in 10 Hz power band when the participant is in rest state (b).

data in 6.10(b). The low frequency oscillation is caused by an ionizer positioned a meter above the head of the participant. Part (b) shows a reduction of -40 dB in signal strength for the same time period when the person is standing under the ionizer.

Furthermore, figure 6.10(a) shows other high amplitude DC variations compared to the based line EEG, which could be caused by movement artefacts. However, if the signal strength is observed against the voltage amplitude a further observation could be made. Figure 6.11 demonstrates that voltage amplitudes higher than 1.5 V and lower than 0.75 V, which fall outside of the base line EEG, is accompanied by high reductions in signal strength. This design lacked an accelerometer, therefore it is not possible to confirm whether all the DC offsets are due to movement or better antenna design could improve the signal quality.

6.5 Discussion

This chapter was focused on presenting a low power wireless module that could be used to record and transmit biopotentials, in particular the EEG. The wireless system was

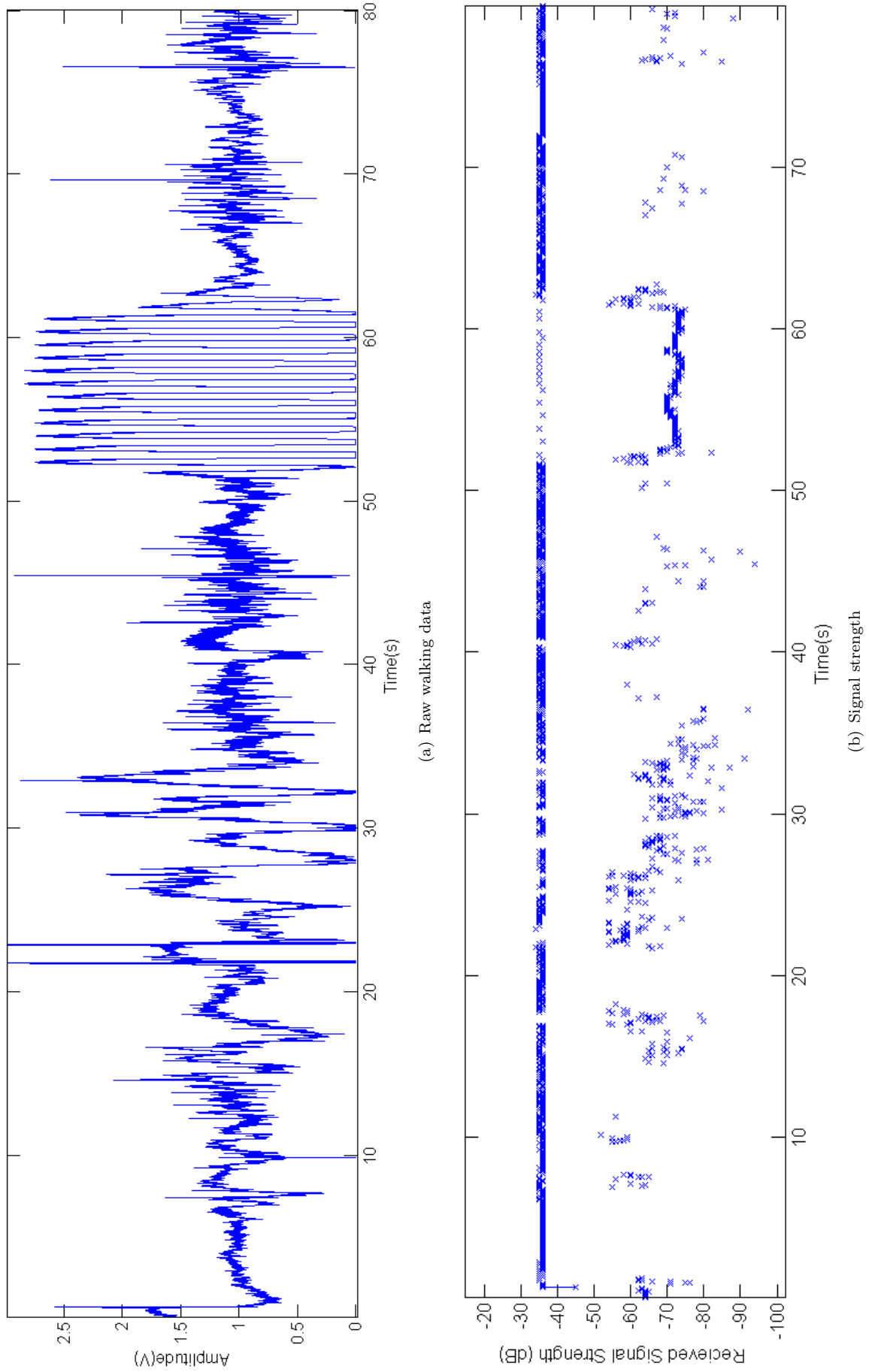


FIGURE 6.10: Comparison of 80 seconds of raw walking data (a) and signal strength (b), a correlation can be observed when the raw data has high DC drifts. The high amplitude low frequency signal between 50 and 60 second is caused by standing under an ionizer.

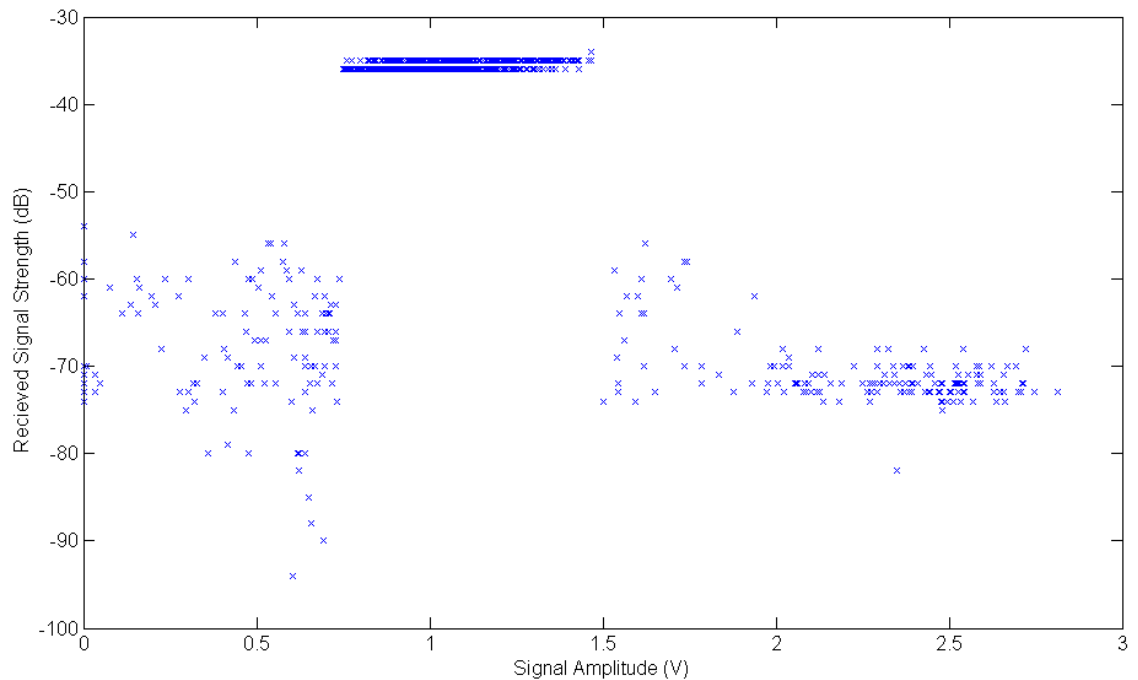


FIGURE 6.11: Received signal strength compared to drift. As drift increases the signal strength decreases. A reduction of -40 dB is observed on average for voltages outside of expected base line EEG, higher than 1.5 V and lower than 0.75 V.

based on IEEE 802.15.4 standard which defines the MAC and PHY layers. A simple network and application layer was developed which allows for forming either point to point communication or a star network. The power consumption is measured at 179 mW for a single differential EEG channel system. A LabView interface is designed to capture the transmitted data and communicate hardware specific alteration to sensor nodes such as data rate and system gain. The biopotentials recorded using this module are then compared to data collected with a wired setup and it shows reduction in 50 Hz frequency presence in the recorded wireless data. Further improvements in power consumption are possible by altering the network layer to allow for the transceiver chip to move to low power mode when not active as the transmission of one second of data takes 32.4 ms. Thus a duty cycle of 1 to 30 could be achieved. Comparing the recorded data with received signal strength shows that inclusion of accelerometer data could help with better identifying the sources of high DC drift when a participant is asked to wear the module and perform certain tasks such as to walk around a room and sitting in a chair. It was shown that

the deviations from the expected baseline EEG signal was accompanied with an average loss of -40 dB in signal strength. This indicates the high drifts are not solely caused by movement artefacts and using an accelerometer would allow distinguishing between the noise caused from movement of the user in contrast with the noise caused by other sources of noise, present in an environment, such as an ionizer.

Chapter 7

Conclusion

In order to confirm, at an early stage in the design process, that the EPS design was both suitable for high quality EEG signal acquisition and that it was compatible with commercial systems and practice, the sensors were interfaced and compared with commercial systems. This enabled a direct comparison between the EPS and wet gel electrode measurements using the same amplifier. The results of this study indicate that the Sussex EPS prototype produces a strictly comparable signal and signal to noise ratio to conventional wet gel electrodes, and is therefore suitable for the acquisition of both free running EEG and Event Related Potentials. First, the EPS prototype measures equivalent ongoing oscillatory activity to the wet gel EEG system, as demonstrated in chapter 3, where measurements of alpha activity were remarkably consistent between these systems. Secondly, the EPS system is suitable for measuring event-related averaged components that correlate with both early-sensory (chapter 4) and perceptual-cognitive processes (chapter 5).

From this exploratory study it seems clear that the EPS prototype has many advantages over conventional EEG sensors, including setup time, elimination of sensor cross-coupling,

lack of a ground electrode and the distortion of electrical potentials encountered when using standard gel electrodes. In the setup of conventional gel electrodes a connection between the scalp and a metal conductor is achieved through the use of an electrolyte solution. The electrical properties of this interface, known as a half-cell potential, is governed by the electrochemical reactions between the two layers. The electrochemical reactions produce fluctuations in the metal-electrolyte potential that can cause an increase in noise levels of up to 10 μV peak-to-peak for Ag/AgCl electrodes as mentioned in chapter 2. Unlike conventional electrodes the EPS has an insulation layer that is placed in front of the electrode, therefore there is no direct resistive electrical contact between the metal and an electrolyte (such as sweat or gel) and as a result half-cell potentials are not an issue with this method of measuring brain activity. Instead a capacitive coupling is formed.

Low frequency noise has been identified as the key performance indicator for capacitively coupled active sensors. We demonstrated that the use of an auto-zero operational amplifier within the prototype sensor yields results which are strictly comparable to wet gel electrodes. The EPS does display a higher sensitivity to motion artefacts, both of the subject and surrounding environment compared to standard wet gel EEG recordings, and this is due to the effect of motion within the local environment on the surrounding electrical fields, discussed in chapter 5. However, within the context of EEG recordings participants are generally instructed to remain as still as possible during the experiment and are also usually located within a separate recording chamber, which minimises the influence of these artefacts on data recorded using the EPS. Both Dry and Insulating electrodes are more susceptible to movement artefacts than wet gel electrodes. However, after the EPS was allowed to settle for approximately a few minutes, they show lower levels of movement artefacts compared to standard wet electrodes. An additional concern with EPS is its sensitivity to electrical sources and static charge. However, it was found that the use of

modest electrical shielding during recording, such as placing a grounded mat where the participant is placed, overcomes these issues.

The EPS technology has been successfully employed for ECG data acquisition, recent developments within this field has seen the sensors miniaturized to the microchip level with a form factor of 10 mm x 10 mm[94], see Figure 7.1 for example, allowing for a host of new applications. Miniaturization of the EPS is also being explored for EEG purposes. The standard 10/20 placement system currently involves the placement of 21 electrodes approximately 6 cm apart. Within the last decade the popularity of high density EEG set-ups has increased (128-256 electrodes) with the aim of localizing sources that drive the scalp recorded EEG signals.

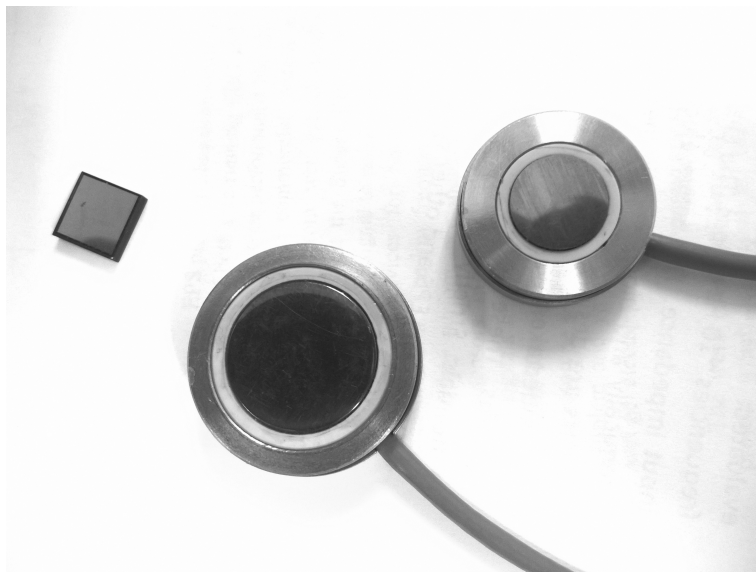


FIGURE 7.1: EPIC: A chip version of EPS commercially available by Plessey Semiconductor with a size of 10mm by 10mm. the prototype sensor have electrode sizes of 12 and 18mm.

While the problem of volume conductance has been widely cited as a critical issue preventing this goal, the fact remains that the scalp recorded EEG does exhibit distinct spatial characteristics, which are not represented with low density EEG recordings. This has led researchers to investigate the number of electrodes necessary to adequately capture the spatial pattern of scalp recorded EEG. Estimates range from electrode spacing of 2-3 cm

to 0.5–1 cm. The sensor distances of between 6–10 mm are required to capture the full spatial texture of the raw EEG signal on a neonatal scalp. Strong variations can be found in EEG signals (VEPs) at the scale of 1 cm when using an ultra-dense electroencephalography (ud-EEG) sensor array. It has been found that the use of such an array would lead to a two-fold increase in the signal to noise ratio compared to a high density electroencephalography (hd-EEG) system. The studies that have been performed so far do not record ud-EEG over the entire head, due to the technical challenges involved, but have used a small dense array of electrodes (e.g. 16 electrodes) placed over a small region of the scalp.

Future miniaturisation of the Sussex EPS sensors would allow the creation of ud-EEG montages that could conceivably cover the entire head. The miniaturised EPS sensors' ability to couple capacitively to the scalp removes some of the major issues facing standard ud-EEG systems, such as the elimination of cross-coupling between electrodes caused by the use of electrolyte or gel on electrodes in close proximity and the large set-up time that would be required for a similar ud-standard EEG system. Using a microchip version of the EPS sensor with dimensions of 10 mm x 10 mm, the resulting ud-montage could be made up of > 1000 electrodes.

The relatively low input impedances of conventional EEG recording systems that use Ag/AgCl electrodes ($10^6 - 10^7 \Omega$) have been shown to significantly distort the scalp recorded electrical potentials due to volume conductance, a general property of electrical currents to follow the path of least resistance, which causes activity from a cortical dipole to spread out the further from the source and also to be smeared out or diverted as it tries to pass through the highly resistant skull. These limitations have been addressed in other imaging techniques by using SQUID magnetometer systems, which have a higher sensitivity compared to Ag/AgCl electrodes and do not require direct contact with the scalp. Unfortunately, SQUID systems are very expensive, mainly due to the

cryogenic cooling of the sensors and the necessity of a magnetically shielded chamber to attenuate the Earth's own large magnetic field and external noise. Also these systems are bulky, heavy and thus not wearable. However, it is clear from the data published using SQUID magnetometers that the recording of signals with no electrical connection to the body affords great benefits, including the reconstruction of the underlying sources of scalp recorded signals.

As demonstrated in this thesis, the combination of a high level of sensitivity and very high impedances found in the EPS allows the accurate measurement of electrical potentials from the brain, within a minimally shielded environment. Additionally, similarly to SQUID recordings the EPS does not require a ground electrode allowing a direct comparison between two different areas of the brain. Future studies investigating the EPS should focus on the remote detection of EEG in a similar (but more cost effective) method to the SQUID magnetometers to assess if a similar increase in the spatial resolution is seen when using the EPS.

The data provided here clearly demonstrates the Sussex EPS provides a suitable alternative, with many added benefits, to standard EEG sensors. The EPS fulfils all of the necessary criteria of a sensor for recording scalp electrical potentials: it draws no real current from the scalp and therefore is safe to use, it has an ultra-high input impedance, and a high tolerance to noise at a relatively low cost.

The EPS sensor's intrinsic lack of cross-coupling and fast set-up time makes the implementation of a whole head ud-EEG array using the EPS an achievable goal. This advancement has the potential to significantly influence future neuroscience research, allowing researchers to investigate more accurately the spatial dynamics of scalp recorded EEG, with the addition of a higher signal to noise ratio and applicability to a broad range of

clinical settings. Additionally, mapping the distribution of scalp recorded electrical potentials remotely, in conjunction with ud-EEG using EPS, theoretically has the potential to resolve either a partial or full reconstruction of the location of the neural sources and therefore assist in unravelling the inverse problem.

Bibliography

- [1] A. Mota, L. Duarte, D. Rodrigues, A. Martins, A. Machado, F. Vaz, P. Fiedler, J. Haueisen, J. Nobrega, and C. Fonseca, “Development of a quasi-dry electrode for EEG recording,” *Sensors and Actuators A: Physical*, vol. 199, no. 0, pp. 310 – 317, 2013. [Online]. Available: <http://www.sciencedirect.com/science/article/pii/S0924424713003014>
- [2] T. A. Dawson, “Recent advances in non-perturbative detection of electric and magnetic fields for physiological monitoring,” *Recent Patents on Biomedical Engineering*, vol. 4, no. 2, pp. 94–102, 2011. [Online]. Available: <http://www.eurekaselect.com/95771/article>
- [3] L. F. Haas, “Hans Berger (1873-1941), Richard Caton (1842-1926), and electroencephalography,” *Neurol Neurosurg Psychiatry*, vol. 74, no. 1, p. 9, 2003. [Online]. Available: <http://jnnp.bmj.com/content/74/1/9.full>
- [4] C. J. Harland, T. D. Clark, and R. J. Prance, “Electric potential probes - new directions in the remote sensing of the human body,” *Measurement Science and Technology*, vol. 13, no. 2, pp. 163–169, 2002. [Online]. Available: <http://stacks.iop.org/0957-0233/13/163>
- [5] R. P. J Malmivuo, *Bioelectromagnetism - Principles and Applications of Bioelectric and Biomagnetic Fields*. New York: Oxford University Press, 1995, iSBN: 0195058232. [Online]. Available: <http://www.bem.fi/>
- [6] P. L. Nunez and R. Srinivasan, *Electric Fields of the Brain: The neurophysics of EEG*, 2nd ed. OUP USA, Jan. 2006, ISBN: 019505038X. [Online]. Available: <http://www.amazon.co.uk/dp/019505038X>
- [7] M. Nuwer, G. Comi, R. Emerson, A. Fuglsang-Frederiksen, J. Gurit, H. Hinrichs, A. Ikeda, F. Luccas, and P. Rappelsberger, “IFCN standards for digital recording of clinical EEG,” *Electroencephalography and clinical Neurophysiology*, no. 106, pp. 259–261, 1998.
- [8] D. Cohen and B. Cuffin, “Demonstration of useful differences between magnetoencephalogram and electroencephalogram,” *Electroencephalography and Clinical Neurophysiology*, vol. 56, no. 1, pp. 38 – 51, 1983. [Online]. Available: <http://www.sciencedirect.com/science/article/pii/0013469483900056>
- [9] A. Ahonen, M. Hamalainen, M. Kajola, J. E. T. Knuutila, O. Lounasmaa, J. Simola, C. Tesche, and V. Vilkmann, “Multichannel SQUID systems for brain research,” *Magnetics, IEEE Transactions on*, vol. 27, no. 2, pp. 2786–2792, Mar 1991.
- [10] S. Baillet, J. Mosher, and R. Leahy, “Electromagnetic brain mapping,” *Signal Processing Magazine, IEEE*, vol. 18, no. 6, pp. 14–30, Nov 2001.

- [11] C. J. Aine, "A conceptual overview and critique of functional neuroimaging techniques in humans: I. MRI/fMRI and PET," *Critical reviews in neurobiology*, vol. 9, no. 2-3, pp. 229–309, 1995. [Online]. Available: <http://europepmc.org/abstract/MED/8581985>
- [12] A. C. Chen, "New perspectives in EEG/MEG brain mapping and PET/fMRI neuroimaging of human pain," *International Journal of Psychophysiology*, vol. 42, no. 2, pp. 147 – 159, 2001. [Online]. Available: <http://www.sciencedirect.com/science/article/pii/S0167876001001635>
- [13] J. L. Andreassi, *Psychophysiology Human Behaviour and Physiological Response*, 5th ed. New York: Psychology Press, 2007, ISBN: 0805849505.
- [14] S. Luck, *An introduction to the event-related potential technique*. MIT Press, Sep. 2005, ISBN: 9780262621960.
- [15] S. J. M. Smith, "EEG in the diagnosis, classification, and management of patients with epilepsy," *Neurol Neurosurg Psychiatry*, no. 76, pp. ii2–ii7, 2005.
- [16] D. M. Tucker, "Spatial sampling of head electrical fields: the geodesic sensor net," *Electroencephalography and Clinical Neurophysiology*, vol. 87, no. 3, pp. 154 – 163, 1993. [Online]. Available: <http://www.sciencedirect.com/science/article/pii/S001346949390121B>
- [17] M. Odabae, W. J. Freeman, P. B. Colditz, C. Ramon, and S. Vanhatalo, "Spatial patterning of the neonatal EEG suggests a need for a high number of electrodes," *NeuroImage*, vol. 68, no. 0, pp. 229 – 235, 2013. [Online]. Available: <http://www.sciencedirect.com/science/article/pii/S1053811912011792>
- [18] Y. Petrov, J. Nador, C. Hughes, S. Tran, O. Yavuzcetin, and S. Sridhar, "Ultra-dense EEG sampling results in two-fold increase of functional brain information," *NeuroImage*, vol. 90, no. 0, pp. 140 – 145, 2014. [Online]. Available: <http://www.sciencedirect.com/science/article/pii/S1053811913012615>
- [19] R. Srinivasan, *High-resolution EEG: theory and practice*, ser. Event-related Potentials: A Methods Handbook, T. C. Handy, Ed. Cambridge, MA: The MIT Press, 2005, ISBN: 0262083337.
- [20] W. J. Freeman, M. D. Holmes, B. C. Burke, and S. Vanhatalo, "Spatial spectra of scalp EEG and EMG from awake humans," *Clinical Neurophysiology*, vol. 114, no. 6, pp. 1053 – 1068, 2003. [Online]. Available: <http://www.sciencedirect.com/science/article/pii/S1388245703000452>
- [21] Emotiv. (2014) Emotiv EPOC. Date Accessed: 2012.01.22. [Online]. Available: <http://emotiv.com/epoc.php>
- [22] NeuroSky. (2014) EEG Biosensor Solutions. Date Accessed: 2012.11.22. [Online]. Available: <http://neurosky.com/products-markets/eeg-biosensors/>
- [23] J. R. Wolpaw, N. Birbaumer, D. J. McFarland, G. Pfurtscheller, and T. M. Vaughan, "Brain computer interfaces for communication and control," *Clinical Neurophysiology*, vol. 113, no. 6, pp. 767 – 791, 2002. [Online]. Available: <http://www.sciencedirect.com/science/article/pii/S1388245702000573>

- [24] K. LaFleur, K. Cassady, A. Doud, K. Shades, E. Rogin, and B. He, “Quadcopter control in three-dimensional space using a noninvasive motor imagery-based brain-computer,” *Journal of Neural Engineering*, vol. 10, no. 4, p. 046003, May 2013. [Online]. Available: <http://stacks.iop.org/1741-2552/10/i=4/a=046003>
- [25] J. E. Huggins, P. A. Wren, and K. L. Gruis, “What would brain-computer interface users want? opinions and priorities of potential users with amyotrophic lateral sclerosis,” *Amyotrophic Lateral Sclerosis*, vol. 12, no. 5, pp. 318–324, 2011, pMID: 21534845. [Online]. Available: <http://dx.doi.org/10.3109/17482968.2011.572978>
- [26] H. Prance, *Sensor Developments for Electrophysiological Monitoring in Healthcare*, ser. Applied Biomedical Engineering, 2011. [Online]. Available: <http://www.intechopen.com/books/export/citation/EndNote/applied-biomedical-engineering/sensor-developments-for-electrophysiological-monitoring-in-healthcare>
- [27] A. Searle and L. Kirkup, “A direct comparison of wet, dry and insulating bioelectric recording electrodes,” *Physiological Measurement*, vol. 21, no. 2, p. 271, 2000. [Online]. Available: <http://stacks.iop.org/0967-3334/21/i=2/a=307>
- [28] Y. Chi, T.-P. Jung, and G. Cauwenberghs, “Dry-contact and noncontact biopotential electrodes: Methodological review,” *Biomedical Engineering, IEEE Reviews in*, vol. 3, pp. 106–119, 2010.
- [29] E. S. Kappenman and S. J. Luck, “The effects of electrode impedance on data quality and statistical significance in ERP recordings,” *Psychophysiology*, vol. 47, no. 5, pp. 888–904, 2010. [Online]. Available: <http://dx.doi.org/10.1111/j.1469-8986.2010.01009.x>
- [30] D. Prutchi and M. Norris, *Design and Development of Medical Electronic Instrumentation: A Practical Perspective of the Design, Construction, and Test of Medical Devices*. Wiley, December 2004, ISBN: 978-0-471-67623-2. [Online]. Available: <http://eu.wiley.com/WileyCDA/WileyTitle/productCd-0471676233.html>
- [31] L. A. Geddes and L. Alexander, *Electrodes and the measurement of bioelectric events*. New York: Wiley-Interscience, 1972, ISBN: 047129490X.
- [32] G. Gargiulo, R. A. Calvo, P. Bifulco, M. Cesarelli, C. Jin, A. Mohamed, and A. van Schaik, “A new EEG recording system for passive dry electrodes,” *Clinical Neurophysiology*, vol. 121, no. 5, pp. 686 – 693, 2010. [Online]. Available: <http://www.sciencedirect.com/science/article/pii/S1388245709007962>
- [33] C. Grozea, C. D. Voinescu, and S. Fazli, “Bristle-sensors low-cost flexible passive dry eeg electrodes for neurofeedback and bci applications,” *Journal of Neural Engineering*, vol. 8, no. 2, p. 025008, 2011. [Online]. Available: <http://stacks.iop.org/1741-2552/8/i=2/a=025008>
- [34] T. O. Zander, M. Lehne, K. Ihme, S. Jatzev, J. Correia, C. Kothe, B. Picht, and F. Nijboer, “A Dry EEG-System for Scientific Research and Brain Computer Interfaces,” *Frontiers in Neuroscience*, vol. 5, no. 53, pp. 1–10, May 2011. [Online]. Available: <http://doc.utwente.nl/79822/>
- [35] C.-Y. Chen, I.-J. Wang, S.-F. Chen, S.-Y. Li, B.-W. Chen, J.-Y. Chang, and C.-T. L. L.-D. Liao, “Gaming control using a wearable and wireless EEG-based brain-computer interface device with novel dry foam-based sensors,” *Journal of Neuroengineering and Rehabilitation*, 2012. [Online]. Available: <http://www.jneuroengrehab.com/content/9/1/5>

- [36] N. Alba, R. Sciabassi, M. Sun, and X. Cui, "Novel Hydrogel-Based Preparation-Free EEG Electrode," *Neural Systems and Rehabilitation Engineering, IEEE Transactions on*, vol. 18, no. 4, pp. 415–423, Aug 2010.
- [37] A. J. Clippingdale, R. J. Prance, T. D. Clark, H. Prance, and T. Spiller, "Ultra-high impedance voltage probes and non-contact electrocardiography," *Institute of Physics*, 1991.
- [38] E. Spinelli and M. Haberman, "Insulating electrodes: a review on biopotential front ends for dielectric skin electrode interfaces," *Physiological Measurement*, vol. 31, no. 10, p. S183, 2010. [Online]. Available: <http://stacks.iop.org/0967-3334/31/i=10/a=S03>
- [39] H. J. Baek, H. J. Lee, Y. G. Lim, and K. S. Park, "Conductive Polymer Foam Surface Improves the Performance of a Capacitive EEG Electrode," *IEEE Transactions on Biomedical Engineering*, vol. 59, no. 12, pp. 3422–3431, December 2012.
- [40] B. A. Taheri, R. T. Knight, and R. L. Smith, "A dry electrode for EEG recording," *Electroencephalography and Clinical Neurophysiology*, pp. 376–383, 1994.
- [41] C. J. Harland, T. D. Clark, and R. J. Prance, "Remote detection of human electroencephalograms using ultrahigh input impedance electric potential sensors," *Applied Physics Letters*, vol. 81, no. 17, pp. 3284–3286, 2002. [Online]. Available: <http://link.aip.org/link/?APL/81/3284/1>
- [42] T. Sullivan, S. Deiss, and G. Cauwenberghs, "A Low-Noise, Non-Contact EEG/ECG Sensor," *Biomedical Circuits and Systems Conference*, pp. 154–157, 2007. [Online]. Available: <http://ieeexplore.ieee.org/stamp/stamp.jsp?tp=&arnumber=4463332&isnumber=4463293>
- [43] K. K. Kim and K.-S. Park, "Effective coupling impedance for power line interference in capacitive-coupled ECG measurement system," in *Information Technology and Applications in Biomedicine, 2008. ITAB 2008. International Conference on*, May 2008, pp. 256–258.
- [44] Y. T. Wang, Y. Wang, C. Maier, T. Jung, G. Cauwenberghs, and Y. Chi, "Dry and Noncontact EEG Sensors for Mobile brain-computer interfaces." *IEEE Transactions on Neural Systems and Rehabilitation Engineering*, vol. 20, no. 2, pp. 228–235, 2012.
- [45] C. J. Harland, T. D. Clark, and R. Prance, "High resolution ambulatory electrocardiographic monitoring using wrist-mounted electric potential sensors," *Measurement Science and Technology*, vol. 14, no. 7, pp. 923–928, 2003. [Online]. Available: <http://stacks.iop.org/0957-0233/14/923>
- [46] P. C. Brath, "Atlas of Cardiovascular Monitoring," *Anesthesiology*, vol. 93, no. 1, p. 312, 2000, ISBN: 0443088918.
- [47] J. R. Hampton, *The ECG in practice*. Elsevier Health Sciences, 2013, ISBN: 9780702046438.
- [48] Agilent. Agilent HP3562A Spectrum Analyser Datasheet. Date Accessed: 2014.09.25. [Online]. Available: <http://www.testequipmentdepot.com/usedequipment/pdf/3562Adatasheet.pdf>

- [49] Analog Devices, “AD8629 Data Sheet,” Tech. Rep., 2014, Date Accessed: 2012.07.13. [Online]. Available: http://www.analog.com/static/imported-files/data_sheets/AD8628_8629_8630.pdf
- [50] H. Ott, *Noise reduction techniques in electronic systems*, ser. A Wiley-Interscience publication. Wiley, 1988, ISBN: 9780471850687. [Online]. Available: <http://books.google.co.uk/books?id=FRooAQAAMAAJ>
- [51] A. Rich. Application Note: Shielding and Guarding. Analog Devices. Date Accessed: 2014.09.28. [Online]. Available: http://www.analog.com/static/imported-files/application_notes/41727248AN_347.pdf
- [52] DuPont. (2014) DuPont. Date Accessed: 2013.04.22. [Online]. Available: http://www2.dupont.com/Kapton/en_US/tech_info/
- [53] B. Fisch and R. Spehlmann, *Spehlmann’s EEG primer*, 2nd ed. Elsevier Science Ltd, May 1991. [Online]. Available: <http://www.elsevier.com/books/fisch-and-spehlmans-eeg-primer/fisch/978-0-444-82148-5>
- [54] TMS International. Refa8 DatasData. Date Accessed: 2013.10.12. [Online]. Available: <http://www.tmsi.com/products/item/refa>
- [55] MathWorks. (2014, September) Xcorr. [Online]. Available: http://uk.mathworks.com/help/signal/ref/xcorr.html#inputarg_scaleopt
- [56] g.tec. g.Electrodes. Date Accessed: 2014.07.12. [Online]. Available: <http://www.gtec.at/Products/Electrodes-and-Sensors/g.Electrodes-Specs-Features>
- [57] P. A. Davis, “Effects of Acoustic Stimulation on the Waking Human Brain,” *Journal of Neurophysiology*, vol. 2, no. 6, pp. 494–499, 1939. [Online]. Available: <http://jn.physiology.org/content/2/6/494>
- [58] B. Blankertz, S. Lemm, M. Treder, S. Haufe, and K.-R. Maller, “Single-trial analysis and classification of ERP components,” *NeuroImage*, vol. 56, no. 2, pp. 814 – 825, 2011, multivariate Decoding and Brain Reading. [Online]. Available: <http://www.sciencedirect.com/science/article/pii/S1053811910009067>
- [59] G. C. Galambos, Robert; Sheatz, “An electroencephalography study of classical conditioning,” *American Journal of Physiology*, vol. 203, no. 1, pp. 173–184, 1962. [Online]. Available: <http://psycnet.apa.org/psycinfo/1964-02139-001>
- [60] S. Clare, “Functional MRI: Methods and Applications,” Ph.D. dissertation, University of Nottingham, October 1997. [Online]. Available: <http://users.fmrib.ox.ac.uk/~stuart/thesis/fmri.pdf>
- [61] J. V. Odom, M. Bach, M. Brigel, G. E. Holder, D. L. McCulloch, A. P. Tormene, and Vaegan, “Standards, recommendations and guidelines,” 02 2013. [Online]. Available: <http://www.iscev.org/standards/pdfs/ISCEV-VEP-Standard-2010.pdf>
- [62] *LaCie electronblue IV monitors*, LaCie Group, Date Accessed: 2014.05.12. [Online]. Available: https://www.lacie.com/download/datasheet/blueiv_en.pdf
- [63] A. Delorme and S. Makeig, “EEGLAB: an open source toolbox for analysis of single-trial EEG dynamics including independent component analysis,” *Journal of Neuroscience Methods*, vol. 134, no. 1, pp. 9 – 21, 2004. [Online]. Available: <http://www.sciencedirect.com/science/article/pii/S0165027003003479>

- [64] J. Lopez-Calderon and S. J. Luck, "ERPLAB: An Open-Source Toolbox for the Analysis of Event-Related Potentials," *Frontiers in Human Neuroscience*, vol. 8, no. 213, 2014. [Online]. Available: http://www.frontiersin.org/human_neuroscience/10.3389/fnhum.2014.00213/abstract
- [65] R. Chavarriaga and J. d. R. Millan, "Learning from EEG Error-related Potentials in Noninvasive Brain-Computer Interfaces," *IEEE Transactions on Neural Systems and Rehabilitation Engineering*, vol. 18, no. 4, pp. 381–388, 2010.
- [66] N. K. Squires, K. C. Squires, and S. A. Hillyard, "Two varieties of long-latency positive waves evoked by unpredictable auditory stimuli in man," *Electroencephalography and Clinical Neurophysiology*, vol. 38, no. 4, pp. 387 – 401, 1975. [Online]. Available: <http://www.sciencedirect.com/science/article/pii/0013469475902631>
- [67] National Instruments. LabVIEW System Design Software. Date Accessed: 2011.05.12. [Online]. Available: <http://www.ni.com/labview/>
- [68] Rohde-Schwarz. R&S RTO Digital Oscilloscopes. Date Accessed: 2012.11.03. [Online]. Available: http://www.rohde-schwarz.com/en/product/rto-productstartpage_63493-10790.html
- [69] National Instruments. NI USB-6210. Date Accessed: 2011.05.12. [Online]. Available: <http://sine.ni.com/nips/cds/view/p/lang/en/nid/203223>
- [70] A. Calder, G. Rhodes, M. Johnson, and J. Haxby, *Oxford Handbook of Face Perception*, ser. Oxford Library of Psychology. OUP Oxford, 2011, ISBN: 9780191620904. [Online]. Available: <http://books.google.co.uk/books?id=2UXx9rdfriQC>
- [71] H. E. M. J. Herrmann, A.-C. Ehlis and A. J. Fallgatter, "Early stages (P100) of face perception in humans as measured with event-related potentials (ERPs)," *Journal of Neural Transmission*, vol. 112, pp. 1073–1081, August 2005. [Online]. Available: <http://www.ncbi.nlm.nih.gov/pubmed/15583954>
- [72] M. Eimer, "The face-specific N170 component reflects late stages in the structural encoding of faces," *NeuroReport*, vol. 11, no. 10, pp. 2319–2324, July 2000. [Online]. Available: <http://www.ncbi.nlm.nih.gov/pubmed/10923693>
- [73] H. Heinze, S. J. Luck, G. Mangun, and S. A. Hillyard, "Visual event-related potentials index focused attention within bilateral stimulus arrays. i. evidence for early selection," *Electroencephalography and clinical neurophysiology*, vol. 75, no. 6, pp. 511–527, 1990.
- [74] Systems Wire & Cable. (2014, September) Low Triboelectric Noise Wire and Cable. [Online]. Available: <http://www.systemswire.com/low-noise-triboelectric-cable.html>
- [75] H. Prance, P. Watson, R. Prance, and S. Beardsmore-Rust, "Position and movement sensing at metre standoff distances using ambient electric field," *Measurement Science and Technology*, vol. 23, no. 11, p. 115101, 2012.
- [76] A. J. Casson, S. Smith, J. S. Duncan, and E. Rodriguez-Villegas, "Wearable EEG: what is it, why is it needed and what does it entail?" in *Engineering in medicine and biology society, 2008. embs 2008. 30th annual international conference of the ieee*. IEEE, 2008, pp. 5867–5870.

- [77] N. S. Dias, J. P. Carmo, P. M. Mendes, and J. H. Correia, "Wireless instrumentation system based on dry electrodes for acquiring eeg signals," *Medical Engineering & Physics*, vol. 34, no. 7, pp. 972 – 981, 2012. [Online]. Available: <http://www.sciencedirect.com/science/article/pii/S1350453311002931>
- [78] G. Deuschl and A. Eisen, *Recommendations for the Practice of Clinical Neurophysiology: Guidelines of the International Federation of Clinical Neurophysiology*, ser. Electroencephalography and clinical neurophysiology: Supplement. Elsevier, 1999. [Online]. Available: <http://books.google.co.uk/books?id=HV2qE7BPEkgC>
- [79] M. D. Holmes, "Dense array EEG: methodology and new hypothesis on epilepsy syndromes," *Epilepsia*, vol. 49, no. s3, pp. 3–14, 2008.
- [80] IEEE. (2012) IEEE 802.11: Wireless LANs. Date Accessed: 2013.07.12. [Online]. Available: <http://standards.ieee.org/about/get/802/802.11.html>
- [81] Bluetooth SIG. (2013) Specification. Date Accessed: 2014.04.22. [Online]. Available: <https://www.bluetooth.org/en-us/specification>
- [82] IEEE, "Approved draft amendment to IEEE standard for information technology-telecommunications and information exchange between systems-part 15.4:wireless medium access control (MAC) and physical layer (PHY) specifications for Low-Rate Wireless Personal Area Networks (LR-WPANs): Amendment to add alternate PHY (amendment of IEEE Std 802.15.4)," *IEEE Approved Std P802.15.4a/D7*, pp. –, 2007, Date Accessed: 2014.07.13.
- [83] ZigBee Alliance, "ZigBee Specification Overview," Date Accessed: 2012.07.13. [Online]. Available: <http://www.zigbee.org/Specifications/ZigBee/Overview.aspx>
- [84] J. Zheng and M. J. Lee, "A comprehensive performance study of IEEE 802.15. 4," 2004, Date Accessed: 2013.05.12.
- [85] S. Ashton, "Ember Corporation. Zigbee network performance, typical results and implications for application design," in *ZigBee Developers' Conference*, 2006.
- [86] The Network Simulator - NS-2. Date Accessed: 2014.09.12. [Online]. Available: <http://www.isi.edu/nsnam/ns/>
- [87] T. R. Burchfield, S. Venkatesan, and D. Weiner, "Maximizing throughput in ZigBee wireless networks through analysis, simulations and implementations," in *Proc. Int. Workshop Localized Algor. Protocols WSNs*, 2007, pp. 15–29.
- [88] FlexiPanel. Pixie DARC datasheet. Date Accessed: 2013.11.12. [Online]. Available: <http://flexipanel.com/Docs/Pixie%20DS481.pdf>
- [89] Microchip, "PICmicro 18C MCU Family Reference Manual," 2000.
- [90] IEEE Standard. (2011) 802.15.4-2011 - IEEE Standard for local and metropolitan area networks–part 15.4: Low-Rate Wireless Personal Area Networks (LR-WPANs). Date Accessed: 2013.07.12. [Online]. Available: <http://standards.ieee.org/findstds/standard/802.15.4-2011.html>
- [91] Nordic Semiconductor. (2014, September) nRF51822 datasheet. Date Accessed: 2014.05.13. [Online]. Available: <https://www.nordicsemi.com/eng/Products/Bluetooth-Smart-Bluetooth-low-energy/nRF51822>

- [92] Y. M. Chi and G. Cauwenberghs, "Wireless non-contact EEG/ECG electrodes for body sensor networks," in *Body Sensor Networks (BSN), 2010 International Conference on*. IEEE, 2010, pp. 297–301.
- [93] I. Obeid, M. A. Nicolelis, and P. D. Wolf, "A multichannel telemetry system for single unit neural recordings," *Journal of Neuroscience Methods*, vol. 133, no. 1, pp. 33–38, 2004.
- [94] Plessey Semiconductors Ltd. (2014) EPIC Ultra High Impedance ECG Sensor PS25251. Date Accessed: 2014.05.12. [Online]. Available: <http://www.plesseysemiconductors.com/doc/?id=291766>

Appendices

A.1 Appendix A

A.1.1 MATLAB

Codes used in MATLAB for analysing recorded data.

A.1.1.1 FFT routine

```
Data=EEG;
Data(1)=[];
n=length(Data);
power= abs(Data(1:floor(n/2))).^2;
nyquist = 1/2;
freq = (1:n/2)/(n/2)*nyquist/scale;
plot(freq,power)
```

A.1.2 C Code

Wireless board firmware developed in C.

A.1.2.1 Sensor Node

```
#include <p18f2520.h>
#include <spi.h>
#include <delays.h>
#include ".\CC2420.h"

#define Freq 5

void RFRX(unsigned char data[],unsigned char * Length);
void RFTX(unsigned char *, unsigned char *, unsigned char *);
```

```
void CHIPCC2420Reset(void);
void ANRead(char *);
void UARTInit(void);
rom unsigned char UARTmessage[] = "helloworl1";
//unsigned char UARTRXmessage[100];
volatile unsigned char ADBUFFER[104];
volatile unsigned char ADBuffer_C = 0;
unsigned char TXbuff[4]={0x41,0x42,0x43,0x44};
unsigned char RXlen;
unsigned char RXbuff[115];

#pragma interrupt UserInterruptHandler
void UserInterruptHandler(void)
{
if (INTCONbits.TMROIE & INTCONbits.TMROIF)
{
INTCONbits.TMROIE = 0;

// TMROH = 0xFF;
TMROL = Freq;
ADBuffer_C++;

ADCON0bits.GO = 1; // a/d on

while (ADCON0bits.NOT_DONE) {Nop();}
Nop();

ADBUFFER[2*ADBuffer_C-2] = ADRESH & 0x03;
ADBUFFER[2*ADBuffer_C-1] = ADRESL;

INTCONbits.TMROIF = 0;
INTCONbits.TMROIE = 1;
}
}

void main(void){

unsigned char seq = 0;

near int UARTcounter;
int TESTcounter;

char Inchar;

unsigned char buff2[10];
char ourmessage[] = "Your message here";
// Delay10KTCYx( 100 );

buff2[0] = 11+2*ADBuffer_C+1; //length
//buff[1] = *pseq;
buff2[1] = 0x61; //FCF Upper
```

```

buff2[2] = 0x88; //FCF Lower
buff2[3] = seq; //Sequence #
buff2[4] = 0x55; //PAN Upper
buff2[5] = 0x55; //PAN Lower
buff2[6] = 0x11; //Dest. Addr. Upper
buff2[7] = 0x11; //Dest. Addr. Lower
buff2[8] = 0x12; //Src. Addr. Upper
buff2[9] = 0x12; //Src. Addr. Lower

TRISAbits.TRISA1 = 0;
/* Configure PORTC2 as an output */
PORTCbits.RC2 = 1; //RESETE initially set high
TRISCbits.TRISC2 = 0; //output: RESETE
/* Configure PORTB0:3 as inputs */
ADCON0 = 0x1C; //turn off analog input
ADCON1 = 0b00001111;
TRISAbits.TRISA3 = 1;
TRISBbits.TRISB0 = 1; //input: FIFO
TRISBbits.TRISB1 = 1; //input: CCA TRISBbits.TRISB2 = 1; //input: SFD
TRISBbits.TRISB3 = 1; //input: FIFO
/* Configure PORTC0 as an output */
PORTCbits.RC0 = 1; //CSn initially set high
TRISCbits.TRISCO = 0; // output: CSn
/* Configure SPI interface */
OpenSPI(SPI_FOSC_4, MODE_00, SMPMID); //Clk/16, CKP=0, CKE=1, SMP=0
PORTAbits.RA1 = 0;
////////// UART Setup //////////

// UARTInit();

////////// Timer Setup //////////
INTCON = 0b10000000;
INTCON2bits.TMROIP=1;
INTCONbits.TMROIF = 0;

INTCONbits.TMROIE = 1; //Interrupt Enable

RCONbits.IPEN = 1;
TOCON = 0b01000101;

TMROL = Freq;
TOCONbits.TMROON = 0;
////////// A/D setup //////////

TRISAbits.TRISA2 = 1;

ADCON1 = 0b00001100;
ADCON0 = 0b00001000;
ADCON2 = 0b10111110; // a/d conv period 64Tosc, right shift result
ADCON0bits.ADON = 1;

```

```
////////// TX setup ////////////
CHIPCC2420Reset();

UARTcounter = 0;
TESTcounter = sizeof(TXbuff)/2;

while(1){

/* if (INTCONbits.TMROIE & INTCONbits.TMROIF)
{

INTCONbits.TMROIE = 0;

// TMROH = 0xFF;
TMR0L = 0x05;
ADBuffer_C++;

ADCON0bits.GO = 1; // a/d on

while (ADCON0bits.NOT_DONE) {Nop();}
Nop();

ADBUFFER[2*ADBuffer_C-2] = ADRESH & 0x03;
ADBUFFER[2*ADBuffer_C-1] = ADRESL;

INTCONbits.TMROIF = 0;
INTCONbits.TMROIE = 1;

}*/

////////// Network Recieve ////////////
if(PORTBbits.RB3)
{
// PORTAbits.RA0 = 1;

RFRX(RXbuff, &RXlen);

// PORTAbits.RA0 = 0;
}

if ( ADBuffer_C >= 50 ){

// PORTAbits.RA1 = 1;
buff2[0] = 11+2*ADBuffer_C; //length
buff2[3] = seq; //Sequence #
RFTX(buff2,(unsigned char *)ADBUFFER,(unsigned char *)&ADBuffer_C);
ADBuffer_C = 0;
seq++;
// PORTAbits.RA1 = 1;

}

}
```

```

if ( PORTAbits.RA3 == 0 ){
TXbuff[0] = 0x01;
buff2[0] = 11+2*TESTcounter; //length
buff2[3] = seq++; //Sequence #
RFTX(buff2,(unsigned char *)TXbuff, (unsigned char *)&TESTcounter );
Delay10KTCYx( 100 );
// PORTBbits.RB4=0;
}

if ( RXbuff[10] == 0x01 ){
RXbuff[10] = 0x00;
TXbuff[0] = 0xFF;
buff2[0] = 11+2*TESTcounter; //length
buff2[3] = seq; //Sequence #
RFTX(buff2,(unsigned char *)TXbuff, (unsigned char *)&TESTcounter );
Delay10KTCYx( 100 );
}
else if(RXbuff[10] == 0x02){
RXbuff[10] = 0x00;
TOCONbits.TMROON = 1;
}
else if(RXbuff[10] == 0x03){
RXbuff[10] = 0x00;
TOCONbits.TMROON = 0;
}

////////////////////////////////// UART RX Test ////////////////////////////////////
/*if(PIR1bits.RCIF){
PORTAbits.RA1 = 1;
Inchar = RCREG;
if ( RCSTAbits.OERR || RCSTAbits.FERR ) // overflow or framing error, reset UART
{
RCSTAbits.CREN = 0;
RCSTAbits.CREN = 1;
}
if (Inchar == '\r'){
PORTAbits.RA1 = 0;
UARTRXmessage[UARTcounter] = '\0';
while(1);
}
else{
UARTRXmessage[UARTcounter] = Inchar;
UARTcounter++;
}
}*/

////////////////////////////////// UART TX Test ////////////////////////////////////
/*
PORTAbits.RA1 = 1;
TXREG =  UARTRXmessage[UARTcounter++];

```

```

//while(!TXSTAbits.TRMT);
if (UARTcounter>99){
UARTcounter = 0;
TXREG = '\n';
while(!TXSTAbits.TRMT);
TXREG = '\r';
//while(!TXSTAbits.TRMT);
PORTAbits.RA1 = 0;
Delay100TCYx( 1 );

if (TESTcounter >4){
TXREG = '\n';
while(!TXSTAbits.TRMT);
TXREG = '\r';
Delay10KTCYx( 200 );
Delay10KTCYx( 200 );
TESTcounter = 0;
}
TESTcounter++;
}*/

}
/*
    while(1){
        RFTX(pseq,ADBUFFER);

Delay1KTCYx( 200 );
PORTAbits.RA1 = 1;
ANRead(ADBUFFER);
PORTAbits.RA1 = 0;

Delay1KTCYx( 200 );
    seq++;

}
*/

}

////////// TX ////////////
void RFTX(unsigned char *buff, unsigned char *pADBuf, unsigned char *ADBufLength){

//PORTAbits.RA1 = 1;
CC2420_WriteReg( CC2420_TXFIFO, buff, 10 );
CC2420_WriteReg( CC2420_TXFIFO, pADBuf, 2*(*ADBufLength) );
CC2420_WriteReg( CC2420_TXFIFO, buff, 16 );
//PORTAbits.RA1 = 0;
CC2420_Command( CC2420_STXON );
// while(!PORTBbits.RB2); // Start of TX
// PORTAbits.RA1 = 1;
// while(PORTBbits.RB2); // End of TX
// PORTAbits.RA1 = 0;

```

```

}

////////// RX //////////
void RFRX(unsigned char data[], unsigned char *Length){

    if(PORTBbits.RB0)
    {
        // PORTAbits.RA0 = 1;
        CC2420_ReadReg( CC2420_RXFIFO, Length, 1 );
        data[0] = *Length;
        CC2420_ReadReg( CC2420_RXFIFO, data+1, *Length );

        // PORTAbits.RA0 = 0;
    }

    //at this point, buff[] contains the received message and len contains the message len
}

void ANRead(char *pADBuf){

    ADCON0bits.GO = 1; // a/d on

    while (ADCON0bits.NOT_DONE) {Nop();}
    Nop();

    *(pADBuf++) = ADRESH & 0x03;

    *pADBuf = ADRESL;

}

////////// UART codes //////////
void UARTInit(void){
    RCSTA = 0b10000000;
    TRISCbits.TRISC7 = 1;
    TRISCbits.TRISC6 = 1;
    BAUDCONbits.BRG16 = 1;
    TXSTA = 0x24;
    RCSTA = 0x90; // 0b10010000;
    SPBRG = 1;
        SPBRGH = 0;
    PIE1bits.RCIE = 0;

}

////////// reset and initialize the chip CC2420 //////////
void CHIPCC2420Reset(void){
    char buff[2];
    int i;
    int Status=0;
    CC2420_Reset();
}

```

```

CC2420_Command(CC2420_SXOSCON);
for(i=0;i<30000;i++);
while(1){
Status = CC2420_Command( CC2420_SNOP );
Status = Status >> 6;
if (Status){
// CC2420_Command( CC2420_SFLUSHTX );

break;
}
CC2420_Reset();
CC2420_Command(CC2420_SXOSCON);
for(i=0;i<30000;i++);
}
CC2420_SetReg( CC2420_MDMCTRL0, 0x0AF2 ); //Write to MDMCTRL0 (turn on auto packet a
CC2420_SetReg( CC2420_MDMCTRL1, 0x0500 ); //Write to MDMCTRL1 (set corr threshold to
CC2420_SetReg( CC2420_SECCTRL0, 0x01C4 ); //Write to secctrl0 (turn off security ena
CC2420_SetReg( CC2420_TXCTRL, 0x0AFF );
CC2420_SetReg( CC2420_IOCFG0, 0x007F ); //Write to IOCFG0 (set the FIFOP threshold)
CC2420_Command( CC2420_SFLUSHRX );
CC2420_Command( CC2420_SFLUSHTX );
buff[0] = 0x55; //Set the PAN id
buff[1] = 0x55;
CC2420_WriteRam( CC2420RAM_SECURITY, CC2420RAM_PANID, buff, 2 );
for(i=0;i<30000;i++);
buff[0] = 0x12; //Set the node short address
buff[1] = 0x12;
CC2420_WriteRam( CC2420RAM_SECURITY, CC2420RAM_SHORTADDR, buff, 2 );
CC2420_Command( CC2420_SFLUSHRX ); //Flush the receive buffer
CC2420_Command( CC2420_SFLUSHRX );
CC2420_Command( CC2420_SRXON ); //Turn on receive mode
for(i=0;i<30000;i++); //Pause for chip to become ready
}

```

A.1.2.2 CC2420 Driver

```

/*
* CC2420.c - Driver for CC2420 Wireless transceiver on PIC18
*
* WASN Development team, ECE480 Group #10, Corrections on Addressing
* made by Mohsen Fatoorechi
*/
//Functions to setup and transmit data over the CC2420
#include <p18cxxx.h>
#include <spi.h>
#include ".\CC2420.h"
#define CC2420_CS_SET PORTCbits.RC0 = 0;
#define CC2420_CS_UNSET PORTCbits.RC0 = 1;
#define _SPI_WRITE(cmd) \
SSPBUF = cmd; \

```

```

if ( SSPCON1 & 0x80 ) \
return ( -1 ); \
else \
{ while( !SSPSTATbits.BF ); }
void CC2420_Reset(void)
{
int i;
PORTCbits.RC2 = 0; //RESETh set low
for(i=0;i<30000;i++);
PORTCbits.RC2 = 1; //RESETh set high
for(i=0;i<30000;i++);
}
unsigned char CC2420_Command( char command )
{
unsigned char STATUS;
CC2420_CS_SET
_SPI_WRITE(command)
STATUS = SSPBUF;
CC2420_CS_UNSET
return ( STATUS ); // if WCOL bit is not set return non-negative#
}
unsigned char CC2420_SetReg( char reg, unsigned long data)
{
CC2420_CS_SET
/* Write the address to the SPI */
_SPI_WRITE(reg)
/* Write the data to the spi, stop if there was a SPI error */
_SPI_WRITE((data&0xFF00)>>8)
_SPI_WRITE(data&0x00FF)
CC2420_CS_UNSET
return ( 0 ); // if WCOL bit is not set return non-negative#
}
unsigned char CC2420_WriteReg( char reg, unsigned char data[], unsigned char length )
{
char pos = 0;
CC2420_CS_SET
/* Write the address to the SPI */
_SPI_WRITE(reg)
/* Write the data to the spi, stop if there was a SPI error */
for(pos = 0; pos < length; pos++) {
_SPI_WRITE(data[pos])
}
CC2420_CS_UNSET
return ( 0 ); // if WCOL bit is not set return non-negative#
}
unsigned char CC2420_ReadReg( char reg, unsigned char* data, unsigned char length )
{
char pos = 0;
CC2420_CS_SET
/* Write the address to the SPI */
_SPI_WRITE((reg & 0x3F) | 0x40) // write byte to SSPBUF register with read bit set

```

```

/* Write the data to the spi, stop if there was a SPI error */
for(pos = 0; pos < length; pos++) {
    _SPI_WRITE(0)
    data[pos] = SSPBUF;
}
CC2420_CS_UNSET
return ( 0 ); // if WCOL bit is not set return non-negative#
}
/*
Valid banks are
*/
unsigned char CC2420_WriteRam( char bank, char address,
char data[], unsigned char length )
{
    char pos = 0;
    CC2420_CS_SET
    /* Write the address to the SPI */
    _SPI_WRITE(address | 0x80)
    _SPI_WRITE( bank & 0xC0)
    /* Write the data to the spi, stop if there was a SPI error */
    for(pos = 0; pos < length; pos++) {
        _SPI_WRITE(data[pos])
    }
    CC2420_CS_UNSET
    return ( 0 ); // if WCOL bit is not set return non-negative#
}
unsigned char CC2420_ReadRam( char bank, char address,
char* data, unsigned char length )
{
    char pos = 0;
    CC2420_CS_SET
    /* Write the address to the SPI */
    _SPI_WRITE(address | 0x80)
    _SPI_WRITE((bank | 0x20) & 0xE0)
    /* Write the data to the spi, stop if there was a SPI error */
    for(pos = 0; pos < length; pos++) {
        _SPI_WRITE(0)
        data[pos] = SSPBUF;
    }
    CC2420_CS_UNSET
    return ( 0 ); // if WCOL bit is not set return non-negative#
}

```

A.1.3 LabView

Block Diagram design for Wireless communication interface Figures [A.1](#) and [A.2](#).

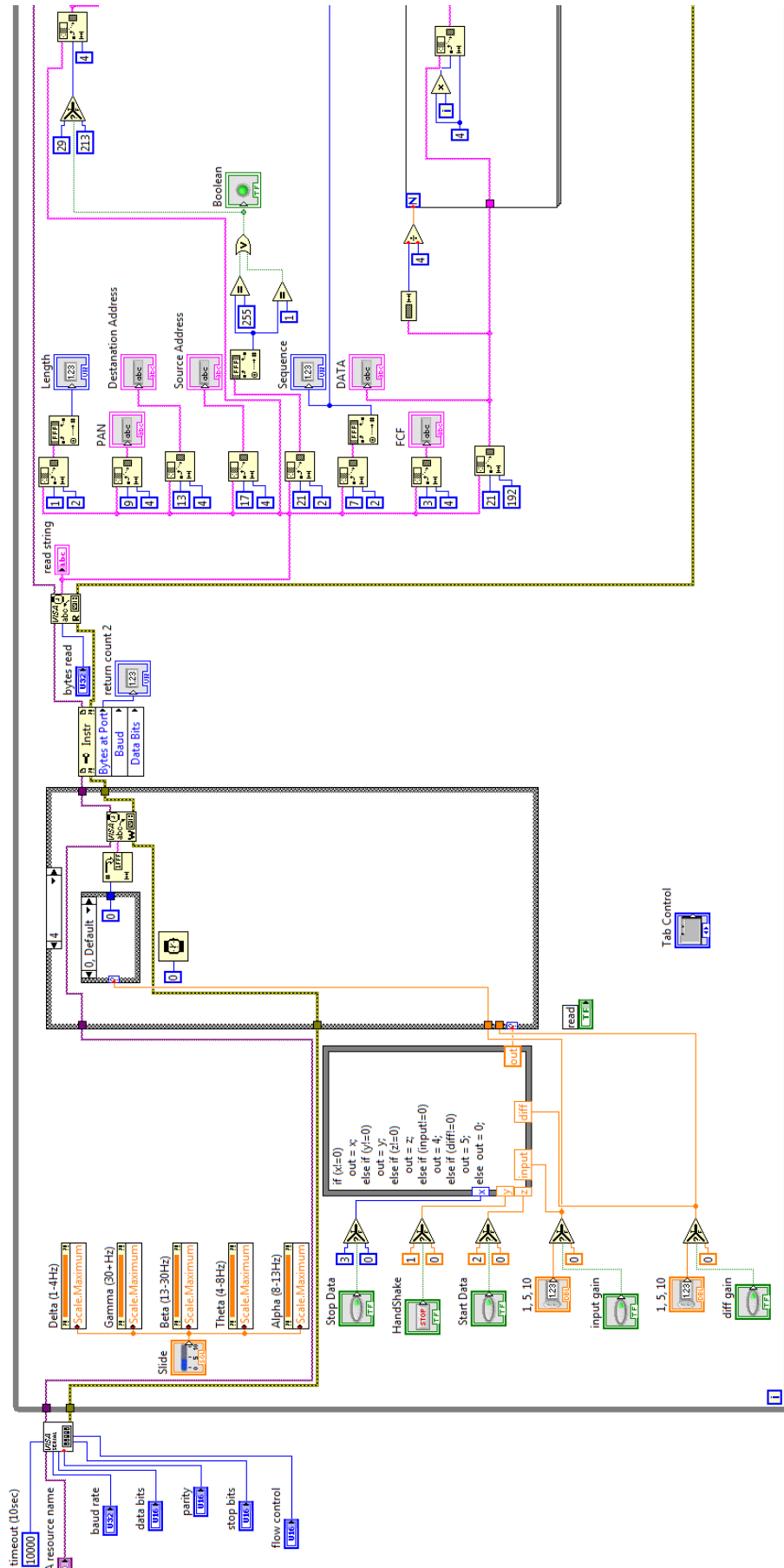


FIGURE A.1: LabView Block Diagram Part 1 for wireless interface

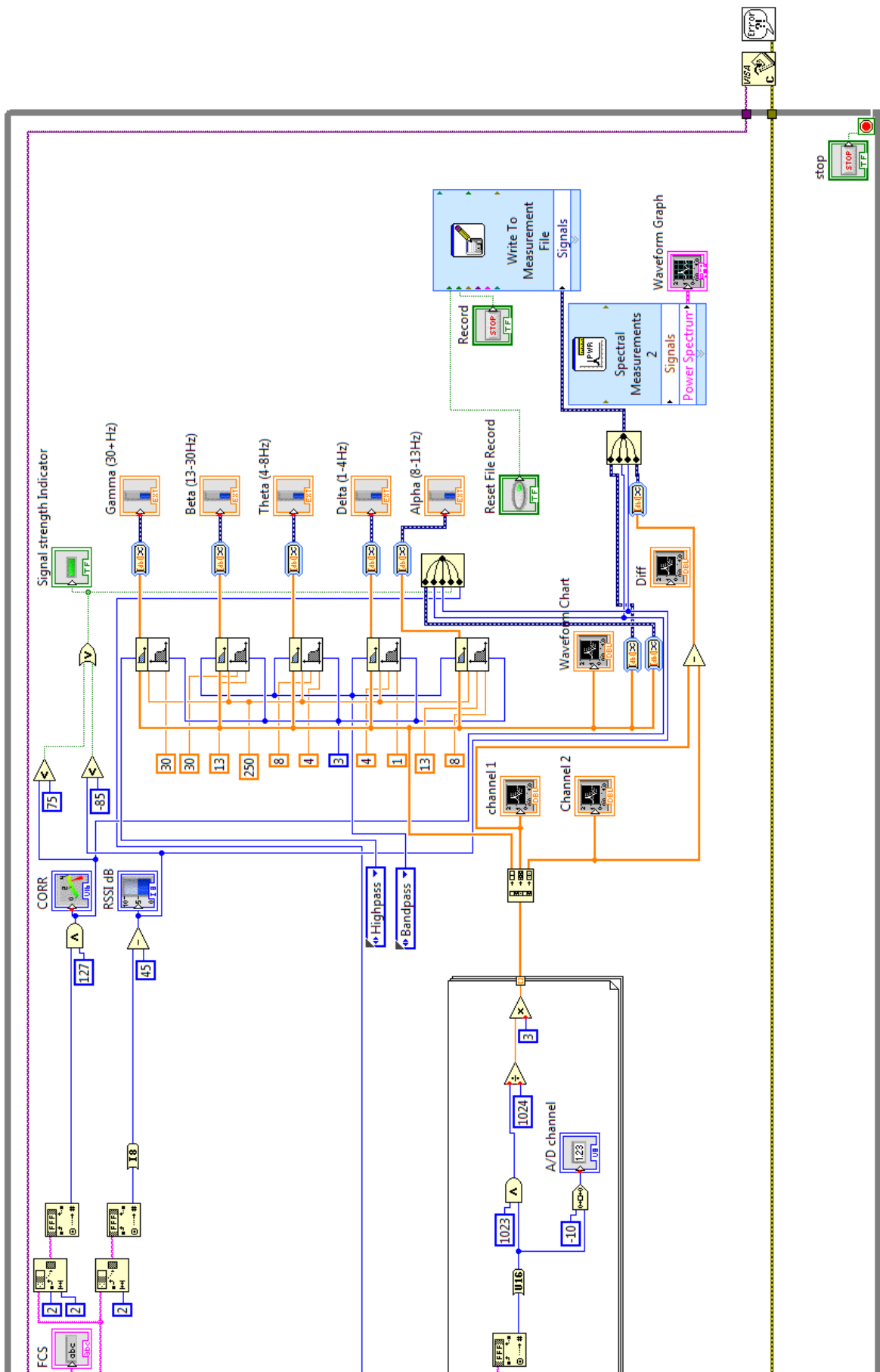


FIGURE A.2: LabView Block Diagram Part 2 for wireless interface

A.2 Appendix B

A.2.1 g.tec

Full result for all channels recorded with g.USBamp as shown in figure A.3. The cap used by g.tec was fitted with 8 sensors and the ninth graph represent the result for EPS data.

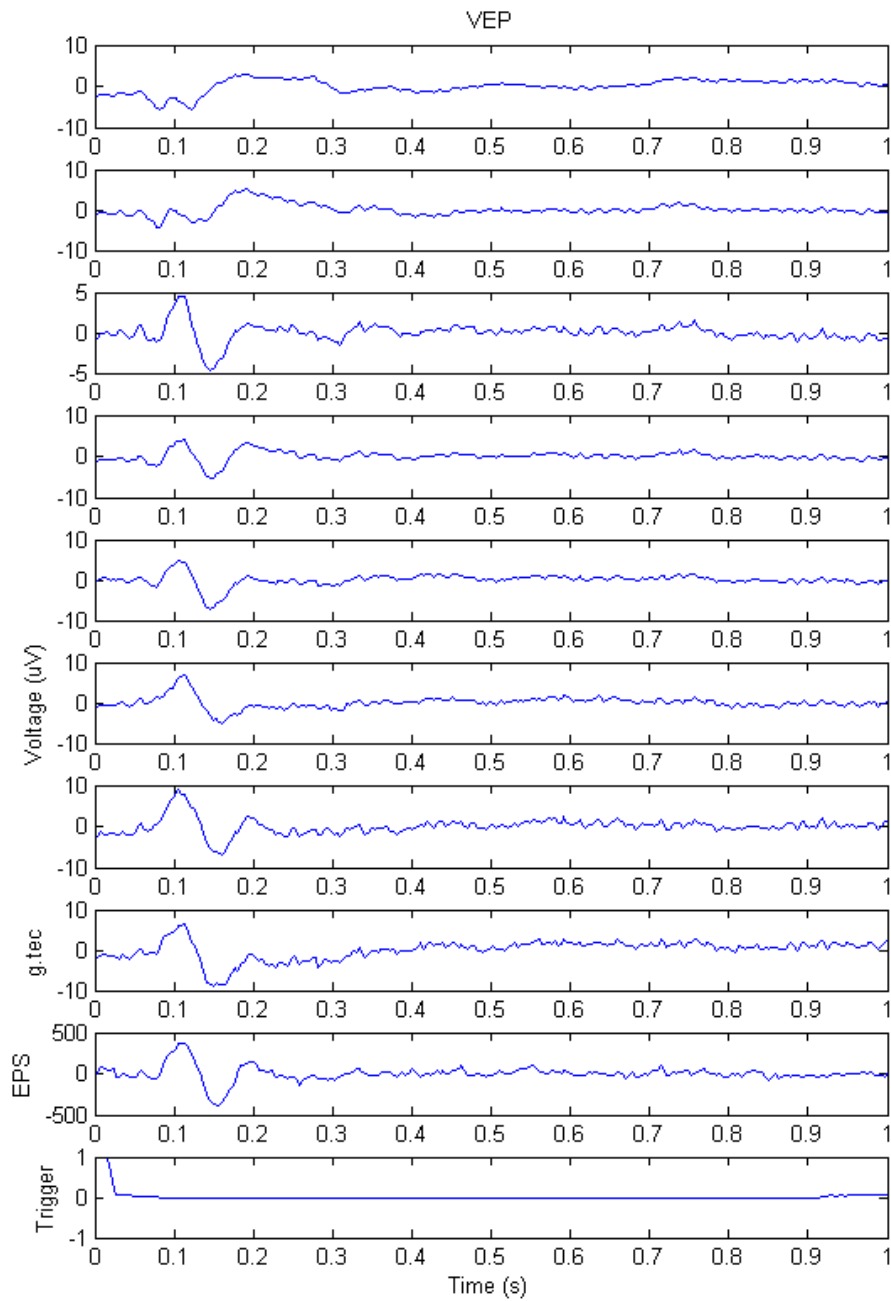


FIGURE A.3: Alpha Blocking Frequency domain, comparison between the EPS and active g.tec gel sensors

A.3 Appendix C

A.3.1 UART Converter

An example of other circuits used is the UART to USB converter [A.4](#).

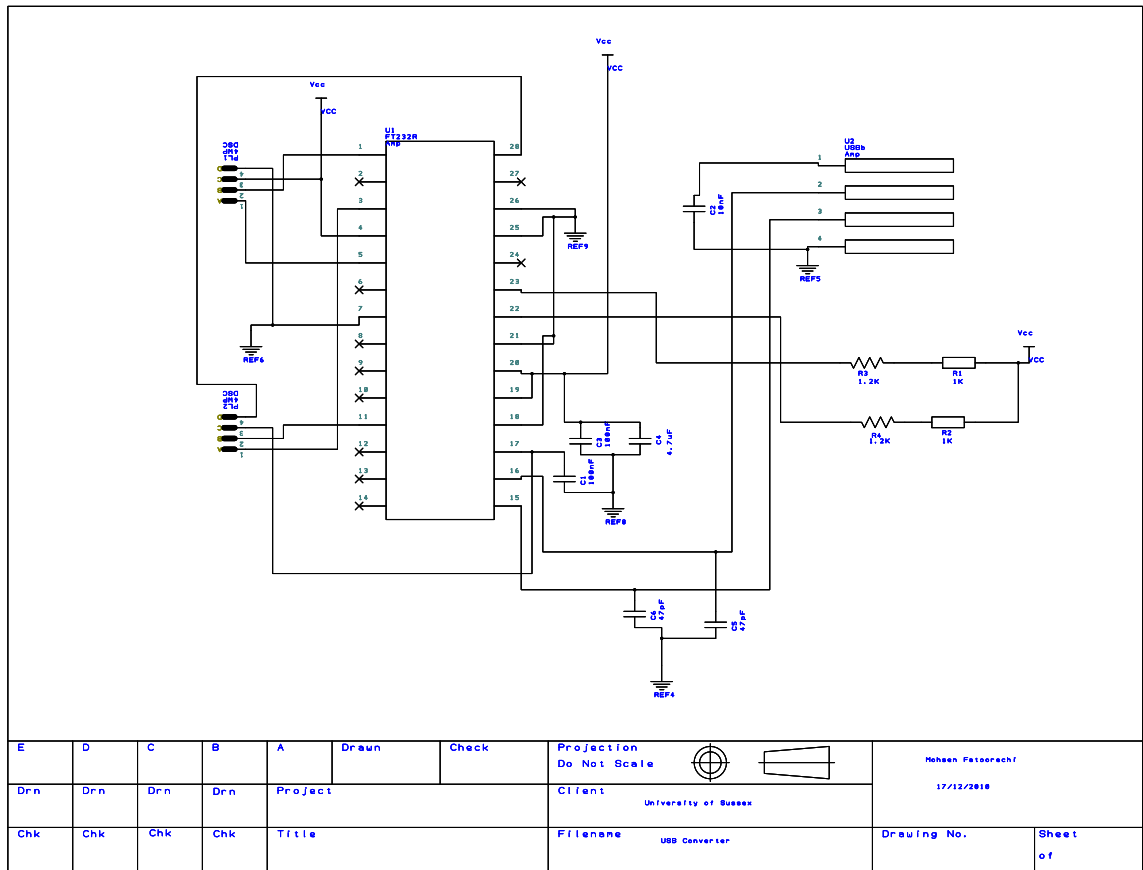


FIGURE A.4: USB to UART Converter using FT232R chip

A.3.2 gtec Interface

Interface box for EPS sensor to g.tec amplifier [A.5](#).

A.3.3 Wireless Communication Board Design

Schematic design for wireless communication board based on the IEEE 802.15.4 standard [A.6](#) and [A.7](#).

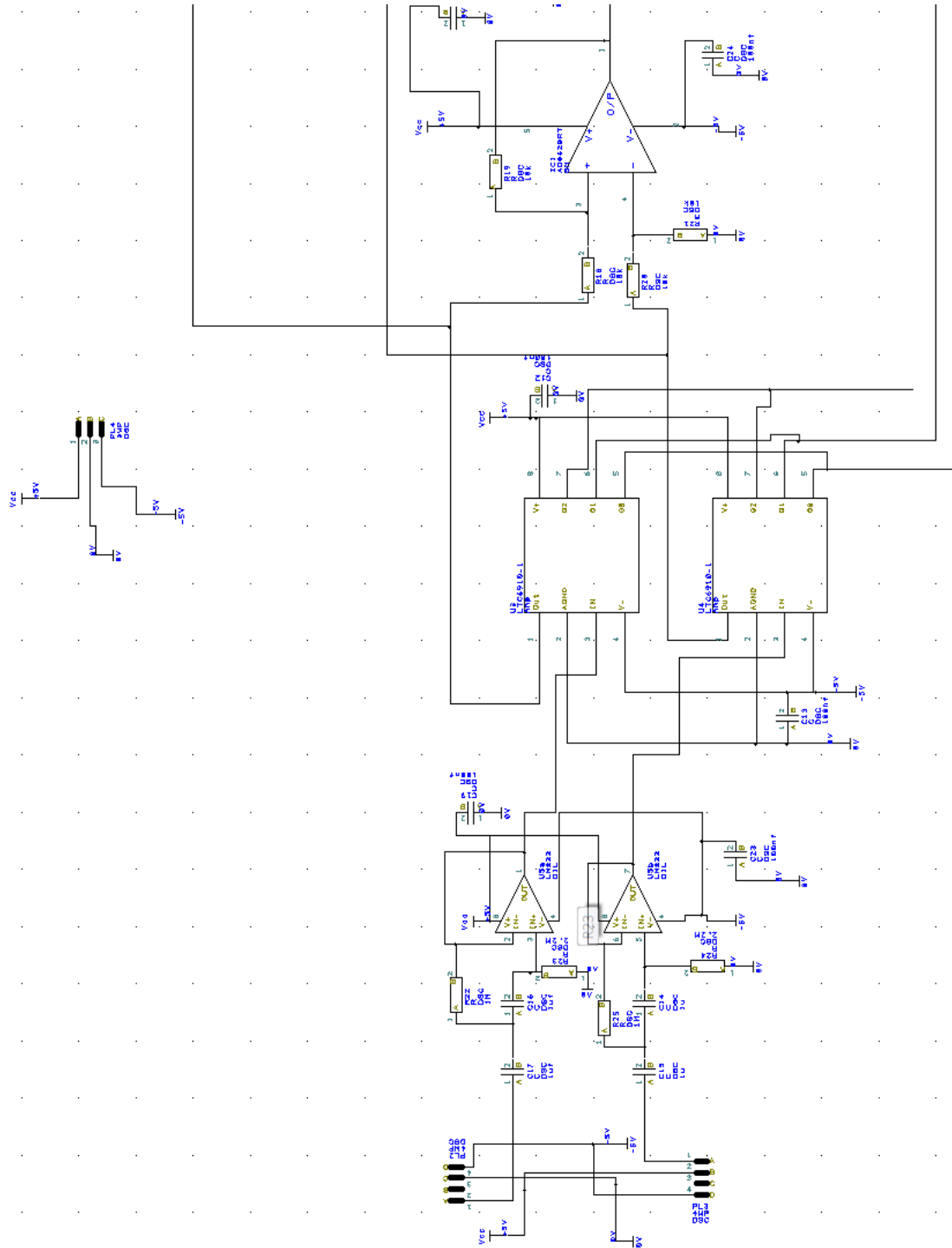


FIGURE A.6: Wireless Board Part 1

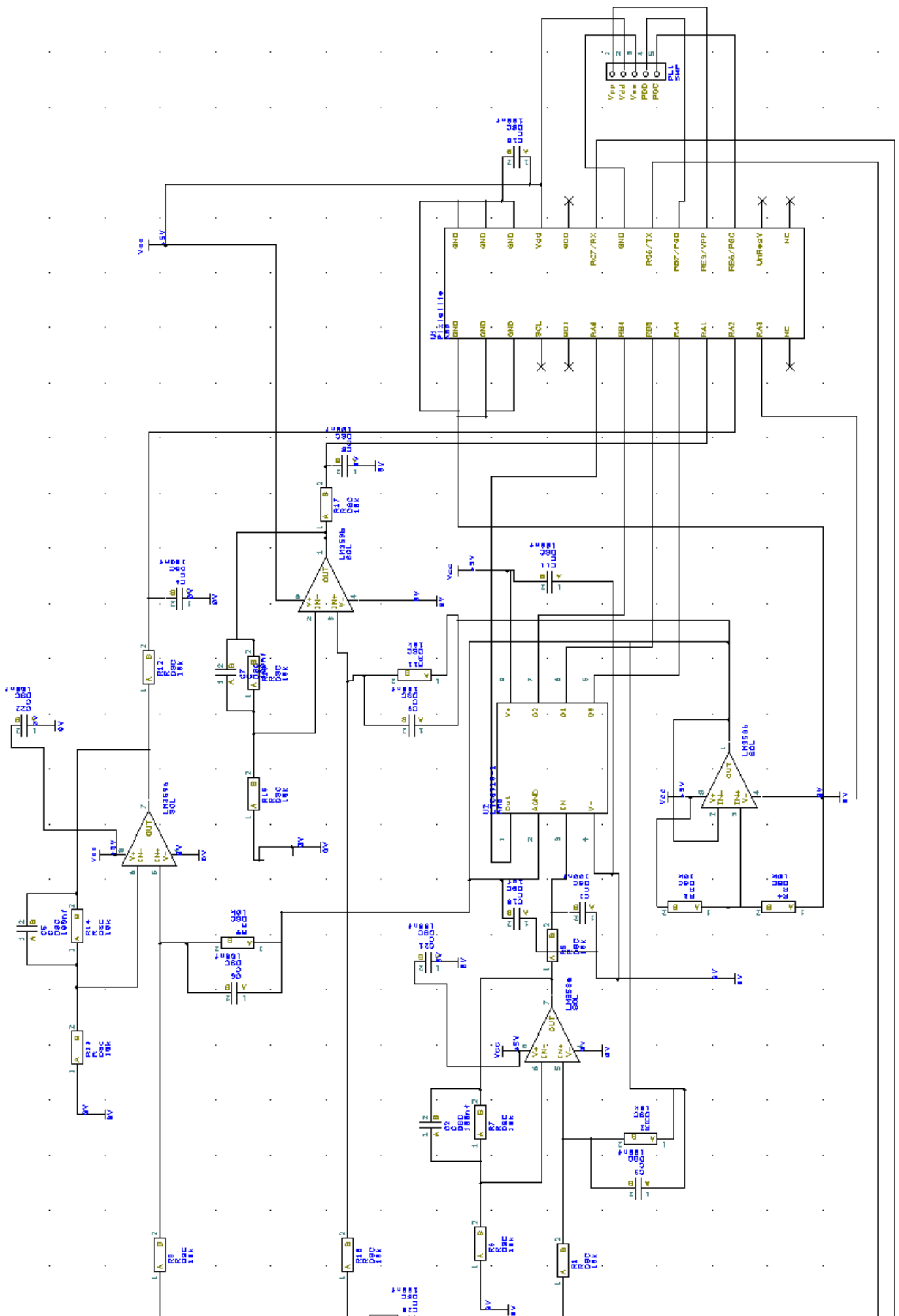


FIGURE A.7: Wireless Board Part 2